

3 Polymer Rheology and Non-Newtonian Fluid Mechanics

- 3.1 Rheological Behavior, Rheometry, and Rheological Material Functions of Polymer Melts, 80
- 3.2 Experimental Determination of the Viscosity and Normal Stress Difference Coefficients, 94
- 3.3 Polymer Melt Constitutive Equations Based on Continuum Mechanics, 100
- 3.4 Polymer Melt Constitutive Equations Based on Molecular Theories, 122

In Chapter 2 we discussed the engineering science of transport phenomena and Newtonian fluid mechanics. Only *simple fluids* such as gases and small liquid molecules exhibit Newtonian behavior. High molecular weight polymer melts are structurally *complex fluids* in that their macromolecules can assume many *conformations*, which become more *stretched* under flow, while gradually *recovering* into *random* conformations upon removal of the flow stresses. The state of macromolecular conformations profoundly affects intermolecular interactions during flow and, therefore, the viscosity of polymer melts strongly depends on the flow velocity gradients, rendering them non-Newtonian and their viscosity a *rheological material function*, not just a material parameter, as with Newtonian fluids. Furthermore, polymer melts also exhibit, in addition to a viscous nature, an elastic response, since conformations recover from stretched to random. Therefore, melts are *viscoelastic materials*.

A major portion of all the polymer processing shaping operations and elementary steps involves either isothermal or, most often, nonisothermal flow of polymer melts in geometrically complex conduits. Before dealing with the realistic polymer processing flow problems, it is therefore appropriate to examine separately the rheological (flow) behavior of polymer melts in simple flow situations and in the absence of temperature gradients. Our aims are to clarify the physical meaning of terms such as non-Newtonian or viscoelastic behavior, primary normal stress coefficient, and viscosity functions, to discuss briefly, from a primarily physical viewpoint, the constitutive equations that either quantitatively or semiquantitatively describe the observed behavior of polymer melts, and to examine the experimental methods that yield the rheological information needed to characterize polymer melt flow behavior in simple flows.

It is important to note that the rheological material functions obtained experimentally, using *rheometers*, are evaluated in simple flows, which are often called *viscometric* or *rheometric*. A viscometric flow is defined as one in which only one component of the velocity changes in only one spatial direction, $v_x(y)$. Yet these material functions are used to describe the more complex flow situations created by polymer processing equipment. We assume, therefore, that while evaluated in *simple flows*, the *same rheological* properties also apply to complex ones.

The combined effects of flow, geometric channel complexities, and coupled thermo-mechanical phenomena necessitate the use of numerical solutions. In the past 25 years a large number of increasingly powerful numerical simulation packages have been developed commercially taking advantage of the exponential growth in available and affordable computational power to enable solutions of nonisothermal processing flows of non-Newtonian polymer melts. We will describe some of these in the relevant chapters.

3.1 RHEOLOGICAL BEHAVIOR, RHEOMETRY, AND RHEOLOGICAL MATERIAL FUNCTIONS OF POLYMER MELTS

Three kinds of viscometric flows are used by rheologists to obtain rheological polymer melt functions and to study the rheological phenomena that are characteristic of these materials: steady simple shear flows, dynamic (sinusoidally varying) simple shear flows, and extensional, elongational, or shear-free flows.

Steady Simple Shear Flows

This type of flow is obtained either by the relative motion of the rheometer surfaces inducing simple drag flow on the fluid, or by an externally created pressure drop inducing pressure flow on the fluid as shown in Fig. 3.1, parts 1a, 2a, and 3. These flows have the following general flow field: $v_1 = v_1(x_2)$, $v_2 = v_3 = 0$, leading to a single nonzero shear rate component $\dot{\gamma}_{12} \neq 0$. The coordinates x_i for each of the steady shear flows are also shown on Fig. 3.1. The maximum shear rates that are attainable in the simple shear drag flows are very low, below $\dot{\gamma} < 1 \text{ s}^{-1}$, because of secondary flow-induced instabilities generated at the melt sample periphery edges. On the other hand, the operational shear rate range for the externally applied *pressure-induced* capillary flow rheometer is $1 < \dot{\gamma} < 10^4 \text{ s}^{-1}$, covering a range which coincides with most if not all processing flows.

Dynamic (Sinusoidally Varying) Drag Simple Shear Flows

Dynamic (sinusoidally varying) drag simple shear flows are shown in Fig. 3.1, parts 1b and 2b. They are obtained by applying a sinusoidally varying angular displacement $A(\omega, t) = A_0 \sin \omega t$ in the same rheometers that generate steady simple shear flows. Since polymer melts are viscoelastic, the resulting time-varying shear stress has both an in-phase (viscous) and an out-of-phase (elastic) component.

The steady and dynamic drag-induced simple shear-flow rheometers, which are limited to very small shear rates for the steady flow and to very small strains for the dynamic flow, enable us to evaluate rheological properties that can be related to the macromolecular structure of polymer melts. The reason is that very small sinusoidal strains and very low shear rates do not take macromolecular polymer melt conformations far away from their equilibrium condition. Thus, whatever is measured is the result of the response of not just a portion of the macromolecule, but the contribution of the entire macromolecule.

Extensional, Elongational or Shear-free Flows

Extensional, elongational or shear-free flows play a dominant role in the post die-forming step, such as stretching of melt strands in spinning, uniaxial stretching of molten films

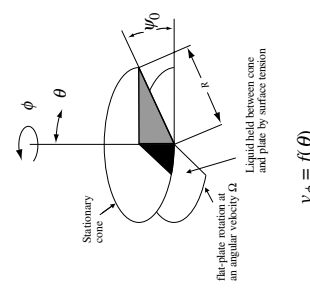
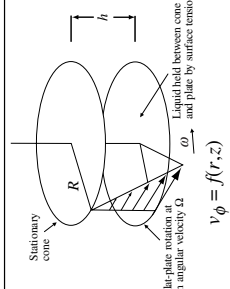
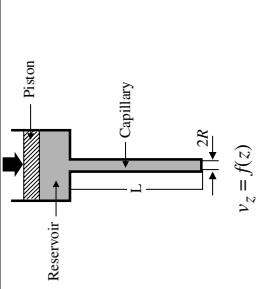
Flow	Coordinates x_1 x_2 x_3	Shear Rate	Experimental Results		Rheological Functions Obtained
			Apply	Measure	
1. Cone and plate	$v_1 \neq 0, v_2 = v_3 = 0$ $\dot{\gamma}_{12} \neq 0$ 	$\dot{\gamma}_{12}$ $\dot{\gamma} = \frac{\sin \theta}{r} d \left(\frac{v_\phi \sin \theta}{d\theta} \right)$ $\Omega = \frac{r}{\psi_0} \dot{\gamma} = C$	(a). Ω (Steady) $\dot{\gamma} < 1 \text{ s}^{-1}$ (b). $A = A_0 \sin \omega t$ A_0 : small (Dynamic)	(P) Torque $\propto \dot{\gamma}^n$ Normal force on plate (N) Torque $\propto \dot{\gamma}$ (P) Torque = $f(\omega, t)$ $= C_1 \sin \omega t + C_2 \cos \omega t$ Normal force on plate (N) Torque only $T = T_0 \sin \omega t$	(P) $\eta(\dot{\gamma}), \Psi_1(\dot{\gamma}^2), \Psi_2(\dot{\gamma}^2)$ (N) $\mu(T)$ (P) $\eta^*(\omega) = \eta' - i\eta''$; $G' = \eta' \omega$; $G'' = \eta'' \omega$ (N) $\mu(T)$
2. Parallel disks (torsional flow)		$\dot{\gamma} = \frac{dv_\theta}{dz}$ $\dot{\gamma} = \frac{\Omega r}{h}$	(a). Ω (Steady) $\dot{\gamma} < 1 \text{ s}^{-1}$ (b). $A = A_0 \sin \omega t$ A_0 : small (Dynamic)	(P) Torque $\propto \dot{\gamma}^n$ Normal force on plate (N) Torque $\propto \dot{\gamma}$ $Torque = f(\omega, t)$ $= C' \sin \omega t + C'' \cos \omega t$ Normal force on plate	(P) $\eta(\dot{\gamma})$; $(\Psi_1(\dot{\gamma}^2) - \Psi_2(\dot{\gamma}^2))_R$ (N) $\mu(T)$ (P) $\eta^*(\omega), G'(\omega), G''(\omega)$
3. Capillary (Poiseuille flow)		$\dot{\gamma} = \frac{dv_z}{dr}$ (P) $\dot{\gamma} = C_1 r^{1/n}$ (N) $\dot{\gamma} = C_2 r$	Piston speed (flow rate: Q)	Pressure Drop (P) $\Delta P \propto Q^n$ $n < 1$ (N) $\Delta P \propto Q$	(P) $\eta(\dot{\gamma})$; Capillary entrance pressure losses, extrudate swell (N) $\mu(T)$

Fig. 3.1 Examples of simple, viscometric, shear-flow rheometer geometries. 1a, 2a and 3 are *steady* while 1b and 2b are *dynamic* rheological property rheometers. (P) denotes polymer melts, while (N) denotes Newtonian fluids.

exiting a flat film die, or the biaxial stretching of a tubular film exiting a blown film die to form a “bubble.” However, as with shear rheometers, the extensional rheometer flows are simpler than the previously mentioned real flows, because they are spatially uniform, isothermal, and shear-free. The general form of the rate of deformation matrix for incompressible fluids is

$$\dot{\boldsymbol{\gamma}} = \dot{\epsilon} \begin{bmatrix} 1 & 0 & 0 \\ 0 & m & 0 \\ 0 & 0 & -(1+m) \end{bmatrix} \quad (3.1-1)$$

Three uniform, steady extensional flows, which are related to post-die flows and useful to study rheological behavior, and the ability of constitutive equations to predict such behavior, are listed below, and are shown on Fig. 3.2.

Figure 3.2 (Case 1) shows a simple uniaxial extensional flow created by the uniform stretching of a rectangular or a thin filament in the 1 direction. For this flow, $\dot{\epsilon}_{22} = -\dot{\epsilon}_{11}/2$, and because of the incompressibility assumption, $\dot{\epsilon}_{22} = \dot{\epsilon}_{33}$. Thus, in Eq. 3.1-1, $m = -0.5$, giving the following rate of deformation matrix

$$\dot{\boldsymbol{\gamma}} = \begin{bmatrix} \dot{\epsilon} & 0 & 0 \\ 0 & -\dot{\epsilon}/2 & 0 \\ 0 & 0 & -\dot{\epsilon}/2 \end{bmatrix} \quad (3.1-2)$$

For this simple uniaxial extensional flow to be steady, the instantaneous rate of change of the 1 direction length (l) must be constant

$$\frac{1}{l} \frac{dl}{dt} = \dot{\epsilon} = \text{const.} \quad (3.1-3)$$

Defining $a = l/l_0$, we rewrite the preceding equation:

$$\frac{1}{a} \frac{da}{dt} = \dot{\epsilon} \quad (3.1-4)$$

upon integration with l_0 being the length at $t = 0$

$$a(t) = l(t)/l_0 = e^{\dot{\epsilon}t} \quad (3.1-5)$$

Thus, in order to create a steady simple uniaxial extensional flow, the rheometer must cause the thin filament length to increase exponentially in time.

Figure 3.2 shows planar extensional flow generated by the uniform stretching of a thin wide sheet or film in one direction only, while allowing the thickness in the perpendicular direction to decrease. Thus, $\dot{\epsilon}_{11} = -\dot{\epsilon}_{33}$ and $\dot{\epsilon}_{22} = 0$. Therefore, $m = 0$ in Eq. 3.1-1, giving

$$\dot{\boldsymbol{\gamma}} = \dot{\epsilon}_{pl} \begin{bmatrix} 1 & 0 & 0 \\ 0 & 0 & 0 \\ 0 & 0 & -1 \end{bmatrix} \quad (3.1-6)$$

Again, an exponential film length increase is necessary in order to obtain constant $\dot{\epsilon}_{pl}$.

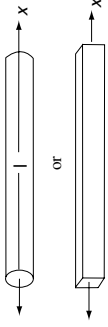
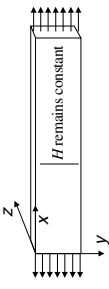
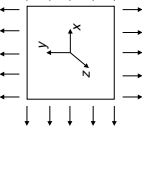
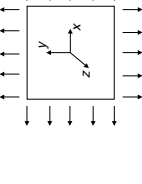
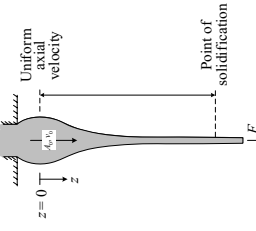
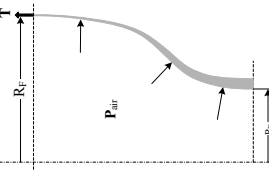
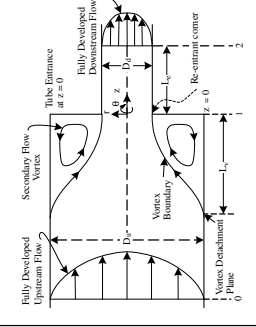
Steady Uniform Extensional Flow		Coordinates x_1 x_2 x_3	Apply	Obtain	Rheological Properties
1. Simple uniaxial extension		x r θ	$l = l_0 e^{\dot{\epsilon} t}$ ($\dot{\epsilon} < 1 s^{-1}$)	$F_1(t), A_1(t)$	<p>Ⓐ $\bar{\eta}(\dot{\epsilon}) = -\frac{F_1}{A_1}$; (steady)</p> <p>$\bar{\eta}^+(\dot{\epsilon}, t) = -\frac{F_1(t)}{A_1(t)}$; (growth)</p> <p>Ⓑ $\bar{\eta}(T) = 3\mu(T)$</p>
		x y z			
2. Planar extension		x y z	$l = l_0 e^{\dot{\epsilon}_{pl} t}$ ($\dot{\epsilon}_{pl} < 1 s^{-1}$)	$F_1(t), A_1(t)$	<p>$\bar{\eta}(\dot{\epsilon}_{pl}) = -\frac{F_1}{A_1}$; (steady)</p> <p>$\bar{\eta}^+(\dot{\epsilon}_{pl}, t) = -\frac{F_1(t)}{A_1(t)}$; (growth)</p>
3. Equibiaxial extension		x y z	$l_1(t) = l_2(t) = l_0 e^{\dot{\epsilon}_{bt} t}$ ($\dot{\epsilon}_{bt} < 1 s^{-1}$)	$F(t), A(t)$	<p>$\bar{\eta}(\dot{\epsilon}_{bt}) = -\frac{F}{A}$; (steady)</p> <p>$\bar{\eta}^+(\dot{\epsilon}_{bt}, t) = -\frac{F_1(t)}{A_1(t)}$; (growth)</p>
4. Examples of non-uniform die and post-die forming extensional flows					
					
Fiber spinning (Nonuniform uniaxial extension)	Film blowing (Nonuniform biaxial extension)			Stretch blow molding (Nonuniform biaxial extension)	Die entrance flows (Uniaxial extension and shear flow)

Fig. 3.2 Cases 1, 2, and 3 show steady, uniform extensional flows. Case 4 shows examples of more complex nonuniform stretching flows encountered in polymer processing operations.

In an equibiaxial extensional flow, shown in Fig. 3.2, the film is stretched at a constant rate $\dot{\epsilon}_{bi}$ in two directions, allowing the thickness of the incompressible molten film to decrease. Here $\dot{\epsilon}_{11} = \dot{\epsilon}_{22}$ and $\dot{\epsilon}_{33} = -2\dot{\epsilon}_{11}$. Thus $m = 1$ in Eq. 3.1-1 and

$$\dot{\gamma} = \epsilon_{bi} \begin{bmatrix} 1 & 0 & 0 \\ 0 & 1 & 0 \\ 0 & 0 & -2 \end{bmatrix} \quad (3.1-7)$$

It is quite difficult to experimentally produce the preceding three uniform and isothermal flows, and extensional rheometers are therefore often limited to low attainable $\dot{\epsilon} \sim 1 \text{ s}^{-1}$ and short duration. Nevertheless, polymer processing engineers have to deal with nonuniform, nonisothermal extensional flows with polymer melts which, if they are crystallizable, undergo rapid crystal nucleation and anisotropic growth of the crystalline phase. As mentioned in Chapter 1, these phenomena in actual post-die forming operations cause the formation of unique structures and morphologies, called *structuring*, which greatly affect product properties. For further reading on experimental rheology, the reader is referred to the extensive available literature (e.g., Refs. 1–4).

Let us now turn again to Figs. 3.1 and 3.2 to examine the experimental results obtained with polymer melts in rheometers and the differences between them and those obtained with Newtonian fluids, thus gaining a specific understanding of what *non-Newtonian* behavior means in the response of polymeric melt to deformation.

Rheological Response of Polymer Melts in Steady Simple Shear-Flow Rheometers

Non-Newtonian Viscosity In the *cone-and-plate* and *parallel-disk torsional* flow rheometer shown in Fig. 3.1, parts 1a and 2a, the experimentally obtained torque, and thus the τ_{12} component of the shear stress, are related to the shear rate $\dot{\gamma} = \dot{\gamma}_{12}$ as follows: for Newtonian fluids $\tau_{12} \propto \dot{\gamma}$, implying a *constant* viscosity, and in fact we know from Newton's law that $\tau_{12} = -\mu\dot{\gamma}$. For polymer melts, however, $\tau_{12} \propto \dot{\gamma}^n$, where $n < 1$, which implies a *decreasing* shear viscosity with increasing shear rate. Such materials are called *pseudoplastic*, or more descriptively, *shear thinning*.¹ Defining a non-Newtonian viscosity,² η ,

$$\tau_{12} = \eta(\dot{\gamma})\dot{\gamma} \quad (3.1-8)$$

and assuming that the shear rate dependence of η can be expressed by simple power dependence, which agrees well with experimental measurements of many polymeric melts over a broad shear rate range, we get the following relationship

$$\eta(\dot{\gamma}) = m\dot{\gamma}^{n-1} \quad (3.1-9)$$

1. The term *pseudoplastic* is somewhat outdated because there is nothing "pseudo" in the flow behavior of polymers. In this book we use the term *shear thinning*, which well describes the phenomenon.

2. Non-Newtonian viscosity is sometimes called *apparent viscosity*, presumably because it changes with shear rate. In this book we call it *non-Newtonian viscosity*.

This relationship, as we will see in Section 3.3, is called the Power Law fluid model, and is used extensively in modeling flows in polymer processing.

In conclusion, we thus find that polymer melts are non-Newtonian in that they have a *viscosity that depends on the shear rate* $\dot{\gamma}_{12}$, or the shear stress τ_{12} in steady shear flows. This is the most important non-Newtonian property that we encounter in polymer processing.

Normal Stresses In the steady *cone-and-plate* and *parallel-disk torsional* flow rheometers, again with polymer melts, we observe experimentally a phenomenon that is totally unexpected and unpredictable by Newtonian rheological behavior, namely a *normal force*, F_N , acting on both pairs of plates. For a Newtonian fluid, the only stress component needed to support the single shear rate components $\dot{\gamma} = \dot{\gamma}_{12}$ is shear stress component τ_{12} . This stress component gives rise to the experimentally needed torque, as noted earlier. How can the normal force F_N on the rheometer plates be explained? On the grounds of physical macromolecular behavior, we can reason that the flow in the direction that the velocity points, defined as direction 1, tends to orient the macromolecules in that direction, somewhat like rubber bands stretched around a cylinder. But stretched polymer melt macromolecules want to revert to their equilibrium coiled conformations. This creates *tensile stresses* in the 1 direction, τ_{11} (which act as “strangulation” forces) as well as stresses in the normal direction in which the velocity changes, defined as direction 2, τ_{22} . These normal stresses would be relieved if the rheometer spacing were increased. Thus, in order to maintain the plate spacing constant, we have to impose on the sheared melt a normal force F_N . Because of the difficulties associated with the absolute value of pressure in a flow system (see Chapter 2), we define normal stress differences rather than individual components, such as the *primary* normal stress difference $\tau_{11} - \tau_{22}$. In fact, as we will see later, the measurement of the normal force F_N in the cone and plate rheometer is a direct measure of this normal stress difference.

A graphic example of the consequences of the existence of τ_{11} stress in simple steady shear flows is demonstrated by the well-known Weissenberg *rod-climbing* effect (5). As shown in Fig. 3.3, it involves another simple shear flow, the Couette (6) torsional concentric cylinder flow,³ where $x_1 = \theta$, $x_2 = r$, $x_3 = z$. The flow creates a shear rate $\dot{\gamma}_{12} = \dot{\gamma}$, which in Newtonian fluids generates only one stress component τ_{12} . Polyisobutylene molecules in solution used in Fig. 3.3(b) become oriented in the 1 direction, giving rise to the shear stress component in addition to the normal stress component τ_{11} .

Furthermore, when the cone-and-plate rheometer is outfitted with pressure taps at various radial positions, the experimentally obtained *pressure distribution* is found to be increasing with decreasing radial distance. This, as we will see later, enables us to compute the *secondary* normal stress difference, namely, $\tau_{22} - \tau_{33}$, where direction 3 is the third neutral spatial direction.

Next we define the two normal stress difference functions that arise in simple shear flows

$$\tau_{11} - \tau_{22} = \Psi_1(\dot{\gamma})\dot{\gamma}_{12}^2 \quad (3.1-10)$$

3. The Couette apparatus was developed by Maurice Couette in 1890 as a means for measuring the viscosity of a fluid at small imposed angular velocities of the cylinders.

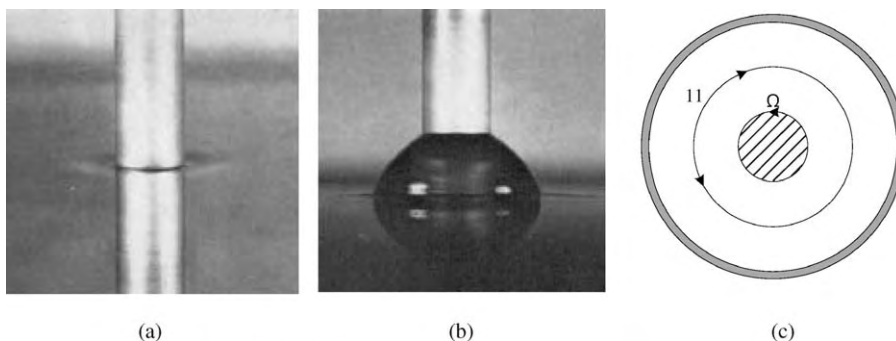


Fig. 3.3 A 9.52-mm D aluminum rod rotating at 10 rps in a wide-diameter cylinder containing (a) Newtonian oil, and (b) polyisobutylene (PIB) solution, which exhibits the rod-climbing Weissenberg effect [from G. S. Beavers and D. D. Joseph, *J. Fluid Mech.*, **69**, 475 (1975)]. (c) Schematic representation of the flow direction flow-induced τ_{11} , causing rod climbing. For Newtonian fluids, $\tau_{11} = 0$, since the small and simple Newtonian fluid molecules are incapable of being “oriented” by the flow.

and

$$\tau_{22} - \tau_{33} = \Psi_2(\dot{\gamma})\dot{\gamma}_{12}^2 \quad (3.1-11)$$

The coefficients Ψ_1 and Ψ_2 , like non-Newtonian viscosity, are also found to be shear rate dependent. The non-Newtonian property of exhibiting normal stresses in shear flows plays an important role in processing under situations in which shear stresses vanish, as in extrudate swell, discussed later in this section.

Capillary Flow Rheometry Next we examine the experimentally obtained results with the capillary flow rheometer shown in Fig. 3.1, which are directly relevant to polymer processing flows, since the attainable shear rate values are in the range encountered in polymer processing. The required pressure drop ΔP does not increase linearly with increases in the volumetric flow rate Q , as is the case with Newtonian fluids. Rather, increasingly smaller increments of ΔP are needed for the same increases in Q . The Newtonian Poiseuille equation, relating flow rate to pressure drop in a tube, is linear and given by

$$\Delta P = \frac{8\mu L}{\pi R^4} Q \quad (3.1-12)$$

On the other hand, for polymer melts, we obtain experimentally a nonlinear relationship

$$\Delta P \propto Q^n \quad (n < 1) \quad (3.1-13)$$

Again, this dependence may reasonably be attributed to a *decreasing* viscosity with *increasing* shear rate. With decreasing viscosity, resistance to flow at higher flow rates decreases as well. It is this decreasing viscosity with increasing shear rates that enables

processing machinery to operate at high rates of production and avoid excessive heat generation that may damage the polymer.

Another important ramification of shear-thinning behavior in capillary or tube flow, relevant to polymer processing, relates to the shape of the *velocity profiles*. Newtonian and shear-thinning fluids are very different, and these differences have profound effects on the processing of polymer melts. The former is parabolic, whereas the latter is flatter and pluglike. The reason for such differences emerges directly from the equation of motion. The only nonvanishing component for steady, incompressible, fully developed, isothermal capillary flow, from Table 2.2, is

$$\frac{1}{r} \frac{d}{dr}(r\tau_{rz}) = -\frac{dP}{dz} \tag{3.1-14}$$

Integrating with the boundary condition $\tau_{rz}(0) = 0$

$$\tau_{zr} = \tau(r) = Cr = -\left(\frac{\Delta P}{2L}\right)r \tag{3.1-15}$$

Equation 3.1-14 holds for all fluids, since it is a physical law. This is shown in Fig. 3.4(a).

But when a rheological model relating $\tau(r)$ versus $\dot{\gamma}(r)$ is substituted into Eq. 3.15, two different shear rate and velocity profiles are obtained. For Newtonian fluids, $\tau(r) = -\mu\dot{\gamma}(r)$, the shear rate profile is

$$\dot{\gamma}(r) = \frac{\Delta P}{2\mu L}r \tag{3.1-16}$$

indicating that the Newtonian shear rate increases linearly with r , as shown in Fig. 3.4(b), whereas for shear-thinning melts, using the Power Law model $\tau(r) = -m\dot{\gamma}(r)^n$, we get

$$\dot{\gamma}(r) = \left(\frac{\Delta P}{2mL}\right)^{1/n} r^{1/n} \tag{3.1-17}$$

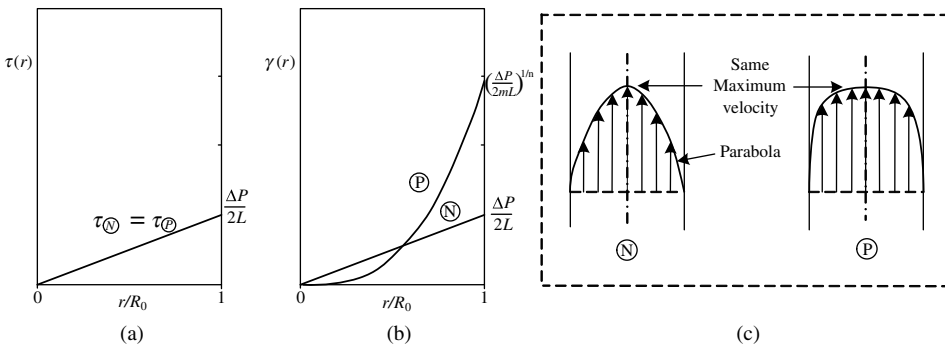


Fig. 3.4 The (a) shear stress, (b) shear rate, and (c) velocity profiles of a Newtonian and a shear-thinning fluid flowing in a capillary of dimensions R is under the influence of the same ΔP , that is, $\tau(r)$.

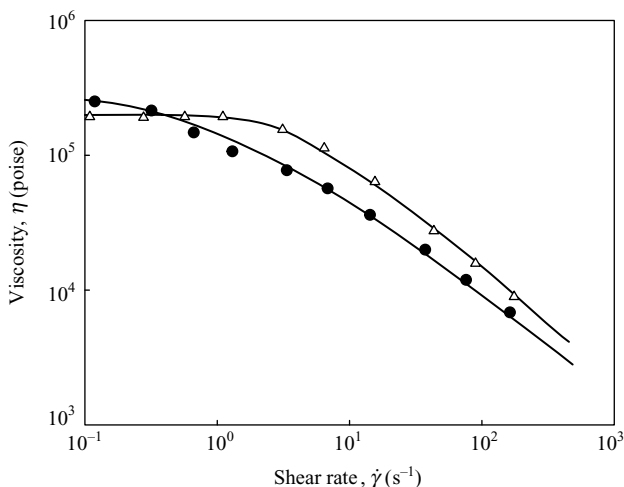


Fig. 3.5 Logarithmic plot of the shear rate-dependent viscosity of a narrow molecular weight distribution $PS(\Delta)$ at $180^\circ C$, showing the Newtonian plateau and the Power Law regions and a broad distribution $PS(\bullet)$. [Reprinted with permission from W. W. Graessley et al., *Trans. Soc. Rheol.*, **14**, 519 (1970).]

Thus for shear-thinning melts, that is, $n < 1$, the shear rate profile, $\dot{\gamma}(r)$, dependence is *stronger than the first power*, as shown again in Fig. 3.4(b). Consequently, as shown in Fig. 3.4(c), shear-thinning polymer melts flow in pressure-induced flows with very high shear rates near the walls, while there is a core of the fluid that is sheared very little. Because of this, and the high polymer melt viscosity, the melt layers next to the wall heat up, while the core flows isothermally. Thus, figuratively speaking, at high shear rates where both shear rate and temperature are high near the capillary wall, the wall polymer melt layer acts almost as a lubricant, while the core flows almost in plug flow. The shear viscosity $\eta(\dot{\gamma})$ of polymer melts typically decreases dramatically with increasing shear rates in the process range of $\dot{\gamma}$ (as shown on Fig. 3.5).

Polymer melts exhibit capillary exit and entrance behavior, which is different than that of Newtonian fluids. Polymer melt extrudates “swell,” that is, increase in diameter, following the capillary exit. This is, again, a ramification of the existence of tensile stresses in the flow direction, encountered earlier. The extrudates in the stress-free boundary region following the exit relieve this axial tension by contracting, and thus expanding radially. Just ahead of the capillary entrance, polymer melts undergo a more complex combined extension and shear flow. The *entrance* pressure drops generated are much higher for melts, because their elongational viscosity is higher than the Newtonian, as we will see later in this section. We will discuss both the preceding phenomena in Chapter 13.

Rheological Response of Polymer Melts to Small, Sinusoidally Varying Shear Deformations, $\gamma(\omega, t) = \gamma_0 \sin \omega t$

The shear rate field that results from such cyclic deformation is

$$\frac{d\gamma}{dt} = \dot{\gamma}(\omega t) = \gamma_0 \omega \cos \omega t = \dot{\gamma}_0 \cos \omega t \quad (3.1-18)$$

The cyclic stress needed to support the imposed strain and flow field is experimentally found to be

$$\tau(\omega, t) = \tau_0' \sin \omega t + \tau_0'' \cos \omega t \quad (3.1-19)$$

The first term of the needed stress is *in phase* with the applied strain; it is, therefore, an *elastic* stress, since elastic materials respond to a stress only by deforming. The second term of Eq. 3.1-19, which is *out of phase* with the applied strain, is in phase with the shear rate, Eq. 3.1-18; it is, therefore, a *viscous* stress, since viscous fluids respond to a stress by flow, where flow is a time-increasing strain and its measure is shear rate (see Section 2.7). The conclusion from the response of polymer melts to small cyclic deformations, then, is that they are *viscoelastic* materials. Their viscous nature is due to the ability of polymer chain segments to *drag* past one another, while their elastic nature is due to the ability of stretched chain segments to *recoil*, thus restoring their coiled configurations, and acting as elastic springs.

An equivalent representation of Eq. 3.1-19, in terms of rheological functions, is

$$\tau(\omega, t) = \dot{\gamma}^0 \eta''(\omega) \sin \omega t + \dot{\gamma}^0 \eta'(\omega) \cos \omega t \quad (3.1-20)$$

where η' and η'' are components of the complex viscosity

$$\eta^*(\omega) = \eta' - i\eta'' \quad (3.1-21)$$

For Newtonian fluids, $\tau(\omega, t) = \mu \cos \omega t$, $\eta' = \mu$, and $\eta'' = 0$.

The viscoelastic response of polymer melts, that is, Eq. 3.1-19 or 3.1-20, become *nonlinear* beyond a level of strain γ_0 , specific to their macromolecular structure and the temperature used. Beyond this strain limit of linear viscoelastic response, η' , η'' , and η^* become functions of the applied strain. In other words, although the applied deformations are cyclic, large amplitudes take the macromolecular, coiled, and entangled structure far away from equilibrium. In the linear viscoelastic range, on the other hand, the frequency (and temperature) dependence of η' , η'' , and η^* is indicative of the specific macromolecular structure, responding to only small perturbations away from equilibrium. Thus, these dynamic rheological properties, as well as the commonly used dynamic moduli

$$G'(\omega) = \omega \eta'' \quad \text{and} \quad G''(\omega) = \omega \eta' \quad (3.1-22)$$

are widely used for the *characterization* of the macromolecular structure by both polymer scientists and engineers (7,8).

The dependence of η' , η'' , G' , and G'' on frequency reflects the ability of macromolecular systems to flow like Newtonian fluids if the experimental time allowed them, $t_{\text{exp}} = 1/\omega$, is very large compared to the time that they require to fully respond macromolecularly. This temperature-dependent, material-characteristic time is commonly called the *relaxation time*, λ , although it is actually a relaxation spectrum (7). Conversely, when t_{exp} is very short, that is, ω is very high compared to λ , the macromolecular system can only respond like an elastic solid, able only to undergo deformation and not flow. In

terms of the dimensionless *Deborah number*,⁴

$$\text{De} = \frac{\lambda}{t_{\text{exp}}} = \lambda\omega \quad (3.1-23)$$

Polymer melts act, qualitatively speaking, as *elastic solids* for $\text{De} \gg 1$, as *viscous liquids* for $\text{De} \ll 1$, and *viscoelastic materials* in the range in-between. Finally, since both (ω) and $(\dot{\gamma})$ represent rates of change of deformation, it is not surprising that both $\eta^*(\omega)$ and $\eta(\dot{\gamma})$ are rate dependent and shear thinning. As a matter of fact, $\eta^*(\omega)$, which can be evaluated experimentally to very low frequency ranges, as low as 10^{-2} s^{-1} , often forms an extension to $\eta(\dot{\gamma})$ obtained by capillary flow at higher shear rates, as high as 10^4 s^{-1} (9). Thus, the viscosity function can be obtained over six orders of magnitude of frequency/shear rate, yielding information on both molecular structure and processing. Dynamic simple shear-flow rheometers yield information on the first normal stress difference N_1 through the out-of-phase component of the complex viscosity η'' or its equivalent in-phase modulus $G' = \eta''\omega$. The experimentally determined function $2G'(\omega)$ tracks $N_1(\dot{\gamma}^2)$ determined from steady flow cone-and-plate experiments (10,11). Laun (12) suggested another empiricism relating G' and N_1 that fits the data over wider ranges of shear rate and frequencies given by

$$N_1 = \tau_{11} - \tau_{22} = 2G'\eta''(\omega) \left[1 + \left(\frac{\eta''}{\eta'} \right)^2 \right]^{0.7} \Bigg|_{\omega=\dot{\gamma}}$$

In summary, steady and dynamic simple shear rheometric results are complementary: at very low $(\dot{\gamma})$ or (ω) values they both yield useful macromolecular structure characterization. Moreover, $\eta^*(\omega)$ in the range $\omega < 10 \text{ s}^{-1}$ forms an extension of $\eta(\dot{\gamma})$ obtained by capillary rheometry at $\dot{\gamma} > 10 \text{ s}^{-1}$, a range that is relevant to processing.

Rheological Response of Polymer Melts in Steady, Uniform, Extensional Flows

Turning to Fig. 3.2, Case 1, we see that the tensile force F_1 needed to sustain the applied constant extensional rate $\dot{\epsilon}$, either levels off to a constant $F_1(\dot{\epsilon})$ or exhibits strain hardening increasing with time, occasionally in an unbounded fashion; the force is then represented as $F^+(\dot{\epsilon}, t)$. For this uniform extensional flow

$$\frac{F_1}{A} = \tau_{11} + P \quad (3.1-24)$$

where

$$-P = \tau_{22} = \tau_{33} \quad (3.1-25)$$

4. The dimensionless Deborah number was defined and coined by Prof. Marcus Reiner from the Technion–Israel Institute of Technology, and one of the fathers of rheology, in an after-dinner speech at the 4th International Congress on Rheology in Providence, Rhode Island. The Prophetess Deborah, said Marcus, “knew” rheology, because in her song [Judges 5:5] she says “The mountains flowed before the Lord” [הָרִים בָּזְלוּ מִפְּנֵי יְהוָה], so not only did she know that mountains, like everything else, flow but she knew that they flowed before the Lord and not before man for man has a too short lifespan to notice. The ratio of relaxation time to observation time clearly illuminates this point (*Phys. Today*, January 1964).

We define a material function $\bar{\eta}$, commonly called the *elongational* or *extensional viscosity*, through the primary normal stress difference $\tau_{11} - \tau_{22}$; thus, for the case of $F_1(\dot{\epsilon})$, it is given by

$$\bar{\eta}(\dot{\epsilon}) = -\frac{F_1/A}{\dot{\epsilon}} = -\left(\frac{\tau_{11}(\dot{\epsilon}) - \tau_{22}}{\dot{\epsilon}}\right) \quad (3.1-26)$$

and for $F_1^+(\dot{\epsilon}, t)$, the elongational viscosity is given by

$$\bar{\eta}^+(\dot{\epsilon}, t) = -\left(\frac{\tau_{11}(\dot{\epsilon}, t) - \tau_{22}}{\dot{\epsilon}}\right) \quad (3.1-27)$$

Experimentally, in both cases, we have

$$\bar{\eta}(\dot{\epsilon}) = \frac{-F_1(\dot{\epsilon})/A_1}{\dot{\epsilon}} \quad (3.1-28)$$

or

$$\bar{\eta}^+(\dot{\epsilon}, t) = \frac{-F_1(\dot{\epsilon}, t)/A_1}{\dot{\epsilon}} \quad (3.1-29)$$

For a Newtonian fluid in a simple elongational flow, the constitutive equation becomes

$$\boldsymbol{\tau} = -\mu\dot{\boldsymbol{\gamma}} = -\mu \begin{pmatrix} +2\dot{\epsilon} & 0 & 0 \\ 0 & -\dot{\epsilon} & 0 \\ 0 & 0 & -\dot{\epsilon} \end{pmatrix} \quad (3.1-30)$$

thus

$$\tau_{11} - \tau_{22} = -\mu(2\dot{\epsilon} + \dot{\epsilon}) = -3\mu\dot{\epsilon} \quad (3.1-31)$$

Combining Eqs. 3.1-31 and 3.1-26, we obtain the so-called Trouton relation, which defines the *Trouton viscosity* (13).

$$\bar{\eta} = 3\mu \quad (3.1-32)$$

For polymer melts where the low shear rate limiting viscosity value is η_0 , $\bar{\eta} = 3\eta_0$ (14). Examples of extensional viscosity growth, either to a steady $\bar{\eta}(\dot{\epsilon})$ value or to a strain-hardening-like mode, are shown in Fig. 3.6 for the linear nonbranched polystyrene (PS), a high density polyethylene (HDPE) that is only slightly branched with short branches, and a long chain-branched low density polyethylene (LDPE) (15).

We observe that strain-hardening stress and viscosity growth are associated with long chain branching. Long chain branching is a chain structural feature that impedes large macromolecular rearrangements of flow motions because it creates *entanglements*. With this in mind, and the fact that in steady uniform extensional flow, the length is increased *exponentially* to maintain $\dot{\epsilon} = \text{const}$, it is not surprising that even at $\dot{\epsilon} = 10^{-2} \text{ s}^{-1}$, the extensional viscosity still exhibits strain hardening. The Deborah number $\text{De} = \lambda 10^{-2}$ is still larger than unity for LDPE, denoting very long relaxation times $\lambda > 100 \text{ s}$. Similar

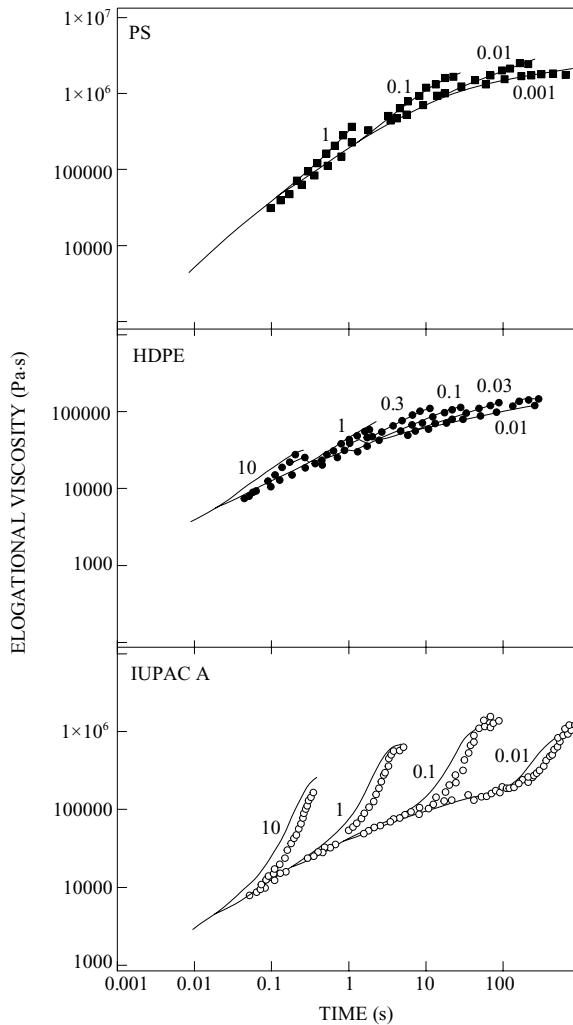


Fig. 3.6 Extensional growth viscosity versus time for polystyrene (top), HDPE, and LDPE. [S. A. Khan, R. K. Prud'homme, and R. G. Larson, *Rheol. Acta*, **26**, 144 (1987).]

results with LDPE are obtained for both the equibiaxial and planar extensional flows, as shown in Fig. 3.7.

Turning to Fig. 3.2, Case 4, we note that the extensional flows encountered by fibers, films, and tubes in *fiber spinning*, *film blowing*, and *stretch blow molding* are not uniform; the strand/film varies in thickness in the stretching direction(s). This extensional flow rheometry once again involves simpler flow, and the rheological results obtained are used to analyze or interpret more complicated, nonuniform, post-die forming flows.

Finally, it is worth discussing briefly the *flow singularity* at the exit corner of pressure-flow dies used for forming fibers and film, which are consequently stretched to orient and structure them. At that location we have to reconcile the fact that the wall melt flow layer must, in nearly zero distance, accelerate from a zero to a finite velocity. Irrespective of the details of this high acceleration, the surface layer undergoes high extensional rate flows,

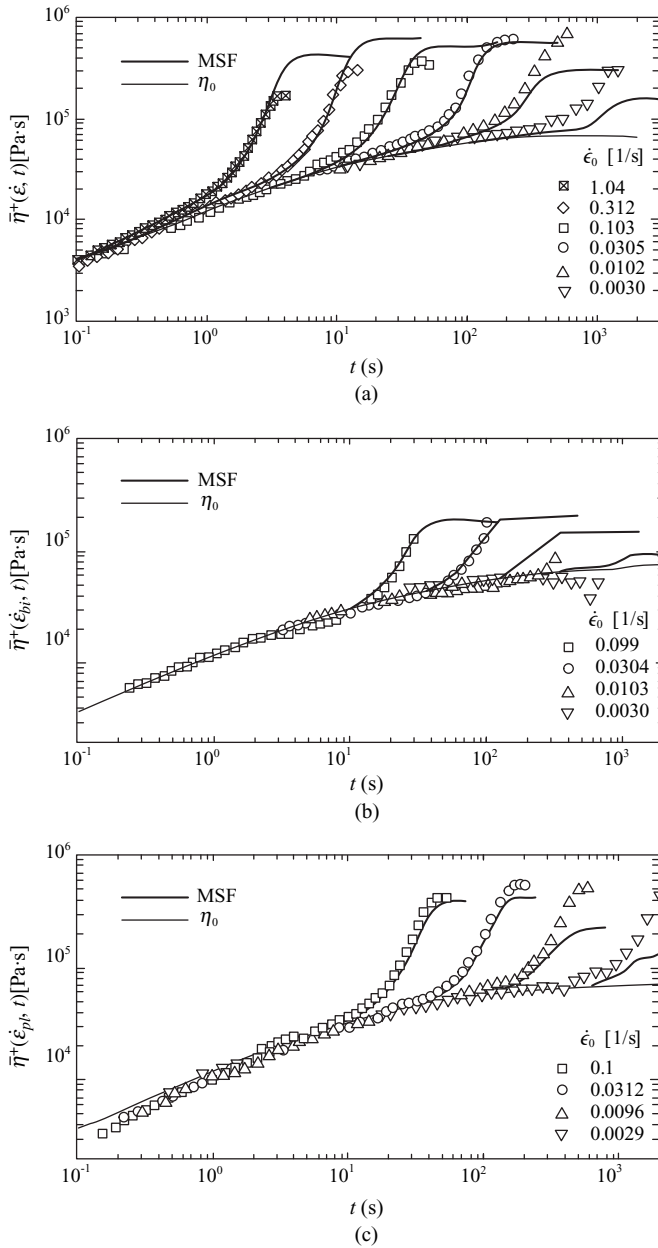


Fig. 3.7 (a) Uniaxial, (b) equibiaxial, and (c) planar extensional viscosities for a LDPE melt. [Data from P. Hachmann, Ph.D. Dissertation, ETH, Zurich (1996).] Solid lines are predictions of the molecular stress function model constitutive equation by Wagner et al. (65,66) to be discussed in Section 3.4.

and consequently, is exposed to potentially very high extensional stresses. Local crack development can occur at critical stresses equal to those needed to rupture the melt, due to its inability to disentangle, thus acting as a fracturing solid. Such phenomena may be the cause of the “shark-skin” (16–19) melt fracture, which is discussed in Chapter 12.

3.2 EXPERIMENTAL DETERMINATION OF THE VISCOSITY AND NORMAL STRESS DIFFERENCE COEFFICIENTS

This section describes two common experimental methods for evaluating η , Ψ_1 , and Ψ_2 as functions of shear rate. The experiments involved are the steady capillary and the cone-and-plate viscometric flows. As noted in the previous section, in the former, only the steady shear viscosity function can be determined for shear rates greater than unity, while in the latter, all three viscometric functions can be determined, but only at very low shear rates. Capillary shear viscosity measurements are much better developed and understood, and certainly much more widely used for the analysis of polymer processing flows, than normal stress difference measurements. It must be emphasized that the results obtained by both viscometric experiments are independent of any constitutive equation. In fact, one reason to conduct viscometric experiments is to test the validity of any given constitutive equation, and clearly the same constitutive equation parameters have to fit the experimental results obtained with *all* viscometric flows.

Example 3.1 Capillary Flow Rheometry The experimental setup used in capillary viscometry is shown schematically in Fig. 3.1, Case 3. Care is taken to have a uniform temperature and to eliminate the piston frictional effects in the reservoir. Either constant pressure or constant flow rate experiments are conducted, depending on the available instrument. At very slow flow rates, with shear rates below 1 s^{-1} , the surface tension of the emerging extrudate, gravity, and the frictional forces between the piston and the reservoir cannot be neglected; thus, the viscosity values obtained in this range are usually too high. A capillary viscometer yields viscosity data up to shear rates, where the phenomenon of melt fracture occurs (see Chapter 12). At high shear rates, the danger of having a high level of viscous dissipation of energy, and thus nonisothermal flow, as pointed out earlier, is very real.

The starting point of our analysis is the z -component momentum equation

$$\frac{dP}{dz} = -\frac{1}{r} \frac{d}{dr}(\tau_{rz}) \quad (\text{E3.1-1})$$

which is valid for all incompressible fluids and is subject to the assumptions of steady and isothermal flow. Integrating Eq. E 3.1-1, we obtain

$$\tau_{rz} = \tau_w \left(\frac{r}{R} \right) \quad (\text{E3.1-2})$$

where τ_w is the shear stress at the “wall” ($r = R$) given by

$$\tau_w = \left(\frac{P_0 - P_L}{2L} \right) R \quad (\text{E3.1-3})$$

The shear stress at the wall τ_w can be experimentally evaluated by measuring R , L , and $P_0 = P_L$.

By assuming only that the polymer melt is viscous and time independent, and that the viscosity is a function of the shear rate, $\eta(\dot{\gamma})$, without the need to specify any specific viscosity function, we can state that for capillary flow at the wall,

$$\tau_w = -\eta \dot{\gamma}_{rz} \big|_R = \eta \dot{\gamma}_w \quad (\text{E3.1-4})$$

where $\dot{\gamma}_w$ is the shear rate at the wall.

Having the shear stress at the wall from Eq. E3.1-3 as a function of pressure drop, Eq. E3.1-4 suggests that if in some way the shear rate at the wall, $\dot{\gamma}_w$, could be evaluated experimentally from the flow rate at the corresponding pressure drops, the viscosity function could be determined. This is indeed possible because of the volumetric flow rate Q , which can be expressed independently of any constitutive equation as follows

$$Q = 2\pi \int_0^R r v_z(r) dr = 2\pi \left[\left(\frac{r^2 v_z(r)}{2} \right) \Big|_0^R - \int_0^R \frac{r^2}{2} dv_z \right] \quad (\text{E3.1-5})$$

Assuming no slip at the wall of the capillary, we note that the first term on the right-hand side of Eq. E3.1-5 is zero and it becomes

$$Q = -\pi \int_0^R r^2 \left(\frac{dv_z}{dr} \right) dr \quad (\text{E3.1-6})$$

From Eq. E3.1-2, $r = \tau_{yz}R/\tau_w$, a relationship that can be utilized to change the integration variable in Eq. E3.1-6, to obtain the following equation

$$Q = \frac{-\pi R^3}{\tau_w^3} \int_0^{\tau_w} \left(\frac{dv_z}{dr} \right) \tau_{rz}^2 d\tau_{rz} \quad (\text{E3.1-7})$$

Next, Eq. E3.1-7 is differentiated (20) with respect to τ_w using the Leibnitz formula of differentiating an integral⁵ to give

$$\frac{1}{\pi R^3} \left[\tau_w^3 \frac{dQ}{d\tau_w} + 3\tau_w^2 Q \right] = -\tau_w^2 \left(\frac{dv_z}{dr} \right)_{r=R} = \dot{\gamma}_w \tau_w^2 \quad (\text{E3.1-8})$$

Equation E3.1-8 indicates that we can obtain the desired shear rate at the wall if we know the flow rate corresponding to the particular shear stress at the wall and the *change* in flow rate (i.e., the slope of the flow-rate function) at that point. Equation E3.1-8 with Eq. E3.1-3 can be written as

$$\dot{\gamma}_w = -\frac{1}{\pi R^3} \left[3Q + \Delta P \frac{dQ}{d(\Delta P)} \right] \quad (\text{E3.1-9})$$

Finally, we can rewrite Eq. E3.1-9 as

$$\dot{\gamma}_w = \frac{3\Gamma_w}{4} + \frac{\tau_w}{4} \frac{d\Gamma_w}{d\tau_w} \quad (\text{E3.1-10})$$

where Γ is the *Newtonian* shear rate at the wall

$$\Gamma_w = \frac{4Q}{\pi R^3} \quad (\text{E3.1-11})$$

5. The Leibnitz formula:

$$\frac{d}{dx} \int_{a_1(x)}^{a_2(x)} f(s, x) ds = \int_{a_1(x)}^{a_2(x)} \frac{\partial f}{\partial z} ds + \left[f(a_2, x) \frac{da_2}{dx} - f(a_1, x) \frac{da_1}{dx} \right]$$

Either Eq. E3.1-9 or Eq. E3.1-10, known as the “Rabinowitsch” or “Weissenberg–Rabinowitsch” equations, can be used to determine the shear rate at the wall $\dot{\gamma}_w$ by measuring Q and ΔP or τ_w and Γ_w (21). Thus, in Eq. E3.1-4 both τ_w and $\dot{\gamma}_w$ can be experimentally measured for *any* fluid having a shear rate–dependent viscosity as long as it does not slip at the capillary wall. Therefore, the viscosity function can be obtained.

Experimentally, it is found that for polymer melts $\dot{\gamma}_w \geq \Gamma_w$, with the inequality, as noted in Section 3.1, becoming more pronounced at higher shear rates.

Finally, because the results obtained in capillary viscometry, especially for capillaries of small L/R , are influenced by both extensional and shear flow phenomena associated with the fluid spatial accelerations at the capillary entrance, it is necessary to correct the values of τ_w given in Eq. E3.1-3. Chapter 13 covers the nature, magnitude, and significance of these, commonly known as “Bagley” corrections.

The Rabinowitsch equation has been used in the long capillary viscometry data found in Appendix A. Figure E3.1 shows long capillary τ_w vs. Γ_w and τ_w vs. $\dot{\gamma}_w$ results with and without the Rabinowitsch correction.

Example 3.2 Cone-and-Plate Flow Rheometry The cone-and-plate flow apparatus is shown schematically in Fig. E3.2a. The polymer melt flows in the space formed by the rotating cone and stationary plate.

The experimentally measured quantities are:

1. The cone rotational frequency Ω
2. The resulting torque needed to turn the cone \mathcal{J}
3. The total force normal to the fixed plate (thrust) F_N .
4. The pressure distribution on the fixed plate as a function of r :

$$\pi_{\theta\theta}(r)|_{\theta=\pi/2} = P + \tau_{\theta\theta}(r)|_{\theta=\pi/2} \tag{E3.2-1}$$

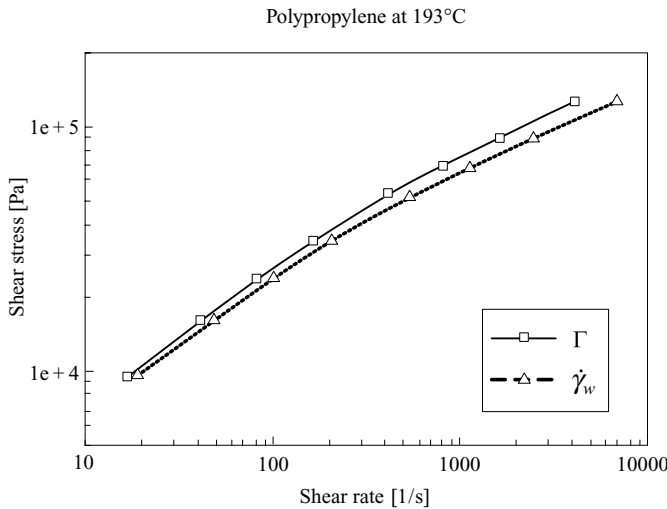


Fig. E3.1 Shear stress vs. shear rate with and without Rabinowitsch correction. [Courtesy of V. Tan, Polymer Processing Institute (PPI), Newark, NJ.]

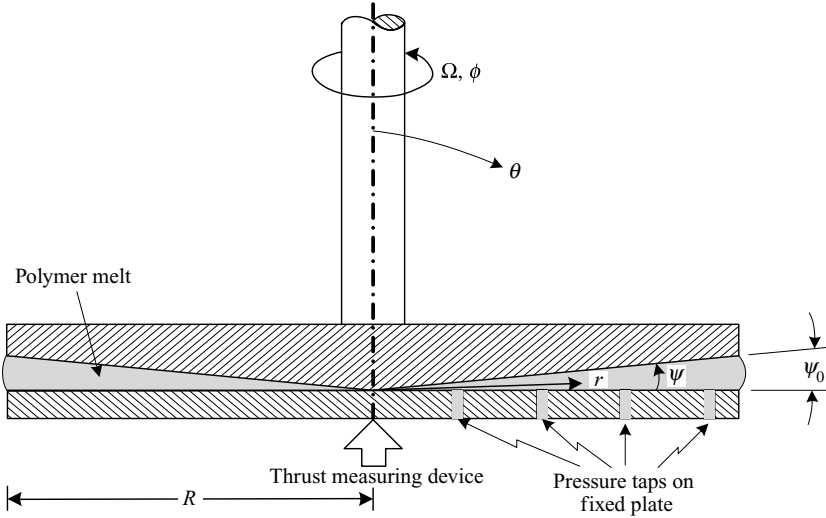


Fig. E3.2a Schematic representation of the cone and plate viscometer.

We note that with the cone-and-plate rheometers, fracture of the polymer melt is observed at shear rates exceeding 10^{-2} or 10^{-1} s^{-1} . Fracture is initiated at the melt-air interface at the perimeter. This has been attributed to the fact that the elastic energy becomes greater than the energy required to fracture the polymer melt at those shear rates (22). Irrespective of the origin of the fracture, it limits the operation of the cone-and-plate instrument to below the previously mentioned shear rates.

The velocity field between the cone and the plate is “visualized” as that of liquid cones described by θ -constant planes, rotating rigidly about the cone axis with an angular velocity that increases from zero at the stationary plate to Ω at the rotating cone surface (23). The resulting flow is a unidirectional shear flow. Moreover, because of the very small ψ_0 (about $1^\circ - 4^\circ$), *locally* (at fixed r) the flow can be considered to be like a torsional flow between parallel plates (i.e., the liquid cones become disks). Thus

$$v_\phi = \Omega r \frac{z}{z_0} \quad (\text{E3.2-2})$$

where z and z_0 can be expressed in terms of the angle $\psi = \pi/2 - \theta$

$$z = r \sin \psi \equiv \psi \quad (\text{E3.2-3})$$

and

$$z_0 = r \sin \psi_0 \equiv r\psi_0 \quad (\text{E3.2-4})$$

Inserting Eqs. E3.2-3 and E3.2-4 into Eq. E3.2-2, the following velocity profile is obtained

$$v_\phi = \Omega r \left(\frac{\psi}{\psi_0} \right) \quad (\text{E3.2-5})$$

Accordingly, the only nonvanishing component of the rate of deformation tensor is $\dot{\gamma}_{\theta\phi} = \dot{\gamma}_{\phi\theta} = (1/r)(\partial v_\phi / \partial \theta)$, and from Eq. E3.2-5 we obtain

$$\dot{\gamma}_{\theta\phi} = -\frac{\Omega}{\psi_0} = \text{constant} \quad (\text{E3.2-6})$$

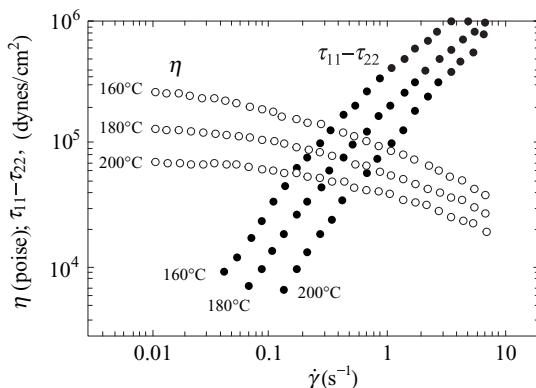


Fig. E3.2b The viscosity η and first (primary) normal stress difference $\tau_{11} - \tau_{22}$ of LDPE evaluated using the Weissenberg rheogoniometer (cone and plate). LDPE is Tenite 800 of density 0.918 g/cm^3 , and $\bar{M}_n = 25,800$. [Reprinted with permission from I. Chen and D. C. Bogue, *Trans. Soc. Rheol.*, **16**, 59 (1972).]

The preceding relationship establishes that the cone-and-plate flow is viscometric, where ϕ is direction 1, that is, the direction of motion, θ is direction 2, that is, the direction in which the velocity changes, and r is direction 3, that is, the neutral direction. Furthermore, the flow field is such that shear rate is constant in the entire flow field, as it is in the flow between parallel plates.

The torque on the shaft of the cone is due to the action of the shear stress $\tau_{\theta\phi}$ on its surface

$$\mathcal{J} = 2\pi \int_0^R (r\tau_{\theta\phi}) r dr \quad (\text{E3.2-7})$$

where $\tau_{\theta\phi}$ is constant, since $\dot{\gamma}_{\theta\phi}$ is constant throughout the flow field. Upon integration, we obtain

$$\tau_{\theta\phi} = \frac{\mathcal{J}}{\left(\frac{2}{3}\pi R^3\right)} \quad (\text{E3.2-8})$$

This expression suffices to determine experimentally the shear stress. Having evaluated both $\tau_{\theta\phi}$ and $\dot{\gamma}_{\theta\phi}$, we can readily obtain the viscosity function $\eta(\dot{\gamma}_{\theta\phi})$. Figure E3.2b gives such data for low-density polyethylene. The data extend beyond the commonly accepted upper limit of shear rate for polymer melts, probably because of the low average molecular weight of the polymer.

To obtain experimental information on normal stresses, we employ and mathematically manipulate the r component of the equation of momentum, which (neglecting centrifugal forces) is

$$-\frac{\partial P}{\partial r} - \frac{1}{r^2} \frac{\partial}{\partial r} (r^2 \tau_{rr}) + \frac{\tau_{\theta\theta} + \tau_{\phi\phi}}{r} = 0 \quad (\text{E3.2-9})$$

Introducing $\pi_{ii} = \tau_{ii} + P$ (no sum)

$$\frac{\pi_{\theta\theta} + \pi_{\phi\phi}}{r} - \frac{1}{r^2} \frac{\partial}{\partial r} (r^2 \pi_{rr}) = 0 \quad (\text{E3.2-10})$$

Upon rearrangement and integration, and taking into account that the negative of the secondary normal stress difference, $\pi_{rr} - \pi_{\theta\theta}$, is a constant (since $\dot{\gamma}_{\theta\phi}$ is constant), and that π_{θ} at $\theta = \pi/2$ (the plate) is a function of the radius, we have

$$[\pi_{\theta\theta}(r) - \pi_{\theta\theta}(R)]_{\theta=\pi/2} = [(\tau_{\phi\phi} - \tau_{\theta\theta}) + 2(\tau_{\theta\theta} - \tau_{rr})] \ln\left(\frac{r}{R}\right) \quad (\text{E3.2-11})$$

The left-hand side of Eq. E3.2-11 can be experimentally evaluated; thus, the quantity in brackets on the right-hand side can be determined.

The normal force on the stationary plate can be expressed as

$$F_N = 2\pi \int_0^R \pi_{\theta\theta} r \, dr - \pi R^2 P_{atm} \quad (\text{E3.2-12})$$

With the help of Eq. E3.2-11 and the relation $P_{atm} = \pi_{rr}(R)$, we obtain, after integration of Eq. E3.2-12, the simple relation for the primary normal stress difference function

$$\tau_{11} - \tau_{22} = \tau_{\phi\phi} - \tau_{\theta\theta} = \frac{-2F_N}{\pi R^2} \quad (\text{E3.2-13})$$

Figure E3.2b shows experimental data for the primary normal stress difference for LDPE.

In summary, and in terms of the viscometric flow notation, we conclude the following about the experimental capabilities of the cone-and-plate viscometric flow:

1. The viscosity function η can be determined with the aid of Eqs. E3.2-6 and E3.2-8.
2. The primary normal stress difference, $\tau_{11} - \tau_{22} = \tau_{\phi\phi} - \tau_{\theta\theta}$, can be calculated through Eq. E3.2-13, and the coefficient Ψ_1 can be calculated from Eq. 3.1-10.
3. The secondary normal stress difference, $\tau_{22} - \tau_{33} = \tau_{\theta\theta} - \tau_{rr}$, can be determined subsequent to the evaluation of $\tau_{11} - \tau_{22}$ using Eq. E3.2-11, and the coefficient Ψ_2 can be calculated from Eq. 3.1-11.

These conditions are subject to the limitation for polymer melts that the applied shear rate $\dot{\gamma} = \Omega/\psi_0$ must be below that which gives rise to fracture in the fluid sample. For solutions of polymers, the upper limit of shear rate (or Ω), however, is one at which the centrifugal forces become important.

Figure E3.2b presents the primary normal stress difference data for LDPE, and Fig. E3.2c presents the primary and secondary normal stress-difference data for a 2.5% polyacrylamide solution, again using a cone-and-plate rheometer.

We note that the primary normal stress coefficient Ψ_1 is positive, whereas the secondary normal stress coefficient Ψ_2 is negative, but with a lot of scatter in the data. It is difficult to measure $(\tau_{22} - \tau_{33})$ and its value is in doubt, but the ratio $-(\tau_{11} - \tau_{22})/(\tau_{22} - \tau_{33})$ appears to be about 0.1.

Bird et al. (24) pointed out a simple method of estimating the primary normal stress difference from viscosity data. The method is approximate, originating with the Goddard-Miller (G-M) (25) constitutive equation (Eq. 3.3-8), and it predicts that

$$\Psi_1(\dot{\gamma}) = \frac{4K}{\pi} \int_0^{\infty} \frac{\eta(\dot{\gamma}) - \eta(\dot{\gamma}')}{(\dot{\gamma}')^2 - \dot{\gamma}^2} d\dot{\gamma}' \quad (\text{3.2-1})$$

where K is an empirical constant. Good fit to data results are obtained, with K equaling about 2 for solutions and 3 for melts.

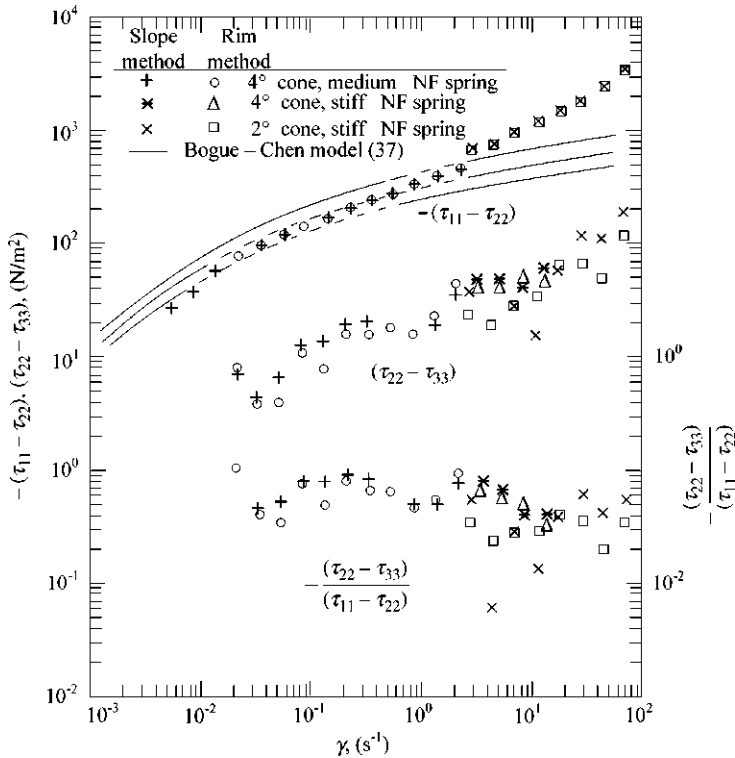


Fig. E3.2c Values for $-(\tau_{11} - \tau_{22})$, $(\tau_{22} - \tau_{33})$ and the ratio $-(\tau_{11} - \tau_{22})/(\tau_{22} - \tau_{33})$ for 2.5% acrylamide solution measured with a cone-and-plate rheometer. [Reprinted with permission from E. B. Christiansen and W. R. Leppard, *Trans. Soc. Rheol.*, **18**, 65 (1974).]

3.3 POLYMER MELT CONSTITUTIVE EQUATIONS BASED ON CONTINUUM MECHANICS

There is a multitude of constitutive equations proposed for polymer melts. However, only a few have been used to solve actual polymer processing problems. Nevertheless, we feel, as we did in the first edition of this book, that it is instructive to trace their origin and to indicate the interrelationship among them. We will do this quantitatively, but without dealing in detail with the mathematical complexities of the subject. The following three families of empirical equations will be discussed:

1. The *generalized Newtonian fluid models* (GNF), which are widely used in polymer processing flow analysis, since they are capable of describing well the very strong shear rate dependence of melts.
2. The *linear viscoelastic models* (LVE), which are widely used to describe the dynamic rheological response of polymer melts below the strain limit of the linear viscoelastic response of polymers. The results obtained are characteristic of and depend on the macromolecular structure. These are widely used as rheology-based structure characterization tools.

3. The *nonlinear viscoelastic models* (VE), which utilize continuum mechanics arguments to cast constitutive equations in coordinate frame-invariant form, thus enabling them to describe all flows: steady and dynamic shear as well as extensional. The objective of the polymer scientists researching these nonlinear VE empirical models is to develop constitutive equations that predict *all* the observed rheological phenomena.

Here we follow the systematic and clear classification and description of the constitutive equations of Bird et al. (14), and we refer the reader who is interested in the detailed development of the subject to that source. There is general agreement that, by and large, the constitutive equations for polymer melts and solutions are special cases of a very general constitutive relation, according to which the stress at any point in a flowing fluid and at any time depends on the entire flow history of the fluid element occupying that point. Because it does not depend on the flow history of adjacent elements, the dependence is “simple,” and the general relation is called the *simple fluid* constitutive equation (26).

One physical restriction, translated into a mathematical requirement, must be satisfied: that is that the simple fluid relation must be “objective,” which means that its predictions should not depend on whether the fluid rotates as a rigid body or deforms. This can be achieved by casting the constitutive equation (expressing its terms) in special frames. One is the *co-rotational* frame, which follows (translates with) each particle and rotates with it. The other is the *co-deformational* frame, which translates, rotates, and deforms with the flowing particles. In either frame, the observer is oblivious to rigid-body rotation. Thus, a constitutive equation cast in either frame is objective or, as it is commonly expressed, “obeys the principle of material objectivity”. Both can be transformed into fixed (laboratory) frame in which the balance equations appear and where experimental results are obtained. The transformations are similar to, but more complex than, those from the substantial frame to the fixed (see Chapter 2). Finally, a co-rotational constitutive equation can be transformed to a co-deformational one.

Goddard (27) expressed the notion of the simple fluid constitutive equation in a co-rotational integral series. The integral series expansion had been used in the co-deformational frame by Green and Rivlin (28) and Coleman and Noll (29). The co-rotational expansion takes the form:

$$\begin{aligned} \tau(x, t) = & - \int_{-\infty}^t G_1(t-t') \dot{\mathbf{\Gamma}}' dt' \\ & - \frac{1}{2} \int_{-\infty}^t \int_{-\infty}^t G_{11}(t-t', t-t'') [\dot{\mathbf{\Gamma}}' \cdot \dot{\mathbf{\Gamma}}'' + \dot{\mathbf{\Gamma}}'' \cdot \dot{\mathbf{\Gamma}}'] dt'' dt' - \dots \end{aligned} \tag{3.3-1}$$

where G_1, G_{11}, \dots are characteristic material functions, $\dot{\mathbf{\Gamma}}$ is the corotating rate of strain (velocity gradient) tensor, t', t'' are integration variables, and t is the present time. Equation 3.3-1 is in an unusable form. There are two alternative routes through which useful constitutive equations can be obtained:

1. Expand $\dot{\Gamma}$ in a Taylor series about $t' = t$

$$\dot{\Gamma}(t, t') = \dot{\gamma}(t) - (t - t') \frac{\mathcal{D}\dot{\gamma}}{\mathcal{D}t} + \dots \quad (3.3-2)$$

where

$$\frac{\mathcal{D}\dot{\gamma}}{\mathcal{D}t} = \frac{\partial\dot{\gamma}}{\partial t} + \{\mathbf{v} \cdot \nabla\dot{\gamma}\} + \frac{1}{2}(\{\boldsymbol{\omega} \cdot \dot{\gamma}\} - \{\dot{\gamma} \cdot \boldsymbol{\omega}\}) \quad (3.3-3)$$

is the co-rotational derivative or *Jaumann* derivative measuring the time rate of change of $\dot{\gamma}$ as measured by an observer who is translating and rotating with the local fluid velocity and vorticity. Keeping only the first two terms of the Taylor series (which means that the flow under consideration is *almost* steady), one can obtain the *second-order fluid* constitutive equation

$$\boldsymbol{\tau} = -\alpha_1 \dot{\gamma} + \alpha_2 \frac{\mathcal{D}\dot{\gamma}}{\mathcal{D}t} - \alpha_{11} \{\dot{\gamma} \cdot \dot{\gamma}\} - \dots \quad (3.3-4)$$

where α_i are constants related to G_1, G_{11}, \dots . For *steady shear flows*, the *Criminale–Ericksen–Filbey* (CEF) constitutive equation can be obtained (30):

$$\boldsymbol{\tau} = -\eta \dot{\gamma} - \left(\frac{1}{2} \Psi_1 + \Psi_2 \right) \{\dot{\gamma} \cdot \dot{\gamma}\} + \frac{1}{2} \Psi_1 \frac{\mathcal{D}\dot{\gamma}}{\mathcal{D}t} \quad (3.3-5)$$

where η, Ψ_1 , and Ψ_2 are the viscosity, first normal stress-difference coefficient, and second normal stress difference coefficient functions, respectively. They are all functions of the magnitude of the rate of strain tensor $\dot{\gamma} = \sqrt{(\dot{\gamma} : \dot{\gamma})}/2$. Because many polymer processing flows are steady shear flows, and because of the physical significance of the material functions η, Ψ_1 , and Ψ_2 , the CEF equation is considered in detail in Example 3.3.

If the normal stress coefficient functions Ψ_1 and Ψ_2 are ignored, the CEF equation reduces to the GNF equation

$$\boldsymbol{\tau} = -\eta \dot{\gamma} \quad (3.3-6)$$

This equation reduces for an incompressible *Newtonian fluid* to Newton's law, which in tensorial form is given by

$$\boldsymbol{\tau} = -\mu \dot{\gamma} \quad (3.3-7)$$

2. If, in Eq. 3.3-1 a single integral term is retained, the *Goddard–Miller* (G–M) constitutive equation is obtained (17, 25):

$$\boldsymbol{\tau} = - \int_{-\infty}^t G(t-t') \dot{\Gamma} dt' \quad (3.3-8)$$

For *small* deformation flows it is evident from Eqs. 3.3-2 and 3.3-3 that $\dot{\Gamma}$ equals $\dot{\gamma}$, thus the G–M equation yields the LVE fluid (14, 28, 29):

$$\boldsymbol{\tau} = - \int_{-\infty}^t G(t-t') \dot{\boldsymbol{\gamma}}(t') dt' \quad (3.3-8a)$$

where $G(t-t')$ is the *relaxation modulus*, which can take specific forms, depending on the LVE “mechanical model” used to simulate the real LVE behavior. For example, if a single Maxwell element, consisting of a “spring” G and a “dashpot” μ in a series is used, the *Maxwell* constitutive equation is obtained

$$\boldsymbol{\tau} + \lambda_0 d\boldsymbol{\tau}/dt = -\eta_0 \dot{\boldsymbol{\gamma}} \quad (3.3-9)$$

where $\lambda_0 = \eta_0/G$. When $\lambda_0 = 0$ ($G \rightarrow \infty$), the Newtonian constitutive equation for an incompressible fluid, Eq. 3.3-7, is obtained.

Including a velocity gradient in the time derivative, we obtain the *Jeffreys model* (31)

$$\boldsymbol{\tau} + \lambda_1 \frac{d}{dt} \boldsymbol{\tau} = -\eta_0 \left(\dot{\boldsymbol{\gamma}} + \lambda_2 \frac{d}{dt} \dot{\boldsymbol{\gamma}} \right) \quad (3.3-10)$$

From the G–M equation, while still in the co-rotational frame, we can choose a specific form of the relaxation modulus. Thus, for a single Maxwell element we can obtain

$$\boldsymbol{\tau} + \lambda_0 \frac{\mathcal{D}\boldsymbol{\tau}}{\mathcal{D}t} = -\eta_0 \dot{\boldsymbol{\gamma}} \quad (3.3-11)$$

This is called the *Zaremba-Fromm-DeWitt* (ZFD) equation.

As stated earlier, the simple fluid concept can be expressed in a series of co-deformational integrals (14, 28, 29)

$$\begin{aligned} \boldsymbol{\tau} = & - \int_{-\infty}^t G_1(t-t') \dot{\boldsymbol{\gamma}}^{[1]'} dt' \\ & - \frac{1}{2} \int_{-\infty}^t \int_{-\infty}^t G_2(t-t', t-t'') \left[\dot{\boldsymbol{\gamma}}^{[1]'} \cdot \dot{\boldsymbol{\gamma}}^{[1]''} + \dot{\boldsymbol{\gamma}}^{[1]''} \cdot \dot{\boldsymbol{\gamma}}^{[1]'} \right] dt'' dt' - \dots \end{aligned} \quad (3.3-12)$$

where G_1, G_2, \dots , are material functions and $\dot{\boldsymbol{\gamma}}^{[1]}$ is the co-deforming rate of strain tensor using covariant differentiation. If contravariant derivatives are used (14)

$$\begin{aligned} \boldsymbol{\tau} = & - \int G^1(t-t') \dot{\boldsymbol{\gamma}}_{[1]}' dt' \\ & - \frac{1}{2} \int_{-\infty}^t \int_{-\infty}^t G^2(t-t', t-t'') \left[\dot{\boldsymbol{\gamma}}_{[1]}' \cdot \dot{\boldsymbol{\gamma}}_{[1]}' + \dot{\boldsymbol{\gamma}}_{[1]}' \cdot \dot{\boldsymbol{\gamma}}_{[1]}' \right] dt'' dt' - \dots \end{aligned} \quad (3.3-13)$$

where G^1, G^2, \dots are material functions and $\dot{\boldsymbol{\gamma}}_{[1]}$ is the co-deforming rate of strain tensor using contravariant differentiation.

As was the case with Eq. 3.3-1, Eqs. 3.3-12 and 3.3-13 are also not usable in their current form. But the same means for making them usable are available (see Ref. 14: Fig. 9.6-1 and Table 9.4-1). Two specific steps to simplify the equation are as follows:

1. For *almost steady flows* one can expand $\dot{\gamma}^{[1]}$ or $\dot{\gamma}_{[1]}$ about $t = t'$ and obtain *second-order* fluid constitution equations in the co-deforming frame. When steady shear flows are considered, the CEF equation is obtained, which, in turn, reduces to the GNF equation for $\Psi_1 = \Psi_2 = 0$ and to a Newtonian equation if, additionally, the viscosity is constant.
2. Setting G_1, G_2, \dots , or G^1, G^2, \dots , equal to zero, Eqs. 3.3-11 and 3.3-12 reduce to G-M-type equations. For example,

$$\boldsymbol{\tau} = - \int_{-\infty}^t G(t-t') \dot{\gamma}_{[1]}' dt' \quad (3.3-14)$$

is the so-called *Oldroyd (32)–Walters (33)–Fredrickson (34)* equation. This equation, when integrated by parts, yields the *Lodge rubber-like liquid* equation (23)

$$\boldsymbol{\tau} = \int_{-\infty}^t M(t-t') \boldsymbol{\gamma}_{[0]}' dt' \quad (3.3-15)$$

where $M(t-t') = dG(t-t')/dt'$ and $\boldsymbol{\gamma}_{[0]}$ is the strain tensor in a co-deforming frame using contravariant differentiation.

For small deformations, Eq. 3.3-14 reduces to the LVE Eqs. 3.3-9 and 3.3-10 ($\dot{\gamma}_{[1]}' = \dot{\gamma}$). On the other hand, for large deformations, while still in the co-deforming frame, one can use a particular linear viscoelastic model to represent $G(t-t')$ in Eq. 3.3-14. If, as before, a single Maxwell element is used, one can obtain the following analog to Eq. 3.3-11

$$\boldsymbol{\tau} + \lambda_0 \boldsymbol{\tau}_{(1)} = -\eta_0 \dot{\boldsymbol{\gamma}} \quad (3.3-16)$$

where $\boldsymbol{\tau}_{(1)}$ is a co-deforming time derivative (14) equal to

$$\boldsymbol{\tau}_{(1)} = \frac{D}{Dt} \boldsymbol{\tau} - \left\{ (\nabla \mathbf{v})^\dagger \cdot \boldsymbol{\tau} + \boldsymbol{\tau} \cdot (\nabla \mathbf{v}) \right\} \quad (3.3-17)$$

Together with Eq. 3.3-17, Eq. 3.3-16 is the *White–Metzner* constitutive equation, which has been used frequently as a nonlinear viscoelastic model. Of course, for small deformations, $\boldsymbol{\tau}_{(1)} = d\boldsymbol{\tau}/dt$, and the single Maxwell fluid equation (Eq. 3.3-9) is obtained.

Finally, a number of commonly used constitutive equations are derived from Eq. 3.3-13 by specifying G^1, G^2, \dots instead of specifying only G^1 and setting G^2, \dots equal to zero. Moreover, in these equations, M_i are allowed to be functions of the invariants of the strain or rate-of-strain tensors, since there is experimental evidence supporting this dependence (35). Examples of such usable integral co-deformational constitutive equations are:

$$\boldsymbol{\tau} = + \int_{-\infty}^t \left[M_1(t-t', I_{\boldsymbol{\gamma}'_{[0]}}, II_{\boldsymbol{\gamma}'_{[0]}}) \boldsymbol{\gamma}_{[0]}' + M_2(t-t', I_{\boldsymbol{\gamma}'_{[0]}}, II_{\boldsymbol{\gamma}'_{[0]}}) \left\{ \boldsymbol{\gamma}_{[0]}' \cdot \boldsymbol{\gamma}_{[0]}' \right\} \right] dt' \quad (3.3-18)$$

which is the *Bernstein–Kearsley–Zappas* (BKZ) (36) constitutive equation, and

$$\boldsymbol{\tau} = + \int_{-\infty}^t M(t-t', II_{\dot{\boldsymbol{\gamma}}}(t)) \left[\left(1 + \frac{\epsilon}{2} \right) \boldsymbol{\gamma}_{[0]}' - \frac{\epsilon}{2} \boldsymbol{\gamma}_{[0]}'^2 \right] dt' \quad (3.3-19)$$

which is the *Bogue* or *Chen-Bogue* (37) and *Bird-Carreau* (38) constitutive equation, depending on the representation of the dependence of M on $II_{\dot{\gamma}}$; ε is a constant.

We have tried to give a quick glimpse of the interrelationships among some commonly used constitutive equations for polymer melts and solutions. None predicts quantitatively the entire spectrum of the rheological behavior of these materials. Some are better than others, becoming more powerful by utilizing more detailed and realistic molecular models. These, however, are more complex to use in connection with the equation of motion. Table 3.1 summarizes the predictive abilities of some of the foregoing, as well as other constitutive equations.

In examples 3.3, 3.4 and 3.5 we discuss three of the models listed above: the LVE, some members of the GNF family and the CEF; the first because it reveals the viscoelastic nature of polymer melts; the second because, in its various specific forms, it is widely used in polymer processing; and the third because of its ability to predict normal stress differences in steady shear flows.

Example 3.3 Small Amplitude Oscillatory Motion of a Linear Viscoelastic Body

We wish to derive the steady state response of a linear viscoelastic body to an externally applied sinusoidal shear strain (dynamic testing) using the constitutive Eq. 3.3-8, which for this viscometric flow reduces to

$$\tau(t) = - \int_{-\infty}^t G(t-t') \frac{d\gamma}{dt'} dt' \quad (\text{E3.3-1})$$

and

$$\frac{d\gamma}{dt'} = \gamma_0 \omega \cos \omega t' \quad (\text{E3.3-2})$$

Let the linear viscoelastic body be represented by a continuous spectrum of relaxation times, that is,

$$G(t-t') = \int_{-\infty}^{+\infty} H(\ln \lambda) e^{-(t-t')/\lambda} d \ln \lambda \quad (\text{E3.3-3})$$

Substituting in the constitutive equation and integrating, we have

$$\begin{aligned} \tau(t) &= - \int_{-\infty}^t \left[\int_{-\infty}^{\infty} H(\ln \lambda) e^{-t/\lambda} e^{+t'/\lambda} d \ln \lambda \right] \gamma_0 \omega \cos \omega t' dt' \\ &= -\omega \gamma_0 \int_{-\infty}^{\infty} H(\ln \lambda) e^{-t/\lambda} \left[\int_{-\infty}^t e^{t'/\lambda} \cos \omega t' dt' \right] d \ln \lambda \\ &= -\gamma_0 \int_{-\infty}^{\infty} \frac{H(\ln \lambda)}{1 + \omega^2 \lambda^2} [\omega \lambda \cos \omega t + \omega^2 \lambda^2 \sin \omega t] d(\ln \lambda) \quad (\text{E3.3-4}) \\ &= -\gamma_0 \left[\int_{-\infty}^{\infty} \frac{H(\ln \lambda) \omega^2 \lambda^2}{1 + \omega^2 \lambda^2} d(\ln \lambda) \right] \sin \omega t \\ &\quad - \gamma_0 \left[\int_{-\infty}^{\infty} \frac{H(\ln \lambda) \omega \lambda}{1 + \omega^2 \lambda^2} d(\ln \lambda) \right] \cos \omega t \end{aligned}$$

TABLE 3.1 Selected Constitutive Equations that Have Been Used for Polymer Melts, and Comments on Their Predictive Abilities^a

Equation	$\eta(\dot{\gamma})$	$\Psi_1(\dot{\gamma}), \Psi_2(\dot{\gamma})$	Stress Overshoot	VE Response
Newtonian fluid (3.3-7)	Constant	Zero	No	No
All GNF fluids (Section 3.3)	$\Psi(\dot{\gamma})$ fit depends on model	Zero	No	No
LVE fluids (3.3-8a)	Constant	Zero	No	Predicts small deformation <i>linear</i> response
G-M (3.3-8)	Good fit can be obtained	$\Psi_2 = -0.5\Psi_1; \Psi_i = f(\dot{\gamma})$ (3.2-1)	Yes; followed by spurious oscillations	Predicts nonlinear response in terms of $G(t-t')$ determined from LVE
ZFD (3.3-11)	Abrupt drop for single element; better fit for several λ_{0i}, η_{0i}	$\Psi_2 = -0.5\Psi_1; \Psi_i = f(\dot{\gamma})$	Yes, followed by spurious oscillations	Yes. The pairs $\eta(\dot{\gamma}), \eta'(\omega)$ and $\frac{1}{2}\Psi_1(\dot{\gamma}), \eta''(\omega)$ are identical; semiquantitatively correct
Second-order fluids (3.3-4)	Constant	Ψ_i are constant and related to each other	No	No
CEF fluids (3.3-5)	$\eta(\dot{\gamma})$ unspecified	$\Psi_i(\dot{\gamma})$ unspecified	No	No
Lodge rubberlike liquid (3.3-15)	Constant	$\Psi_1 = \text{constant}; \Psi_2 = 0$	No; predicts elongational stress growth $\eta^+(t, \dot{\epsilon})$	Yes
White-Metzner (3.3-16); (3.3-17)	Constant	$\Psi_1 = \text{constant}; \Psi_2 = 0$	No	Yes
BKZ (3.3-18)	Predicts $\eta(\dot{\gamma})$	$\Psi_1 = f(\dot{\gamma})$ and related to $\eta(\dot{\gamma})$; this relationship tests out semiquantitatively	Yes	Yes
Bogue (Bird-Carreau) (3.3-19)	Good fit; depends on model for M	Good fit; depends on model for M	Yes	Yes

^a For more details on the predictive abilities of the constitutive equations listed, see Ref. 14.

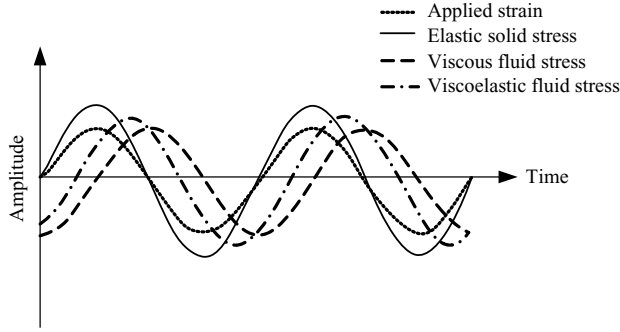


Fig. E3.3 The schematic stress response of elastic, a viscous, and a viscoelastic body to a sinusoidally applied strain.

Thus, according to the result just given, the response of a linear viscoelastic body to a sinusoidal strain (a) lags in time behind the applied strain, and (b) is composed of purely elastic and purely viscous parts. Figure E3.3 illustrates these features.

Furthermore, it is useful to define the following quantities associated with dynamic mechanical testing:

- (a) The in-phase or elastic dynamic modulus

$$G'(\omega) = \int_{-\infty}^{+\infty} \frac{H(\ln \lambda) \omega^2 \lambda^2}{1 + \omega^2 \lambda^2} d(\ln \lambda) \quad (\text{E3.3-5})$$

- (b) The out-of-phase or loss dynamic modulus

$$G''(\omega) = \int_{-\infty}^{+\infty} \frac{H(\ln \lambda) \omega \lambda}{1 + \omega^2 \lambda^2} d(\ln \lambda) \quad (\text{E3.3-6})$$

- (c) The loss tangent or dissipation factor; the ratio of the mechanical energy dissipated to that stored per cycle

$$\tan \delta = \frac{G''}{G'} \quad (\text{E3.3-7})$$

Note that since in this case, the Deborah number, $De = \lambda\omega$, the moduli and the loss tangent, G' , G'' , $\tan \delta$, are *functions of the Deborah number*.

The moduli can be expressed in terms of the *discrete* spectrum of relaxation times given by

$$G(t - t') = \sum_{i=1}^{N_1} G_i e^{-(t-t')/\lambda_i} \quad (\text{E3.3-8})$$

as

$$G' = \sum_{i=1}^{N_1} \frac{G_i \omega \lambda_i^2}{1 + (\omega \lambda_i)^2} \quad (\text{E3.3-9})$$

and

$$G'' = \sum_{i=1}^{N_1} \frac{G_i \omega \lambda_i}{1 + (\omega \lambda_i)^2} \quad (\text{E3.3-10})$$

GNF-based Constitutive Equations

As was pointed out before, the GNF is the generic expression for a whole family of empirical, semiempirical, or molecular model-based equations that were proposed to account for the non-Newtonian, shear-thinning behavior of polymer melts that take the form

$$\boldsymbol{\tau} = -\eta\dot{\boldsymbol{\gamma}} \quad (3.3-20)$$

GNF-based constitutive equations differ in the specific form that the shear rate dependence of the viscosity, $\eta(\dot{\boldsymbol{\gamma}})$, is expressed, but they all share the requirement that the non-Newtonian viscosity $\eta(\dot{\boldsymbol{\gamma}})$ be a function of only the three scalar invariants of the rate of strain tensor. Since polymer melts are essentially incompressible, the first invariant, $I_{\dot{\boldsymbol{\gamma}}} = 0$, and for steady shear flows since $v_1 = f(x_2)$, and $v_2 = v_3 = 0$ the third invariant, $III_{\dot{\boldsymbol{\gamma}}} = 0$, and therefore the non-Newtonian viscosity can only be a function of the second invariant $\eta(\dot{\boldsymbol{\gamma}}) = f(II_{\dot{\boldsymbol{\gamma}}})$. In practice, this functionality is expressed via the *magnitude* of $\dot{\boldsymbol{\gamma}}$, and is given by

$$\dot{\boldsymbol{\gamma}} = \sqrt{\frac{1}{2}II_{\dot{\boldsymbol{\gamma}}}} \quad (3.3-21)$$

For viscometric flows, $II_{\dot{\boldsymbol{\gamma}}} = 2\dot{\gamma}_{12}^2$, and thus the magnitude of $\dot{\boldsymbol{\gamma}}$ is $\dot{\boldsymbol{\gamma}} = |\dot{\gamma}_{12}|$, or the absolute value of the shear rate.

There are numerous fluid models or empirical constitutive equations that comply with the GNF fluid assumptions that were proposed in the literature. They vary in form and in the number of parameters that have to be determined by fitting them to experimental results. Rheological flow curves of non-Newtonian fluids and polymer melts generally exhibit a Newtonian range in the low shear rate range, followed by a broad range of shear-thinning viscosity, and ending in an upper Newtonian range (though the upper range is hardly relevant to polymer melts because of excessive heat generation and the possibility of degradation in this range). These empirical equations have two uses: the primary use is to insert them into the equation of motion to obtain an analytical solution to real processing flow problems. The more complex the empirical model is, the more difficult it is to reach analytical solutions, but even the simplest one converts the equation of motion into a nonlinear set of differential equations as compared to the linear Newtonian equivalent. The second use is to record in a simple way (with the minimum number of required parameters) the experimentally obtained results. This use simply converts a table of results to an algebraic equation. For numerical solutions, such as finite-element methods (FEM), having a more complex empirical equation does not add to the mathematical complexity of the solution. We now review a few of the commonly used empirical equations with an increasing number of parameters.

The Power Law Model

The Power Law model (excluding temperature dependence) is a two-parameter empirical model proposed by Ostwald and de Waele (39). It is based on the experimental observation that by plotting $\ln \eta(\dot{\boldsymbol{\gamma}})$ vs. $\ln(\dot{\boldsymbol{\gamma}})$, a straight line is obtained in the high shear rate region for

many non-Newtonian fluids, including most polymer melts. This suggests the following functional relationship between non-Newtonian viscosity and shear rate

$$\eta(\dot{\gamma}) = m\dot{\gamma}^{n-1} \quad (3.3-22)$$

where $m(\text{Ns}^n/\text{m}^2)$ and the dimensionless n are parameters, commonly called the consistency and Power Law index, respectively. Thus a Power Law constitutive equation can be arrived at:

$$\boldsymbol{\tau} = -m\dot{\gamma}^{n-1} \dot{\boldsymbol{\gamma}} = -m \left[\sqrt{\frac{1}{2}(\dot{\boldsymbol{\gamma}} : \dot{\boldsymbol{\gamma}})} \right]^{n-1} \dot{\boldsymbol{\gamma}} \quad (3.3-23)$$

The parameter m is a sensitive function of temperature, obeying an Arrhenius-type relationship

$$m = m_0 \exp \left[\frac{\Delta E}{R} \left(\frac{1}{T} - \frac{1}{T_0} \right) \right] \quad (3.3-24)$$

where m_0 is the value of m at T_0 , and ΔE is the flow activation energy. For mathematical convenience, a simpler relationship is frequently used

$$m = m_0 e^{-a(T-T_0)} \quad (3.3-25)$$

where a is an empirical parameter. Equation 3.3-25 holds well over relatively narrow temperature ranges.

The following comments can be made about the Power Law equation and the viscosity or “flow curve,” as, for example, that shown in Fig. 3.5:

- The upper limit of the Newtonian plateau is dependent on \overline{M}_w and the melt temperature. Commonly, it is roughly in the region $\dot{\gamma} = 10^{-2} \text{s}^{-1}$. Low viscosity fiber-forming Nylon and polyethylene terephthalate (PET) are important exceptions, as their Newtonian plateau extends to higher shear rates.
- This upper limit decreases with increasing \overline{M}_w , with increasing molecular weight distribution (MWD) at constant \overline{M}_w , and with decreasing melt temperature. On physical grounds, it is considered to terminate roughly where the Deborah number reaches unity.
- If the Power Law equation is used in pressure flows, where $0 \leq \dot{\gamma} \leq \dot{\gamma}_{\max}$, an error is introduced in the very low shear rate Newtonian region. In flow rate computation, however, this is not a very significant (40).
- The transition from the Newtonian plateau to the Power Law region is sharp for monodispersed polymer melts and broad for polydispersed melts (see Fig. 3.5).
- The slope of the viscosity curve in the Power Law region is not exactly constant. The flow index n decreases with increasing shear rate. Thus the Power Law equation holds exactly only for limited ranges of shear rate, for a given value of n .

In conclusion, despite its limitations, the Power Law model is one of the most widely used empirical relations in polymer fluid dynamics, and it gives surprisingly good results, even for nonviscometric and slightly transient flows.

The Ellis Model

The Ellis model (41), is a three-parameter model, in which the non-Newtonian viscosity is a function of the absolute value of the shear stress tensor, τ ,

$$\eta(\tau) = \frac{\eta_0}{1 + (\tau/\tau_{1/2})^{\alpha-1}} \quad (3.3-26)$$

yielding the following constitutive equation

$$\boldsymbol{\tau} = -\eta(\tau)\dot{\boldsymbol{\gamma}} = -\left[\frac{\eta_0}{1 + (\tau/\tau_{1/2})^{\alpha-1}} \right] \dot{\boldsymbol{\gamma}} \quad (3.3-27)$$

where τ is related to the second invariant of the stress tensor as follows

$$\tau = \sqrt{\frac{1}{2} II_{\boldsymbol{\tau}}} \quad (3.3-28)$$

The three parameters are α , which is the slope of the curve $\log(\eta/\eta_0 - 1)$ vs. $\log(\tau/\tau_{1/2})$; $\tau_{1/2}$, which is the shear stress value, where $\eta = \eta_0/2$; and η_0 , which is the zero shear viscosity. Thus the Ellis model matches the low shear Newtonian plateau and the shear-thinning region.

The Cross Model

The Cross and the temperature-dependent Cross-WLF model (42) is an often used GNF-type model accounting for, like the Ellis and Carreau fluids for the viscosity at both low and high shear rates,

$$\eta(\dot{\gamma}, T, P) = \frac{\eta_0(T_1)}{1 + \left[\frac{\eta_0(T)}{\tau^*} \dot{\gamma} \right]^{n-1}} \quad (3.3-29)$$

where n denotes the Power Law index; τ^* the critical stress level at which η transitions from the Newtonian plateau, η_0 , to the Power Law regime; and $\dot{\gamma}$ is the shear rate. If an Arrhenius viscosity temperature dependence is assumed, then a shift factor a_T is defined as

$$\log a_T = \frac{\Delta E}{R} \left(\frac{1}{T_1} - \frac{1}{T_2} \right) \quad (3.3-30)$$

Given the value of the activation energy, ΔE , a master curve $\eta(T, \dot{\gamma})$ can be constructed, and Eq. 3.3-30 becomes

$$\eta = \left[\frac{\eta_0}{1 + \left(\frac{\eta_0}{\tau^*} \frac{\dot{\gamma}}{a_T} \right)^{1-n}} \right] \frac{1}{a_T} \quad (3.3-31)$$

This relation holds well for semicrystalline polymers; for amorphous polymers, it holds for $T > T_g + 100^\circ\text{C}$. Below this region free volume effects predominate necessitating the use of the Arrhenius–WLF equation

$$\log a_T = \frac{\Delta E}{R} \left(\frac{1}{T_1} - \frac{1}{T_2} \right) - b_1 \left(\frac{T_1 - T_2}{b_2 + T_2 - T_1} \right) \quad (3.3-32)$$

The parameters b_1 and b_2 have to be experimentally determined.

The Carreau Model

The Carreau model (43) is a four-parameter model that accounts for the both the low shear rate Newtonian region and the high shear rate upper Newtonian region that is expected (although polymer melts do not reach this region, because of excessive heating and degradation at these high shear rate values):

$$\frac{\eta(\dot{\gamma}) - \eta_\infty}{\eta_0 - \eta_\infty} = \frac{1}{\left[1 + (\lambda\dot{\gamma})^2 \right]^{(1-n)/2}} \quad (3.3-33)$$

where η_0 is the zero shear rate viscosity, η_∞ is the infinite shear-rate viscosity, λ is a parameter with units of (relaxation) time, and n is a dimensionless parameter. Note that the shear-thinning nature of melts is accounted for by the parameter n ($n < 1$), as was the case with the Power Law model. The product $\lambda\dot{\gamma} = \text{De}$ reflects the viscoelastic nature of the melt, which at low De number values $\text{De} \rightarrow 0$ become Newtonian. As De is increased, melts become less viscous and more elastic.

There are numerous other GNF models, such as the Casson model (used in food rheology), the Ellis, the Powell–Eyring model, and the Reiner–Phillippoff model. These are reviewed in the literature. In Appendix A we list the parameters of the Power Law, the Carreau, and the Cross constitutive equations for common polymers evaluated using oscillatory and capillary flow viscometry.

The Bingham Fluid

The Bingham fluid is a two-parameter, somewhat different model from the previous rheological models, in that it has a final yield stress below which there is no flow, whereas above it, the stress is a linear function of the rate of strain

$$\begin{aligned} \eta &= \infty & \tau &\leq \tau_y \\ \eta(\dot{\gamma}) &= \mu_0 + \left(\frac{\tau_y}{\dot{\gamma}} \right) & \tau &> \tau_y \end{aligned} \quad (3.3-34)$$

where τ_y is the yield stress, and μ_0 is the Newtonian viscosity for vanishing yield stress. A typical Bingham plastic fluid is ketchup, but many other fluids have this property, such as “no drip” paints, pastes, and slurries.

Example 3.4 Flow of a Power Law Fluid in Tubes For an isothermal, laminar, fully developed steady pressure flow of an incompressible Power Law model fluid in a horizontal tube without slip, we wish to derive (a) the velocity profile and (b) the flow rate.

(a) For a tubular flow we use the cylindrical coordinate system. Since flow is isothermal and the fluid incompressible, the equation of motion and continuity, together with the

constitutive equation, fully describe the flow. On the basis of symmetry, we assume that there is no θ dependence and that $v_\theta = 0$. Fully developed flow implies that $\partial v_z / \partial z = 0$, and hence the equation of continuity reduces to

$$\frac{\partial}{\partial r}(rv_r) \quad (\text{E3.4-1})$$

which can be integrated to give $rv_r = C$, where C is a constant. Since $v_r = 0$ at the tube radius, we conclude that $C = 0$, and therefore $v_r = 0$. Hence, the only nonvanishing velocity component is v_z , which is a function only of r . Turning to the equation of motion in Table 2.2, the three components of the equation therefore reduce to

$$\begin{aligned} \frac{\partial P}{\partial r} &= 0 \\ \frac{\partial P}{\partial \theta} &= 0 \\ \frac{\partial P}{\partial z} &= -\frac{1}{r} \frac{\partial}{\partial r}(r\tau_{rz}) \end{aligned} \quad (\text{E3.4-2})$$

Clearly, the left-hand side of the equation is a function only of z , since $P \neq f(r, \theta)$, whereas the right-hand side of the last equation is a function only of r ; therefore, they both must equal a constant, indicating that the pressure gradient is constant along the tube and that partial differentials can be replaced by ordinary differentials. Following integration, we get

$$\tau_{rz} = -\left(\frac{r}{2}\right) \frac{dP}{dz} + C_1 \quad (\text{E3.4-3})$$

where C_1 is an integration constant. The constant C_1 is zero, because at $r = 0$, where the velocity has a maximum and the gradient is zero, the shear stress must vanish as well. Thus the shear stress distribution is given by

$$\tau_{rz} = -\left(\frac{r}{2}\right) \frac{dP}{dz} \quad (\text{E3.4-4})$$

indicating that the shear stress increases linearly from a value of zero at the center to a maximum at the wall. The only nonvanishing velocity gradient in this flow is dv_z/dr , and therefore the rate of deformation tensor of Table 2.3 reduces to

$$\dot{\boldsymbol{\gamma}} = \begin{pmatrix} 0 & 0 & \frac{dv_z}{dr} \\ 0 & 0 & 0 \\ \frac{dv_z}{dr} & 0 & 0 \end{pmatrix} \quad (\text{E3.4-5})$$

and the Power Law constitutive equation reduces to

$$\tau_{rz} = -m\dot{\gamma}^{n-1} \frac{dv_z}{dr} \quad (\text{E3.4-6})$$

However, $\dot{\gamma}$ in Eq. E3.4-56 is obtained from Eq. E3.4-5 and given by

$$\dot{\gamma} = \sqrt{\frac{1}{2}(\dot{\boldsymbol{\gamma}} : \dot{\boldsymbol{\gamma}})} = \sqrt{\left(\frac{dv_z}{dr}\right)^2} = \left|\frac{dv_z}{dr}\right| \quad (\text{E3.4-7})$$

where the scalar product of the tensor $\dot{\boldsymbol{\gamma}}$ is $2(dv_z/dr)^2$. By substituting Eq. E3.4-7 into Eq. E3.4-6, we get

$$\tau_{rz} = -m \left| \frac{dv_z}{dr} \right|^{n-1} \frac{dv_z}{dr} \quad (\text{E3.4-8})$$

Note that shear rate $\dot{\gamma}$ is the magnitude of the tensor $\dot{\boldsymbol{\gamma}}$, and therefore it must always be positive. Thus we maintain the absolute-value sign over the term that reflects the shear dependence of the viscosity.

Combining Eq. E3.4-8 with Eq. E3.4-4 yields

$$m \left| \frac{dv_z}{dr} \right|^{n-1} \frac{dv_z}{dr} = \frac{r}{2} \left(\frac{dP}{dz} \right) \quad (\text{E3.4-9})$$

In tubular flow for all r , $dv_z/dr < 0$; therefore

$$\left| \frac{dv_z}{dr} \right| = -\frac{dv_z}{dr} \quad (\text{E3.4-10})$$

and Eq. E3.4-9 can be written as

$$-\frac{dv_z}{dr} = \left(-\frac{r}{2mL} \frac{dP}{dz} \right)^s \quad (\text{E3.4-11})$$

where $s = 1/n$. Note that the pressure gradient in the preceding equation is negative, and therefore the term in parenthesis is positive. This equation can be integrated with boundary condition $v_z(R) = 0$ to give

$$v_z(r) = \left(\frac{R}{s+1} \right) \left[-\frac{R}{2m} \frac{dP}{dz} \right]^s \left[1 - \left(\frac{r}{R} \right)^{s+1} \right] \quad (\text{E3.4-12})$$

For Newtonian fluids with $s = 1$, this equation reduces to the classic parabolic profile.

(b) The volumetric flow rate is obtained by integrating Eq. E3.4-12.

$$\begin{aligned} Q &= \int_0^R 2\pi r v_z dr = \frac{\pi R^3}{s+3} \left[-\frac{R}{2m} \frac{dP}{dz} \right]^s \\ &= \frac{\pi R^3}{s+3} \left[-\frac{R}{2m} \frac{\Delta P}{L} \right]^s \end{aligned} \quad (\text{E3.4-13})$$

where $\Delta P = P_0 - P_L$, P_0 is the pressure at $z = 0$, and P_L at $z = L$. Equation E3.4-13 is the Power Law equivalent to the celebrated Newtonian Hagen–Poiseuille equation, with $s = 1$ and $m = \mu$

$$Q = \frac{\pi R^4}{8\mu L} (P_0 - P_L) \quad (\text{E3.4-14})$$

Example 3.5 The CEF Equation in Steady, Fully Developed Flow in Tubes The viscosity functions in both the Power Law model GNF fluid and the CEF fluid are expected to be

the same. Therefore, assuming that the velocity field of a CEF fluid, in steady viscometric flow, will be the same as that of a purely viscous fluid, we can calculate the stress field needed to maintain such a flow. In this Example, we calculate the stress field needed to maintain the pressure-driven tube flow discussed in Example 3.4.

In Section 3.3 we discussed the origins of the CEF equation

$$\boldsymbol{\tau} = -\eta\dot{\boldsymbol{\gamma}} - \left(\frac{1}{2}\Psi_1 + \Psi_2\right)\{\dot{\boldsymbol{\gamma}} \cdot \dot{\boldsymbol{\gamma}}\} + \frac{1}{2}\Psi_1 \frac{\mathcal{D}\dot{\boldsymbol{\gamma}}}{\mathcal{D}t} \quad (\text{E3.5-1})$$

where the material functions η , Ψ_1 , and Ψ_2 are functions of shear rate, and they hold for steady shear flow and account for the shear-thinning viscosity and for normal stresses.

Our starting point is the rate-of-deformation tensor given in Eq. E3.4-5

$$\dot{\boldsymbol{\gamma}} = \begin{pmatrix} 0 & 0 & \dot{\gamma}_{rz} \\ 0 & 0 & 0 \\ \dot{\gamma}_{rz} & 0 & 0 \end{pmatrix} \quad (\text{E3.5-2})$$

To calculate the stresses generated by the CEF fluid, we need to calculate the quantities $\dot{\boldsymbol{\gamma}} \cdot \dot{\boldsymbol{\gamma}}$ and $\mathcal{D}\dot{\boldsymbol{\gamma}}/\mathcal{D}t$ in Eq. E3.5-1. The first one is a simple matrix multiplication, resulting in

$$\{\dot{\boldsymbol{\gamma}} \cdot \dot{\boldsymbol{\gamma}}\} = \begin{pmatrix} \dot{\gamma}_{rz}^2 & 0 & 0 \\ 0 & 0 & 0 \\ 0 & 0 & \dot{\gamma}_{rz}^2 \end{pmatrix} \quad (\text{E3.5-3})$$

Next we calculate

$$\frac{\mathcal{D}}{\mathcal{D}t}\dot{\boldsymbol{\gamma}} = \frac{\partial}{\partial t}\dot{\boldsymbol{\gamma}} + \{\mathbf{v} \cdot \nabla\}\dot{\boldsymbol{\gamma}} + \frac{1}{2}(\{\boldsymbol{\omega} \cdot \dot{\boldsymbol{\gamma}}\} - \{\dot{\boldsymbol{\gamma}} \cdot \boldsymbol{\omega}\}) \quad (\text{E3.5-4})$$

The first term on the right-hand side is zero because the flow is steady. The components of the second term, $\mathbf{v} \cdot \nabla\dot{\boldsymbol{\gamma}}$, we obtain from Table 3.2

$$\begin{aligned} (\mathbf{v} \cdot \nabla\dot{\boldsymbol{\gamma}})_{rz} &= (\mathbf{v} \cdot \nabla)\dot{\gamma}_{rz} - \frac{v_\theta}{r}\dot{\gamma}_{\theta z} \\ &= \left(v_r \frac{\partial}{\partial r} + \frac{v_\theta}{r} \frac{\partial}{\partial \theta} + v_z \frac{\partial}{\partial z}\right)\dot{\gamma}_{rz} - \frac{v_\theta}{r}\dot{\gamma}_{\theta z} \end{aligned} \quad (\text{E3.5-5})$$

Since $v_r = 0$, $v_\theta = 0$, and $\partial v_z/\partial z = 0$ for a developed flow, the term $(\mathbf{v} \cdot \nabla\dot{\boldsymbol{\gamma}})_{rz} = 0$. Similarly, we evaluate all other components and conclude that $\mathbf{v} \cdot \nabla\dot{\boldsymbol{\gamma}} = 0$. The vorticity tensor $\boldsymbol{\omega}$ can be obtained for this flow from Table 3.3

$$\boldsymbol{\omega} = \nabla\mathbf{v} - (\nabla\mathbf{v})^\dagger = \begin{pmatrix} 0 & 0 & \dot{\gamma}_{rz} \\ 0 & 0 & 0 \\ -\dot{\gamma}_{rz} & 0 & 0 \end{pmatrix} \quad (\text{E3.5-6})$$

Next, with Eqs. E.3.5-2 and E3.5-6 we derive

$$\{\boldsymbol{\omega} \cdot \dot{\boldsymbol{\gamma}}\} = \begin{pmatrix} 0 & 0 & \dot{\gamma}_{rz} \\ 0 & 0 & 0 \\ -\dot{\gamma}_{rz} & 0 & 0 \end{pmatrix} \begin{pmatrix} 0 & 0 & \dot{\gamma}_{rz} \\ 0 & 0 & 0 \\ \dot{\gamma}_{rz} & 0 & 0 \end{pmatrix} = \begin{pmatrix} \dot{\gamma}_{rz}^2 & 0 & 0 \\ 0 & 0 & 0 \\ 0 & 0 & -\dot{\gamma}_{rz}^2 \end{pmatrix} \quad (\text{E3.5-7})$$

TABLE 3.2 The Components of $(\mathbf{v} \cdot \nabla \dot{\boldsymbol{\gamma}})$ in Three Coordinate Systems

Rectangular Coordinates^a (x, y, z)

$$(\mathbf{v} \cdot \nabla \dot{\boldsymbol{\gamma}})_{xx} = (\mathbf{v} \cdot \nabla) \dot{\gamma}_{xx} \quad (\mathbf{v} \cdot \nabla \dot{\boldsymbol{\gamma}})_{xy} = (\mathbf{v} \cdot \nabla \dot{\boldsymbol{\gamma}})_{yx} = (\mathbf{v} \cdot \nabla) \dot{\gamma}_{xy}$$

$$(\mathbf{v} \cdot \nabla \dot{\boldsymbol{\gamma}})_{yy} = (\mathbf{v} \cdot \nabla) \dot{\gamma}_{yy} \quad (\mathbf{v} \cdot \nabla \dot{\boldsymbol{\gamma}})_{yz} = (\mathbf{v} \cdot \nabla \dot{\boldsymbol{\gamma}})_{zy} = (\mathbf{v} \cdot \nabla) \dot{\gamma}_{zy}$$

$$(\mathbf{v} \cdot \nabla \dot{\boldsymbol{\gamma}})_{zz} = (\mathbf{v} \cdot \nabla) \dot{\gamma}_{zz} \quad (\mathbf{v} \cdot \nabla \dot{\boldsymbol{\gamma}})_{zx} = (\mathbf{v} \cdot \nabla \dot{\boldsymbol{\gamma}})_{xz} = (\mathbf{v} \cdot \nabla) \dot{\gamma}_{xz}$$

Cylindrical Coordinates^b (r, θ, z)

$$(\mathbf{v} \cdot \nabla \dot{\boldsymbol{\gamma}})_{rr} = (\mathbf{v} \cdot \nabla) \dot{\gamma}_{rr} - \frac{v_\theta}{r} (\dot{\gamma}_{r\theta} + \dot{\gamma}_{\theta r})$$

$$(\mathbf{v} \cdot \nabla \dot{\boldsymbol{\gamma}})_{\theta\theta} = (\mathbf{v} \cdot \nabla) \dot{\gamma}_{\theta\theta} + \frac{v_\theta}{r} (\dot{\gamma}_{r\theta} + \dot{\gamma}_{\theta r})$$

$$(\mathbf{v} \cdot \nabla \dot{\boldsymbol{\gamma}})_{zz} = (\mathbf{v} \cdot \nabla) \dot{\gamma}_{zz}$$

$$(\mathbf{v} \cdot \nabla \dot{\boldsymbol{\gamma}})_{r\theta} = (\mathbf{v} \cdot \nabla \dot{\boldsymbol{\gamma}})_{\theta r} = (\mathbf{v} \cdot \nabla) \dot{\gamma}_{\theta r} + \frac{v_\theta}{r} (\dot{\gamma}_{rr} - \dot{\gamma}_{\theta\theta})$$

$$(\mathbf{v} \cdot \nabla \dot{\boldsymbol{\gamma}})_{\theta z} = (\mathbf{v} \cdot \nabla \dot{\boldsymbol{\gamma}})_{z\theta} = (\mathbf{v} \cdot \nabla) \dot{\gamma}_{\theta z} + \frac{v_\theta}{r} \dot{\gamma}_{rz}$$

$$(\mathbf{v} \cdot \nabla \dot{\boldsymbol{\gamma}})_{rz} = (\mathbf{v} \cdot \nabla \dot{\boldsymbol{\gamma}})_{zr} = (\mathbf{v} \cdot \nabla) \dot{\gamma}_{rz} - \frac{v_\theta}{r} \dot{\gamma}_{\theta z}$$

Spherical Coordinates^c (r, θ, ϕ)

$$(\mathbf{v} \cdot \nabla \dot{\boldsymbol{\gamma}})_{rr} = (\mathbf{v} \cdot \nabla) \dot{\gamma}_{rr} - \frac{2v_\theta}{r} \dot{\gamma}_{r\theta} - \frac{2v_\phi}{r} \dot{\gamma}_{r\phi}$$

$$(\mathbf{v} \cdot \nabla \dot{\boldsymbol{\gamma}})_{\theta\theta} = (\mathbf{v} \cdot \nabla) \dot{\gamma}_{\theta\theta} + \frac{2v_\theta}{r} \dot{\gamma}_{r\theta} - \frac{2v_\phi}{r} \dot{\gamma}_{\theta\phi} \cot \theta$$

$$(\mathbf{v} \cdot \nabla \dot{\boldsymbol{\gamma}})_{\phi\phi} = (\mathbf{v} \cdot \nabla) \dot{\gamma}_{\phi\phi} + \frac{2v_\phi}{r} \dot{\gamma}_{r\phi} + \frac{2v_\theta}{r} \dot{\gamma}_{\theta\phi} \cot \theta$$

$$(\mathbf{v} \cdot \nabla \dot{\boldsymbol{\gamma}})_{r\theta} = (\mathbf{v} \cdot \nabla \dot{\boldsymbol{\gamma}})_{\theta r} = (\mathbf{v} \cdot \nabla) \dot{\gamma}_{r\theta} + \frac{v_\theta}{r} (\dot{\gamma}_{rr} - \dot{\gamma}_{\theta\theta}) - \frac{v_\phi}{r} (\dot{\gamma}_{\phi\theta} + \dot{\gamma}_{r\phi} \cot \theta)$$

$$(\mathbf{v} \cdot \nabla \dot{\boldsymbol{\gamma}})_{r\phi} = (\mathbf{v} \cdot \nabla \dot{\boldsymbol{\gamma}})_{\phi r} = (\mathbf{v} \cdot \nabla) \dot{\gamma}_{r\phi} - \frac{v_\theta}{r} \dot{\gamma}_{\theta\phi} + \frac{v_\phi}{r} [(\dot{\gamma}_{rr} - \dot{\gamma}_{\phi\phi}) + \dot{\gamma}_{r\theta} \cot \theta]$$

$$(\mathbf{v} \cdot \nabla \dot{\boldsymbol{\gamma}})_{\theta\phi} = (\mathbf{v} \cdot \nabla \dot{\boldsymbol{\gamma}})_{\phi\theta} = (\mathbf{v} \cdot \nabla) \dot{\gamma}_{\theta\phi} + \frac{v_\theta}{r} \dot{\gamma}_{r\phi} + \frac{v_\phi}{r} [\dot{\gamma}_{\theta r} + (\dot{\gamma}_{\theta\theta} - \dot{\gamma}_{\phi\phi}) \cot \theta]$$

Source: Reprinted by permission from R. B. Bird, R. C. Armstrong, and O. Hassager, *Dynamics of Polymeric Liquids, 2nd Edition, Vol. I, Fluid Dynamics*, Wiley, New York, 1987.

$$^a(\mathbf{v} \cdot \nabla) = v_x \frac{\partial}{\partial x} + v_y \frac{\partial}{\partial y} + v_z \frac{\partial}{\partial z}$$

$$^b(\mathbf{v} \cdot \nabla) = v_r \frac{\partial}{\partial r} + \frac{v_\theta}{r} \frac{\partial}{\partial \theta} + v_z \frac{\partial}{\partial z}$$

$$^c(\mathbf{v} \cdot \nabla) = v_r \frac{\partial}{\partial r} + \frac{v_\theta}{r} \frac{\partial}{\partial \theta} + \frac{v_\phi}{r \sin \theta} \frac{\partial}{\partial \phi}$$

and

$$\{\dot{\boldsymbol{\gamma}} \cdot \boldsymbol{\omega}\} = \begin{pmatrix} -\dot{\gamma}_{rz}^2 & 0 & 0 \\ 0 & 0 & 0 \\ 0 & 0 & \dot{\gamma}_{rz}^2 \end{pmatrix} \quad (\text{E3.5-8})$$

Thus, Eq. E3.5-4 reduces to

$$\frac{\mathcal{D}}{\mathcal{D}t} \dot{\boldsymbol{\gamma}} = \frac{1}{2} (\{\boldsymbol{\omega} \cdot \dot{\boldsymbol{\gamma}}\} - \{\dot{\boldsymbol{\gamma}} \cdot \boldsymbol{\omega}\}) = \begin{pmatrix} \dot{\gamma}_{rz}^2 & 0 & 0 \\ 0 & 0 & 0 \\ 0 & 0 & -\dot{\gamma}_{rz}^2 \end{pmatrix} \quad (\text{E3.5-9})$$

Table 3.3 Components of the Vorticity Tensor ω in Three Coordinate Systems^a**Rectangular Coordinates** (x, y, z)

$$\omega_{xy} = -\omega_{yx} = \frac{\partial v_y}{\partial x} - \frac{\partial v_x}{\partial y}$$

$$\omega_{yz} = -\omega_{zy} = \frac{\partial v_z}{\partial y} - \frac{\partial v_y}{\partial z}$$

$$\omega_{zx} = -\omega_{xz} = \frac{\partial v_x}{\partial z} - \frac{\partial v_z}{\partial x}$$

Cylindrical Coordinates (r, θ, z)

$$\omega_{r\theta} = -\omega_{\theta r} = \frac{1}{r} \frac{\partial}{\partial r} (rv_\theta) - \frac{1}{r} \frac{\partial v_r}{\partial \theta}$$

$$\omega_{\theta z} = -\omega_{z\theta} = \frac{1}{r} \frac{\partial v_z}{\partial \theta} - \frac{\partial v_\theta}{\partial z}$$

$$\omega_{zr} = -\omega_{rz} = \frac{\partial v_r}{\partial z} - \frac{\partial v_z}{\partial r}$$

Spherical Coordinates (r, θ, ϕ)

$$\omega_{r\theta} = -\omega_{\theta r} = \frac{1}{r} \frac{\partial}{\partial r} (rv_\theta) - \frac{1}{r} \frac{\partial v_r}{\partial \theta}$$

$$\omega_{\theta\phi} = -\omega_{\phi\theta} = \frac{1}{r \sin \theta} \frac{\partial}{\partial \theta} (v_\phi \sin \theta) - \frac{1}{r \sin \theta} \frac{\partial v_\theta}{\partial \phi}$$

$$\omega_{\phi r} = -\omega_{r\phi} = \frac{1}{r \sin \theta} \frac{\partial v_r}{\partial \phi} - \frac{1}{r} \frac{\partial}{\partial r} (rv_\phi)$$

Source: Reprinted with permission from R. B. Bird, R. C. Armstrong, and O. Hassager, *Dynamics of Polymeric Liquids, 2nd Edition, Vol. I, Fluid Dynamics*, Wiley, New York, 1987.

^aAll diagonal components are zero.

Finally, we substitute Eqs. E3.5-2, E3.5-3, and E3.5-9 into Eq. E3.5-1 to obtain the stress field

$$\begin{pmatrix} \tau_{rr} & \tau_{r\theta} & \tau_{rz} \\ \tau_{\theta r} & \tau_{\theta\theta} & \tau_{\theta z} \\ \tau_{zr} & \tau_{z\theta} & \tau_{zz} \end{pmatrix} = -\eta(\dot{\gamma}) \begin{pmatrix} 0 & 0 & \dot{\gamma}_{rz} \\ 0 & 0 & 0 \\ \dot{\gamma}_{rz} & 0 & 0 \end{pmatrix} - \left[\frac{1}{2} \Psi_1(\dot{\gamma}) + \Psi_2(\dot{\gamma}) \right] \begin{pmatrix} \dot{\gamma}_{rz}^2 & 0 & 0 \\ 0 & 0 & 0 \\ 0 & 0 & \dot{\gamma}_{rz}^2 \end{pmatrix} \\ + \frac{1}{2} \Psi_1(\dot{\gamma}) \begin{pmatrix} \dot{\gamma}_{rz}^2 & 0 & 0 \\ 0 & 0 & 0 \\ 0 & 0 & -\dot{\gamma}_{rz}^2 \end{pmatrix} \quad (\text{E3.5-10})$$

From Eq. E3.5-10 we obtain the following nonvanishing stress components:

$$\begin{aligned}\tau_{rz} &= \tau_{zr} = -\eta \dot{\gamma}_{rz} \\ \tau_{rr} &= -\left(\frac{1}{2}\Psi_1 + \Psi_2\right)\dot{\gamma}_{rz}^2 + \frac{1}{2}\Psi_1\dot{\gamma}_{rz}^2 = -\Psi_2\dot{\gamma}_{rz}^2 \\ \tau_{\theta\theta} &= 0 \\ \tau_{zz} &= -\left(\frac{1}{2}\Psi_1 + \Psi_2\right)\dot{\gamma}_{rz}^2 - \frac{1}{2}\Psi_1\dot{\gamma}_{rz}^2 = -(\Psi_1 + \Psi_2)\dot{\gamma}_{rz}^2\end{aligned}\quad (\text{E3.5-11})$$

We therefore observe that unlike in the Power Law model solution with a single shear stress component, τ_{rz} , in the case of a CEF model, we obtain, in addition, two nonvanishing normal stress components. Adopting the sign convention for viscometric flow, where the direction of flow z is denoted as 1, the direction into which the velocity changes r , is denoted as 2, and the neutral direction θ is denoted as direction 3, we get the expressions for the shear stress in terms of the shear rate, the primary, and secondary normal stress differences (see Eqs. 3.1-10 and 3.1-11):

$$\tau_{12} = \tau_{21} = -\eta \dot{\gamma}_{21} \quad (\text{E3.5-12})$$

$$\tau_{11} - \tau_{22} = \tau_{zz} - \tau_{rr} = -\Psi_1 \dot{\gamma}_{21}^2 \quad (\text{E3.5-13})$$

$$\tau_{22} - \tau_{33} = \tau_{rr} - \tau_{\theta\theta} = -\Psi_2 \dot{\gamma}_{21}^2 \quad (\text{E3.5-14})$$

with the three material functions of the CEF equation being identified as follows: $\eta(\dot{\gamma})$ is the viscosity function; $\Psi_1(\dot{\gamma})$ is the first normal stress-difference coefficient; and $\Psi_2(\dot{\gamma})$ is the second normal stress-difference coefficient. Examples of the shear rate dependence of both the viscosity and the coefficient of the first normal stress-difference functions are shown in Fig. E3.5.

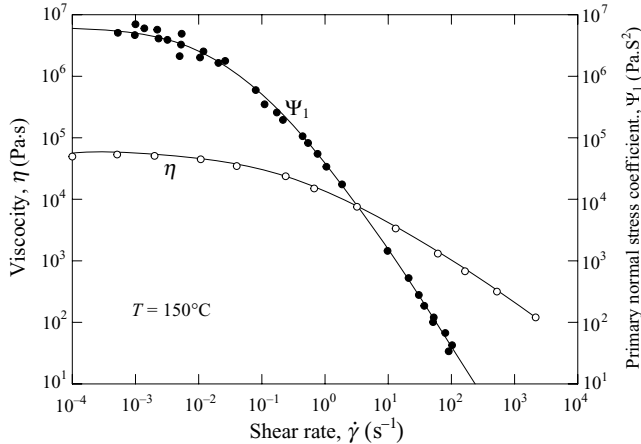


Fig. E3.5 Steady-state shear viscosity η and first normal stress coefficient Ψ_1 , obtained from dynamic measurements versus shear rate for a low-density polyethylene melt, melt I. [H. M. Laun, *Rheol. Acta*, **17**, 1 (1978).]

Example 3.6 Combined Drag and Pressure Flow between Parallel Plates In this example we examine the isothermal, laminar, steady, fully developed combined pressure and drag

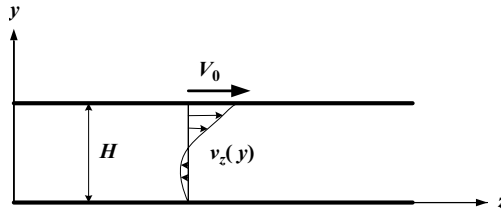


Fig. E3.6a Two parallel plates at a distance H apart with the upper plate moving at constant velocity V_0 . The velocity profile is for a particular flow situation where the pressure is “built up” in the z direction and is sufficiently high to create a “back flow” in the lower part of the channel.

flow of an incompressible Power Law model fluid, between parallel plates in relative motion as shown schematically in Fig. E3.6a. Superimposed on the drag flow there may be a positive or negative pressure gradient. In the figure we show a case where the pressure gradient is positive (i.e., pressure increases in the positive z direction). We present this example for two reasons: first, it is the type of flow that occurs in many types of processing equipment, most notably single-screw extruders, and second, it illustrates the relative complexity introduced in dealing analytically with the *absolute sign* in the Power Law model.

This problem was solved by Hirshberger (44), whose solution we follow. We will derive the velocity profile and the flow rate and demonstrate how to deal with a Power Law model fluid when the flow field where the velocity gradient is negative in one region and positive in the other.

The flow is viscometric because there is only one velocity component, $v_z(y)$, which is changing only in one spatial direction, y . Adopting a rectangular coordinate system, we find in analogy to Example 3.3 that $v_y = v_x = 0$, and therefore the equation of motion reduces to

$$\begin{aligned}\frac{\partial P}{\partial x} &= 0 \\ \frac{\partial P}{\partial y} &= 0 \\ \frac{\partial P}{\partial z} &= -\frac{\partial \tau_{yz}}{\partial y}\end{aligned}\tag{E3.6-1}$$

From the preceding equations we conclude that the pressure is a function of coordinate z only. Consequently, in the last equation the left-hand side is a function of z only, whereas the right-hand side is a function of y only. This is only possible if *both* equal a constant. Thus we conclude that the pressure gradient is constant, that is, pressure rises (or drops) *linearly* with z , and that the shear stress, in the presence of a pressure gradient, is a *linear* function of y , and in the absence of a pressure gradient it is constant across the gap. These observations follow from the momentum balance, and, they are therefore, true for all fluids, Newtonian and non-Newtonian alike.

Following the logic described in Example 3.4, we find that the Power Law model fluid for this viscometric flow reduces to

$$\tau_{yz} = -m \left| \frac{dv_z}{dy} \right|^{n-1} \frac{dv_z}{dy}\tag{E3.6-2}$$

Substituting Eq. E3.6-2 into Eq. E3.6-1 and casting it into dimensionless form, we obtain

$$\frac{d}{d\xi} \left(\left| \frac{dv_z}{dy} \right|^{n-1} \frac{dv_z}{dy} \right) = 6G \quad (\text{E3.6-3})$$

where $u_z = v_z/V_0$, and the dimensionless pressure gradient G is defined as

$$G = \frac{H^{n+1}}{6mV_0^n} \left(\frac{dP}{dz} \right) \quad (\text{E3.6-4})$$

Equation E3.6-3 can be integrated with respect to ξ to give

$$\left| \frac{du_z}{d\xi} \right|^{n-1} \frac{du_z}{d\xi} = 6G(\xi - \lambda) \quad (\text{E3.6-5})$$

where $-6G\lambda$ is an integration constant. The advantage of writing the integration constant this way is that λ acquires a clear physical meaning; it is the location where the shear rate is zero, or the location of the extremum in the velocity profile. We need to know this location in order to rid ourselves of the absolute value in Eq. E3.6-5. Depending on the value of G , there are four velocity profiles that we must consider (Fig. E3.6b). Cases a and b exhibit an extremum in the velocity profile within the flow regime. In the former, the pressure gradient is positive ($dP/dz > 0$); in the latter it is negative ($dP/dz < 0$). Cases c and d exhibit no extremum in the velocity profile within the flow regime, thus, in this case, λ lacks physical meaning, although it still is the location of an extremum value of the mathematical function describing the velocity profile. In Case c, $\lambda < 0$, and in Case d, it is $\lambda > 1$. In Cases c and d, $\dot{\gamma}_{yz} = dv_z/dy$ is positive through the flow regime, whereas in Cases a and b, it changes sign above and below λ .

We note from Eq. E3.6-4 that G may be positive or negative depending on the sign of the pressure gradient. It is, therefore, convenient to introduce at this point a variable accounting for the sign of G

$$\text{sign } G = \frac{G}{|G|} \quad (\text{E3.6-6})$$

We can now rewrite Eq. E3.6-5 as

$$\left| \frac{du_z}{d\xi} \right|^{n-1} \frac{du_z}{d\xi} = 6 \text{ sign } G |G| (\xi - \lambda) \quad (\text{E3.6-7})$$

It can easily be verified that for regions $\xi \geq \lambda$ for both positive and negative pressure gradients (i.e., both Cases a and b), Eq. E3.6-5 can be written as follows:

$$\frac{du_z}{d\xi} = |6G|^s (\xi - \lambda)^s \text{sign } G \quad (\text{E3.6-8})$$

where $s = 1/n$. Similarly, for $\xi \leq \lambda$ we get

$$\frac{du_z}{d\xi} = -|6G|^s (\lambda - \xi)^s \text{sign } G \quad (\text{E3.6-9})$$

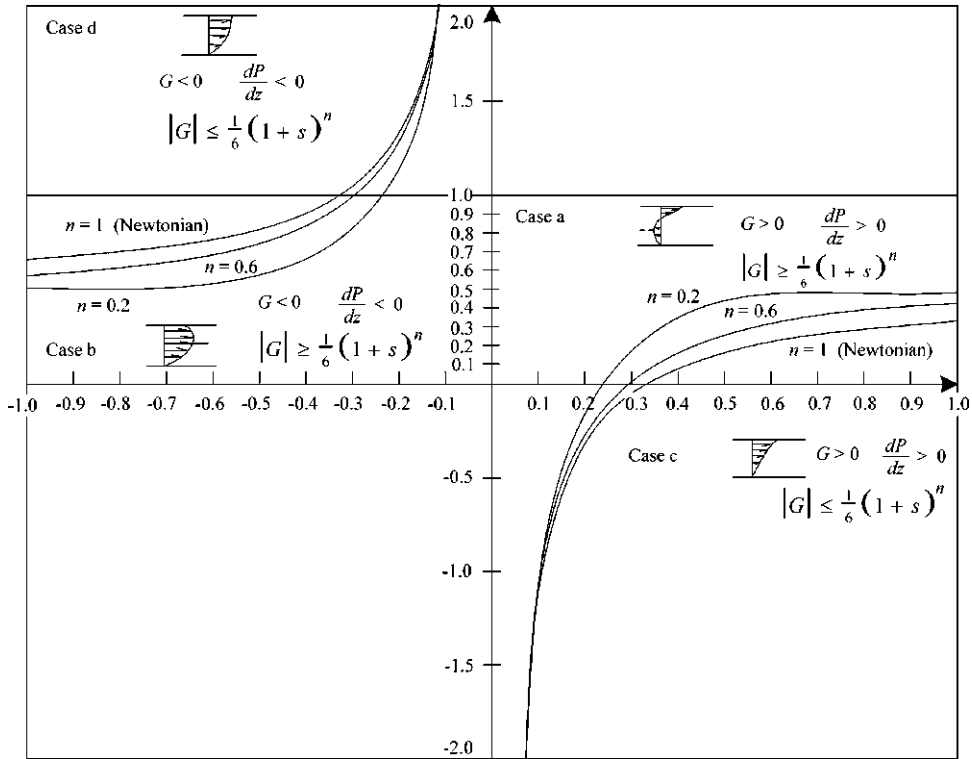


Fig. E3.6b Four regions of the solution of Eq. E3.6-5 corresponding to four types of velocity profiles. In regions (Cases) a and b, the velocity profile exhibits an extremum. In the former the pressure gradient is positive ($dP/dz > 0$); in the latter, it is negative ($dP/dz < 0$). The location of the extremum is at $\xi = \lambda$. In regions c and d, the velocity profile exhibits no extremum in the flow regime. In the former the pressure gradient is positive ($dP/dz > 0$); in the latter, it is negative ($dP/dz < 0$). The curves present solution λ as a function of G from Eq. E3.6-5, for $n = 1$, $n = 0.6$, and $n = 0.2$.

Equations E3.6-8 and E3.6-9 can be integrated subject to boundary conditions $u_z(1) = 1$ and $u_z(0) = 0$, respectively, to give

$$u_z = 1 - \frac{|6G|^s}{(1+s)} \left[(1-\lambda)^{1+s} - (\xi-\lambda)^{1+s} \right] \text{sign } G \tag{E3.6-10}$$

and

$$u_z = \frac{|6G|^s}{(1+s)} \left[(\xi-\lambda)^{1+s} - \lambda^{1+s} \right] \text{sign } G \tag{E3.6-11}$$

Since the velocity is continuous throughout ξ , Eqs. E3.6-10 and E3.6-11 are equal at $\xi = \lambda$, resulting in an equation for the unknown λ as a function of G and $\text{sign } G$

$$\lambda^{1+s} - (1-\lambda)^{1+s} + \frac{1+s}{|6G|^s \text{sign } G} = 0 \tag{E3.6-12}$$

Equation E3.6-12 is a nonlinear algebraic equation that must be solved numerically. However, it provides the limiting values of G for determining a priori whether the flow corresponds to Case a or b. By setting $\lambda = 0$ for $G > 0$, and $\lambda = 1$ for $G < 0$, we obtain the following conditions for the existence of an extremum within the flow region $0 \leq \xi \leq 1$

$$|G| \geq \frac{1}{6}(1+s)^n \quad (\text{E3.6-13})$$

By substituting Eq. E3.6-12 into Eq. E3.6-10, we can rewrite the velocity profile in one equation

$$u_z = \frac{|6G|^s}{(1+s)} \left[|\xi - \lambda|^{1+s} - \lambda^{1+s} \right] \text{sign } G \quad (\text{E3.6-14})$$

subject to the inequality in Eq. E3.6-13.

Turning now to Cases c and d, where no extremum occurs and $du_z/d\xi > 0$, we note that Eq. E3.6-7 can be written for $G > 0$ and $G < 0$, respectively, as

$$\frac{du_z}{d\xi} = (6G)^s (\xi - \lambda)^s \quad G > 0 \quad (\text{E3.6-15})$$

and

$$\frac{du_z}{d\xi} = (-6G)^s (\lambda - \xi)^s \quad G < 0 \quad (\text{E3.6-16})$$

Integration of Eqs. E3.6-15 and E3.6-16 with boundary conditions $u_z(0) = 0$ and $u_z(1) = 1$ results in the following velocity profiles for each of the Cases c and d:

$$u_z = \frac{(6G)^s}{(1+s)} \left[(\xi - \lambda)^{1+s} - (-\lambda)^{1+s} \right] \quad G > 0 \quad (\text{E3.6-17})$$

where λ is obtained from

$$(-\lambda)^{1+s} - (1 - \lambda)^{1+s} + \frac{1+s}{(6G)^s} = 0 \quad G > 0 \quad (\text{E3.6-18})$$

and

$$u_z = \frac{(-6G)^s}{(1+s)} \left[\lambda^{1+s} - (\lambda - \xi)^{1+s} \right] \quad G < 0 \quad (\text{E3.6-19})$$

where λ is obtained from

$$(\lambda)^{1+s} - (\lambda - 1)^{1+s} - \frac{1+s}{(-6G)^s} = 0 \quad G < 0 \quad (\text{E3.6-20})$$

By setting $\lambda = 0$ in Eq. E3.6-18 and $\lambda = 1$ in Eq. E3.6-20, we find the following condition for the flow without an extremum within the flow regime

$$|G| \leq \frac{1}{6}(1+s)^n \quad (\text{E3.6-21})$$

a result that, of course, is predictable from Eq. E3.6-13.

All the velocity profile and the equations for obtaining λ can be collapsed, respectively, into a single equation

$$u_z = \frac{|6G|^s \text{sign } G}{(1+s)} \left(|\xi - \lambda|^{1+s} - |\lambda|^{1+s} \right) = \frac{|\xi - \lambda|^{1+s} - |\lambda|^{1+s}}{|1 - \lambda|^{1+s} - |\lambda|^{1+s}} \quad (\text{E3.6-22})$$

and

$$|\lambda|^{1+s} - |1 - \lambda|^{1+s} + \frac{1+s}{|6G|^s \text{sign } G} = 0 \quad (\text{E3.6-23})$$

In solving for λ in the last equation, we find multiple solutions, but we must recall the following inequalities that help select the right solution

$$\begin{aligned} \text{if } |G| \geq \frac{1}{6}(1+s)^n & \quad \text{then} \quad 0 \leq \lambda \leq 1 \\ \text{if } |G| \leq \frac{1}{6}(1+s)^n & \quad \text{and if } G > 0 \quad \text{then} \quad \lambda \leq 0 \\ \text{if } |G| \leq \frac{1}{6}(1+s)^n & \quad \text{and if } G < 0 \quad \text{then} \quad \lambda \geq 1 \end{aligned}$$

Figure E3.6b, which plots the solution of Eq. E3.6-23 for three n values, also indicates the four solution regions.

Finally, we can integrate the velocity profile to obtain the volumetric flow rate per unit width

$$q = \frac{V_0 H |6G|^s \text{sign } G}{(1+s)(2+s)} \left[(1-\lambda)|1-\lambda|^{1+s} + \lambda|\lambda|^{1+s} - (2+s)|\lambda|^{1+s} \right] \quad (\text{E3.6-24})$$

Figure E3.6c plots the dimensionless flow rate q/q_d , where q_d is the drag flow rate, namely, the flow rate with zero pressure gradient, versus the dimensionless pressure gradient G . The figure shows that, whereas for Newtonian fluids, as expected, there is a linear relationship, non-Newtonian fluids deviate from linearity. The more non-Newtonian the fluid is, the greater is the deviation. Of particular interest is the inflection point indicating, for example, that in screw extruders, even for the isothermal case, increasing die resistance brings about somewhat unexpected changes in flow rate.

3.4 POLYMER MELT CONSTITUTIVE EQUATIONS BASED ON MOLECULAR THEORIES

Molecular theories, utilizing physically reasonable but approximate molecular models, can be used to specify the stress tensor expressions in nonlinear viscoelastic constitutive equations for polymer melts. These theories, called *kinetic theories of polymers*, are, of course, much more complex than, say, the kinetic theory of gases. Nevertheless, like the latter, they simplify the complicated physical realities of the substances involved, and we use approximate “cartoon” representations of macromolecular dynamics to describe the real response of these substances. Because of the relative simplicity of the models, a number of response parameters have to be chosen by trial and error to represent the real response. Unfortunately, such parameters are material specific, and we are unable to predict or specify from them the specific values of the corresponding parameters of other

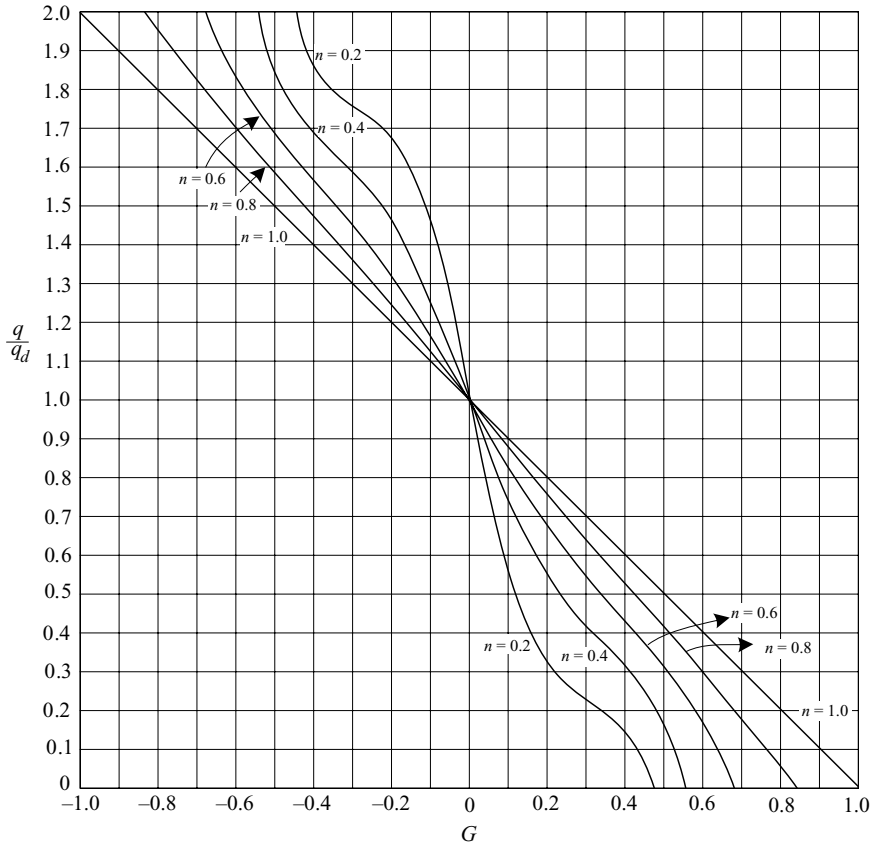


Fig. E3.6c Dimensionless flow rate versus dimensionless pressure gradient, with the Power Law exponent n as a parameter, for parallel-plate flow, as given in Eq. E3.6-24.

substances, even of similar macromolecular structures. In other words, the *kinetic theory* of polymer melts is not *true* molecular theory.

With these comments in mind, we list and briefly discuss the two classes of these theories: the *single molecule* (14) and *entanglement network* theories (23).

Single-molecule Theories

Single-molecule theories originated in early polymer physics work (45) to describe the flow behavior of *very dilute* polymer solutions, which are free of interpolymer chain effects. Most commonly, the macromolecular chain, capable of viscoelastic response, is represented by the well-known *bead-spring* model or “cartoon,” shown in Fig. 3.8(a), which consists of a series of small spheres connected to elastic springs.

Upon flow in the solvent environment, the drag that the solvent exerts on the spheres (representing the viscous nature of the real macromolecule), orients the bead-spring and *stretches* the elastic springs between the beads (which represent the elastic nature of the real macromolecules). The consequent stored energy in the springs is capable of restoring the equilibrium conformations of the bead-springs, but it is resisted by Stokesian drag on

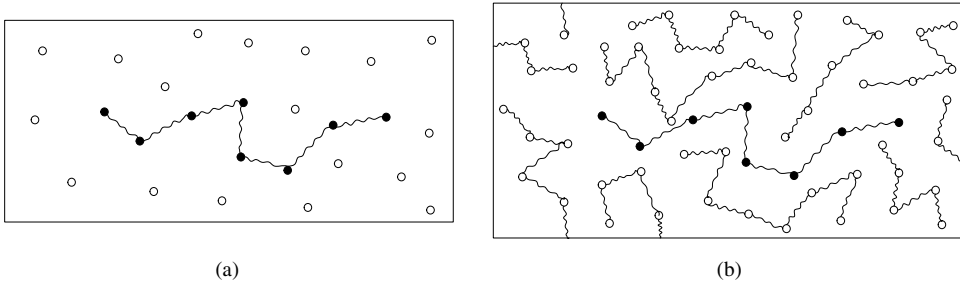


Fig. 3.8 Single-molecule *bead-spring models* for (a) a dilute polymer solution, and (b) an undiluted polymer (a polymer melt with no solvent). In the dilute solution, the polymer molecule can move about in all directions through the solvent. In the undiluted polymer, a typical polymer molecule (black bead) is constrained by the surrounding molecules and tends to execute snakelike motion (“reptation”) by sliding back and forth along its backbone direction (46). [Reprinted by permission from R. B. Bird, W. E. Stewart and E. N. Lightfoot, *Transport Phenomena*, 2nd Edition, Wiley New York (2002).]

the beads, responding with relaxation times that are proportional to the effective solvent drag viscosity and inversely proportional to the elastic spring constant.

Extension of this theory can also be used for treating *concentrated* polymer solution response. In this case, the motion of, and drag on, a single bead is determined by the mean intermolecular force field. In either the dilute or concentrated solution cases, *orientation distribution functions* can be obtained that allow for the specification of the stress tensor field involved. For the concentrated spring-bead model, Bird et al. (46) point out that because of the proximity of the surrounding molecules (i.e., spring-beads), it is easier for the model molecule to move in the *direction of the polymer chain backbone* rather than perpendicular to it. In other words, the polymer finds itself executing a sort of a snake-like motion, called *reptation* (47), as shown in Fig. 3.8(b).

Entanglement Network Theories

Entanglement network theories are based on the following premise: polymer melts are much like cross-linked rubber macromolecular networks, except that their cross-links are due to chain *entanglements* and are *temporary*. Such entanglements are continuously destroyed and formed to establish *network entanglement densities* characteristic of the state of motion of the network, being maximum at equilibrium. Green and Tobolsky (48) extended the rubber elasticity theory (49–52) to liquids with “temporary junctions” with equal probabilities of breaking and reforming. Following Larson (53), the development of the constitutive equation for such liquid with temporary entanglement networks is as follows: Let the probability that a chain breaks loose of a junction point, per unit time, be $1/\lambda$, where λ is of the order of the relaxation time. The probability that the strand does *not* break free in the time interval t' to t (present time), $P_{t',t}$ obeys the differential equation

$$\frac{d}{dt}P_{t',t} = -\frac{1}{\lambda}P_{t',t} \quad (3.4-1)$$

with $P_{t',t} = 1$. Hence

$$P_{t',t} = e^{(t'-t)/\lambda} \quad (3.4-2)$$

When the material is deformed, each strand is stretched affinely until it breaks free from its junction. After it breaks free, it relaxes to a configuration typical of equilibrium. As often as a strand breaks free, another relaxed strand becomes entangled. The probability that a strand breaks free and becomes reentangled in an interval of time between t' and $t' + dt'$ is dt'/λ . The probability that it survives without breaking from time t' to time t is $P_{t',t}$. It obeys the differential equation

$$\frac{d}{dt} P_{t',t} = -\frac{1}{\tau} P_{t',t} \quad (3.4-3)$$

The contribution $d\tau$ to the stress from those *stretched* strands that meet both of these conditions is, according to Eq. 3.4-1,

$$d\tau = \frac{dt'}{\lambda} P_{t',t} G \gamma_{[1]}(t', t) = G \frac{1}{\lambda} e^{(t'-t)/\lambda} \gamma_{[1]}(t', t) dt' \quad (3.4-3a)$$

with $G = (4/5)vk_B T$, where v is the entanglement density and $\gamma_{[1]}$ is the Finger relative strain tensor between the states of the fluid at t and t' . The total stress produced by strands that became reentangled at all past times, t' , is then

$$\tau = \int_{-\infty}^t m(t-t') \gamma_{[1]}(t', t) dt' \quad (3.4-4)$$

where $m(t-t')$ is the so called *memory function*, which is determined by the linear or the nonlinear viscoelastic spectra, depending on the level of strain. For the former case,

$$m(t-t') = \sum_i \frac{G_i}{\lambda_i} \exp[-(t-t')/\lambda_i] \quad (3.4-5)$$

Equations 3.4-3 and 3.4-4 form the molecular theory origins of the Lodge “rubberlike liquid” constitutive Eq. 3.3-15 (23). For large strains, characteristic of processing flows, the nonlinear relaxation spectrum is used in the memory function, which is the product of the linear spectrum and the *damping function* $h(\gamma)$, obtained from the stress relaxation melt behavior after a series of strains applied in stepwise fashion (53)

In the preceding treatment, the “strands”—entire chains or chain segments—are free to move through any path, for example, relaxing to an equilibrium configuration. But as noted in Fig. 3.9, any given polymer chain is able to move only in a *constrained path*, because of the surrounding chains and, therefore, tends to *move and advance* along its backbone direction by, as pointed out before, in a snakelike, reptation motion.

Pierre-Gilles deGennes (47) utilized this concept and coined the term in his work to explain why the relaxation times of entangled melts have a $\lambda \sim M^{3.4}$ dependence. Earlier, the lateral confinement of melt chains to a *tubelike* region had been postulated by Edwards (54). Since these early days of the reptation theory, a very significant volume of work has been dedicated to incorporating features that are physically reasonable and warranted in

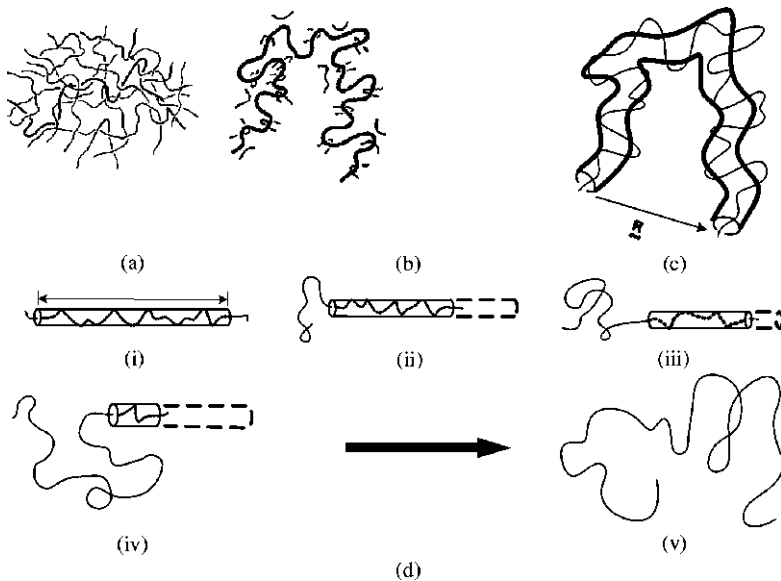


Fig. 3.9. (a) A polymer melt chain entangled in a mesh of other chains. (b) Individual neighboring chain entanglement points that result in (c) the confinement of the given chain to a tubelike region. [(d)(i)–(d)(v)] represents a schematic reptation of the polymer chain out of its (stretched for visualization) tube, requiring a reptation time τ_d . [Reprinted by permission from R. G. Larson, *The Structure and Rheology of Complex Fluids*, Oxford University Press, New York, 1999.]

order to improve the predictions of the corresponding members of the *reptation-based* constitutive equation. But before discussing some of them, it is useful to present a pictorial representation of reptation according to the work of Graessley (55). He considers the polymer chain shown on Fig. 3.9(a), entangled in a mesh of other polymers to be confined by individual chain neighbors in a manner shown in Fig. 3.9(b). As a physical consequence, the polymer chain is confined in a tubelike region shown in Fig. 3.9(c).

Motion within the tube is achieved by a random walk (“primitive path”) of unit steps of the order of the tube diameter, a . When a straight reptation tube is considered, for simplicity, reptation diffusional motion of the chain out of the tube is represented schematically in the steps depicted from Fig. 3.9(d)(i) to Fig. 3.9(d)(v).

Perkins and colleagues (56) have provided graphic and direct evidence of reptation, using a fluorescently stained, very long DNA molecule in an entangled environment of similar unstained DNA molecules. Figure 3.10 shows time-sequence images of such a $60\ \mu\text{m}$ long molecule, which was attached at one end to a small sphere that was pulled through the fluid using a laser-optical trap to form a letter “R.” As seen in the picture sequence, the free end of the DNA undergoes retraction through a tubelike region defined by the surrounding mesh of the invisible neighboring DNA chains.

The retraction follows the path of “R” containing the stretched, strained DNA molecule, strikingly demonstrating reptation. Molecular dynamic computational simulations (a tool of rapidly increasing utility in melt rheology and structuring) also show chain motion that is highly anisotropic, suggesting that diffusion motions of long chains are largely confined in a tube (57), as shown in Fig. 3.11.

The constitutive equations benefiting from the specific representations of reptation theory have the general form of the Lodge rubber-like liquid equation, since they are all

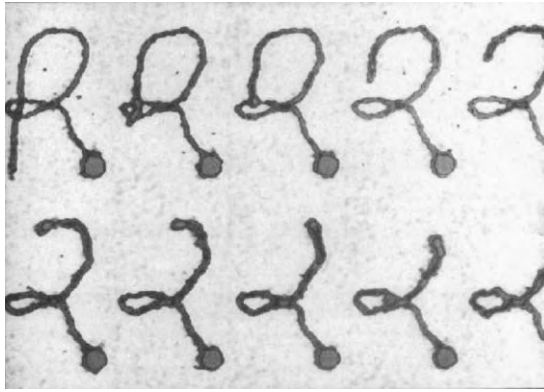


Fig. 3.10. Time sequence of images showing retraction of one end of a fluorescing 60- μm long DNA molecule entangled in a solution of other, nonfluorescing DNA molecules. The fluorescing molecule was attached at one end to a small sphere that was pulled through the solution using a laser-optical trap, to form the letter “R”. The free end then retracts through a tubelike region formed by the surrounding mesh of other, invisible DNA chains. [Reprinted by permission from the cover of *Science*, May 6, 1994 (Copyright 1994, American Association for the Advancement of Science).]

entanglement network theories, treating chain motion, deformations, and entanglements and disentanglements with different degrees of scrutiny and physical assumptions. Thus, the Doi–Edwards equation (58,59) considers the contributors to the stress tensor of the stretched and oriented tube segments due to the flow. This results in the integral form

$$\tau(t) = \int_{-\infty}^t m(t-t') \mathbf{S}_{DE}^{IA}(t') dt' \quad (3.4-6)$$

where \mathbf{S}_{DE}^{IA} , the Doi–Edwards strain measure for tube segments independently aligned

$$\mathbf{S}_{DE}^{IA} = 5 \left\langle \frac{\mathbf{u}' \mathbf{u}'}{(\mathbf{u}')^2} \right\rangle = 5\mathbf{S} \quad (3.4-7)$$

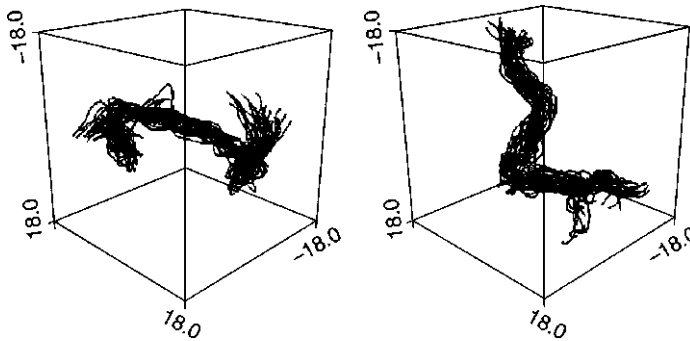


Fig. 3.11. Each of the two images contains superimposed configurations of a chain at many different instants in time in a molecular-dynamics simulation of a melt of such chains in a box. Over the time scale simulated, each chain appears to be confined to a tubelike region of space, except at the chain ends. [Reprinted by permission from K. Kremer and G. S. Grest, *J. Chem. Phys.*, **92**, 5057 (Copyright 1990 American Institute of Physics).]

where \mathbf{S} is the second-order orientation function and \mathbf{u} is the deformation vector. The memory function $m(t - t')$ is expressed as

$$m(t - t') = \frac{G_N^0}{5} \partial F(t - t') / \partial t' \quad (3.4-8)$$

where the plateau modulus is defined from the Treloar theory of rubber elasticity (52):

$$G_n^0 = \frac{3ckTh^2}{a_0^2} \quad (3.4-9)$$

The function $F(t - t')$ is related, as with the temporary network model of Green and Tobolsky (48) discussed earlier, to the survival probability of a tube segment for a time interval $(t - t')$ of the strain history (58,59). Finally, this Doi-Edwards model (Eq. 3.4-5) is for monodispersed polymers, and is capable of moderate predictive success in the non linear viscoelastic range. However, it is not capable of predicting strain hardening in elongational flows (Figs. 3.6 and 3.7).

The *pom-pom polymer reptation model* was developed by McLeish and Larson (60) to represent long chain-branched LDPE chains, which exhibit pronounced strain hardening in elongational flows. This idealized pom-pom molecule has a single backbone confined in a reptation tube, with multiple arms and branches protruding from each tube end, as shown in Fig. 3.12(a). M_b is the molecular weight of the backbone and M_a , that of the arms.

Corresponding dimensionless entanglement lengths are $S_b = M_b/M_e$ for the backbone and $S_a = M_a/M_e$ for the arms, where M_e is the entanglement molecular weight. The dominant contribution to the stress tensor is assumed to arise from the backbone/crossbar segment. Because these branches are entangled with the surrounding molecules, the backbone can readily be stretched in start-up extensional flows, producing strain

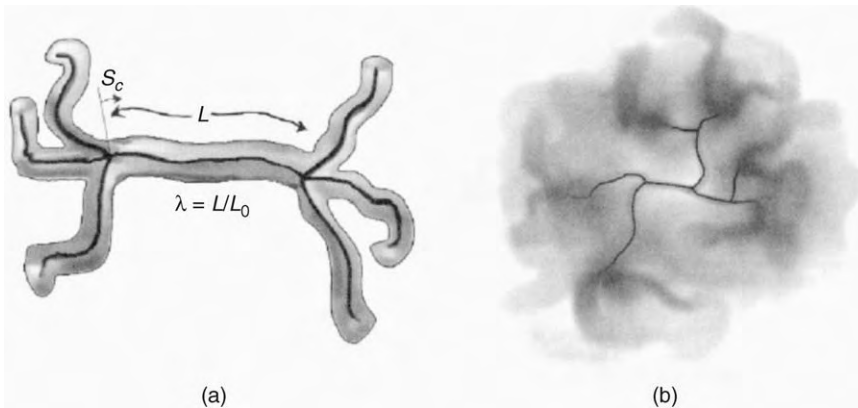


Fig. 3.12 (a) A pom-pom with three arms at each branch point ($q = 3$). At short times the polymer chains are confined to the Doi-Edwards tube. S_c is the dimensionless length of branch point retraction into the tube; λ is the stretch ratio where L is the curvilinear length of the crossbar and L_0 is the curvilinear equilibrium length. (b) Relaxation process of a long-chain-branched molecule such as LDPE. At a given flow rate $\dot{\epsilon}$ the molecule contains an unrelaxed core of relaxation times $\tau > \dot{\epsilon}^{-1}$ connected to an outer “fuzz” of relaxed material of relaxation $\tau < \dot{\epsilon}^{-1}$, behaving as solvent. [Reprinted by permission from N. J. Inkson et al., *J. Rheol.*, **43**(4), 873 (1999).]

hardening when it gets fully stretched and the poms on each end as they “cork” the tube ends. The tension that the poms may be able to sustain and impart on the backbone is qk_B/a , where q is the number of poms and a is the reptation tube diameter. Beyond this, tension in the backbone is sufficient to gradually withdraw the dangling arms into the tube ($S_e > 0$). When this branch point withdrawal is complete, strain-hardening behavior disappears. On the other hand, in start-up of shear flows, the backbone tube stretches only temporarily and eventually goes back to zero as the pom-pom molecule is aligned by the flow, thus producing shear strain softening.

Inkson et al. (61) and McLeish (62) in a recent review have proposed also a *multimode* pom-pom model in an attempt to account for the multiple levels of branching believed to be present in LDPE molecules. Because the precise structure and degree of branching of LDPE molecules are unknown, with no experimental techniques to determine them, the potential exists for these multimode models to “characterize” the LDPE macromolecular structure through fitting with experimental rheological data.

Figure 3.12(b) indicates how a reptating large molecule with multiple branch points relaxes after deformation. The free chain arms relax rapidly, much as the pom-pom arms at the outer branch point. This branch point is able to move one diffusive step after a deep retraction of the chain arms connected to it. This allows the molecular segment in the next (inward) branch point to relax. This, in turn, is repeated until the innermost segment relaxes. The relaxation time of a segment depends hierarchically on the path distance to the nearest free end that can release it from its tube constraint by retraction. The multimode pom-pom models, which utilize a small set of trial-and-error picked modes and utilize experimentally determined discreet relaxation spectra are able to closely account for three rheological functions: $\eta(\dot{\gamma}, t)$, $\bar{\eta}^+(\dot{\epsilon}, t)$, and $\bar{\eta}_{pl}^+(\dot{\epsilon}_{pl}, t)$, simultaneously over four decades of times and rates (61), which is rather remarkable. Still, these models lack the ability to predict the rheological behavior of a structurally slightly different polymer, that is, there is no direct connection to the specific macromolecular characteristics of the polymer melt

Wagner et al. (63–66) have recently developed another family of reptation-based molecular theory constitutive equations, named *molecular stress function* (MSF) models, which are quite successful in closely accounting for all the start-up rheological functions in both shear and extensional flows (see Fig. 3.7). It is noteworthy that the latest MSF model (66) is capable of very good predictions for monodispersed, polydispersed and branched polymers. In their model, the reptation tube diameter is allowed not only to stretch, but also to reduce from its original value. The molecular stress function $f(t)$, which is the ratio of the reduction to the original diameter and the MSF constitutive equation, is related to the Doi–Edwards reptation model integral-form equation as follows:

$$\tau(t) = \int_{-\infty}^t m(t-t') \mathbf{S}_{MSF}(t') dt' = \int_{-\infty}^t m(t-t') f^2 \mathbf{S}_{DE}^{IA}(t') dt' \quad (3.4-10)$$

In the MSF theory, the function, f , in addition to simple reptation, is also related to both the elastic effects of tube diameter reduction, through the Helmholtz free energy, and to dissipative, convective molecular-constraint mechanisms. Wagner et al. arrive at two differential equations for the molecular stress function f : one for linear polymers and one for branched. Both require only two trial-and-error determined parameters.

The constitutive equations discussed previously contain both *linear* and *nonlinear* response parameters. Both have to be evaluated experimentally. The first five to ten terms

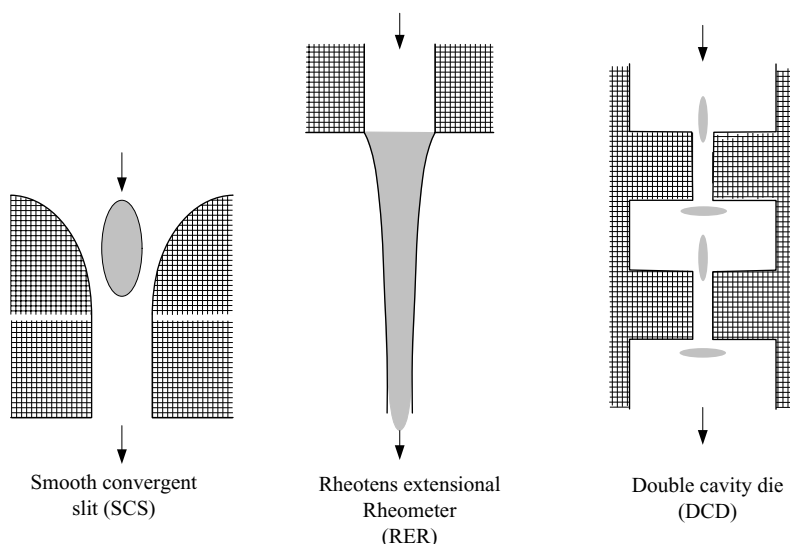


Fig. 3.13 Schematic of three prototype industrial flow (PIF) geometries showing shaded extensional flow regions for each geometry. [Reprinted by permission from J. F. Agassant et al., *Intern. Polym. Proc.*, **17**, 3 (2002).]

of the discrete LVE spectrum constitute a sufficient number of linear response terms. They are derived from small-strain (below the limit of linear viscoelastic response), sinusoidally varying flow experiments, specifically using the experimentally obtained G' , G'' or η^* . Until recently, the nonlinear response parameters have been obtained from flow experiments that are relatively simple (rheometric) and that impose large strains as large step-strain experiments, or extensional flows. Both result in altering the quiescent, entangled macromolecular network of the melts. This practice has left open the question of how relevant the evaluation of all the constitutive equation parameters is, using simple rheometric experiments that do not have the complexity of real processing flows. This question has been the subject of a large-scale investigation by a multidisciplinary network of European polymer researchers, which has been in progress for several years, and is described in by Agassant et al. (67). Two-dimensional, isothermal *prototype industrial flows* (PIF), resembling and closely related to polymer processing practice were used. Three such flows are shown in Fig. 3.13.

The flow birefringence pattern of these flows can be obtained through the use of a pair of flat glass walls. Using image enhancement and the stress-optical law (68),

$$\Delta = C(\tau_{11} - \tau_{22}) \quad (3.4-11)$$

where Δ is the birefringence and C is the stress-optical constant, the principal normal stress difference can be obtained experimentally and enhanced and “skeletalized” by image analysis. This is shown in Fig. 3.14 for the smooth convergent die of the PIFs shown in Fig. 3.13.

Such contours are then compared with numerically derived ones obtained in the following fashion: a nonlinear response constitutive equation is selected (60, 61, 64, 69) to be used with the equation of motion for a given PIF. The numerical solution computational

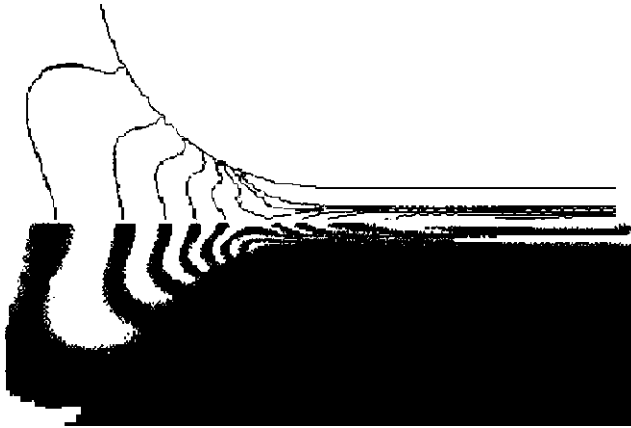


Fig. 3.14 Experimental and matching numerical simulation data for the smooth convergent die geometry of HDPE, Stamyilan HD862 at $T = 190^\circ\text{C}$. [Reprinted by permission from J. F. Agassant et al., *Intern. Polym. Proc.*, **17**, 3 (2002).]

packages required for the solution of the PIFs (as contrasted to the simpler rheometric flows) have to be powerful and the computational demands on both time and computer are daunting. Three different finite-element numerical codes were used: the commercial Fluent Group Polyflow (70), Venus (71), developed at Eindhoven University, and Seve 2 (72), developed at the CEMEF of Ecole des Mines de Paris.

In the example given, the constitutive equation used is a multimode Phan Tien Tanner (PTT). It requires the evaluation of both linear and nonlinear material-response parameters. The linear parameters are a sufficient number of the discrete relaxation spectrum λ_i and η_i pairs, which are evaluated from small-strain dynamic experiments. The values of the two nonlinear material-response parameters are evaluated as follows. Three semiarbitrary initial values of the two nonlinear parameters are chosen and the principal normal stress difference field is calculated for each of them using the equation of motion and the multimode PTT. They are compared at each field point (i, j) to the experimentally obtained normal stress difference and used in the following cost function F

$$F = \left[\sum_{L=1}^n \sum_{j=1}^n \frac{(G_{ij}^{\text{SIM}} - G_{ij}^{\text{exp}})^2}{(G_{ij}^{\text{exp}})^2} \right]^{1/2} \quad (3.4-12)$$

where G_{ij}^{SIM} is the “grey level” of the normalized simulation pattern and G_{ij}^{exp} the corresponding experimental pattern at any (i, j) point. The cost function is then evaluated for each of the three initial nonlinear parameter pairs (69). The simplex optimization method is then employed to arrive at the “optimal” values of the nonlinear parameters, which minimize the value of the cost function. The agreement between the experimentally and numerically obtained birefringence patterns, using the optimal nonlinear parameter pair, is shown in Fig. 3.15; it is very good.

Thus, adequate determination of nonlinear rheological parameters can be obtained, using industrial polymer processing-relevant flows, albeit with very substantial computational efforts, virtually assuring the relevance of the use of the constitutive equation for solving other complex processing flows.

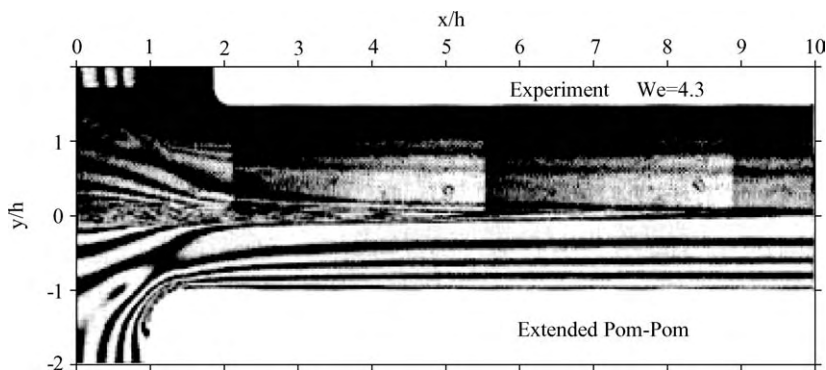


Fig. 3.15 (top) Measured and (bottom) calculated isochromatic fringe patterns for the extended pom-pom model at $We = 4.3$ of LDPE, DSM Stamylan LD 2008 XC43, $T = 150^\circ\text{C}$. [Reprinted by permission from J. F. Agassant et al., *Intern. Polym. Proc.*, **17**, 3 (2002).]

Finally, as we stated at the beginning of this section, all these recent successful molecular theory-based constitutive equations are still not capable of answering the question of what the empirical parameters, chosen by trial and error, will be for a yet-to-be-synthesized polymer, to accurately describe its rheological properties. One expects an answer to this question, if the theory would be based on fundamental molecular properties. The inability to answer this question rests in the fact that molecular theories, such as the previously stated one, are based on physically reasonable, ingeniously conceived and formulated, molecular cartoons. Nevertheless, with available computational power growing exponentially, and the potential synergy between molecular theories and molecular dynamics calculations, predicting the properties of existing macromolecular systems and those yet to come, from “first molecular principles” will not come in the distant future, but sooner.

REFERENCES

1. K. Walters, *Rheometry*, Wiley, New York, 1975.
2. R. I. Tanner, *Engineering Rheology*, Oxford University Press, London, 1985.
3. J. Dealy and K. F. Wissbrun, *Melt Rheology and Its Role in Plastics Processing*, Van Nostrand Reinhold, New York, 1990.
4. C. W. Macosko, Ed., *Rheology: Principles, Measurements and Applications*, Wiley-Interscience, New York, 1994.
5. K. Weissenberg, *Nature*, “A Continuum Theory of Rheological Phenomena,” **159**, 310–311 (1947).
6. M. M. Couette, *Am. Chem. Phys. Ser. VI*, **21**, 433 (1890).
7. J. D. Ferry, *Viscoelastic Properties of Polymers*, Third Edition, Wiley, New York, 1980.
8. H. M. Laun, “Description of the Non-linear Shear Behaviour of a Low Density Polyethylene Melt by Means of an Experimentally Determined Strain Dependent Memory Function,” *Rheol. Acta*, **17**, 1–15 (1978).
9. W. P. Cox and E. H. Mertz, “Correlation of the Complex Viscosity with the Steady Shear Viscosity,” *J. Polymer Sci.*, **28**, 619 (1958).
10. E. B. Christiansen and W. R. Leppard, “Steady-State and Oscillatory Flow Properties of Polymer Solutions,” *Trans. Soc. Rheol.*, **18**, 65–86 (1974).
11. D. G. Baird and D. I. Collias, *Polymer Processing*, Wiley-Interscience, New York, 1998, Chapter 3.

12. H. M. Laun, "Prediction of Elastic Strains of Polymer Melts in Shear and Elongation," *J. Rheol.*, **30**, 459 (1986).
13. F. T. Trouton, *Proc. Roy. Soc.*, **A77**, 426 (1906).
14. R. B. Bird, R. C. Armstrong, and O. Hassager, *Dynamics of Polymeric Fluids*, Second Edition, Vol. I, Wiley, New York, 1987.
15. S. A. Khan, R. K. Prud'homme, and R. G. Larson, "Comparison of the Rheology of Polymer Melts in Shear, and Biaxial and Uniaxial Extensions," *Rheol. Acta*, **26**, 144–151 (1987).
16. F. N. Cogswell, "Stretching Flow Instabilities at the Exits of Extrusion Dies," *J. Non-Newt. Fundam. Mech.*, **2**, 37–47 (1977).
17. J. M. Piau, N. El Kissi, F. Toussaint, and A. Mezghani, "Distortions of Polymer Melt Extrudates and their Elimination Using Slippery Surfaces," *Rheol. Acta*, **34**, 40 (1995).
18. C. Venet and B. Vergnes, "Experimental Characterization of Sharkskin in Polyethylenes," *J. Rheol.*, **41**, 873 (1997).
19. R. P. G. Rutgers and M. R. Mackley, "The Effect of Channel Geometry and Wall Boundary Conditions on the Formation of Extrusion Surface Instabilities for LLDPE," *J. Non-Newt. Fluid Mech.*, **98**, 185 (2001).
20. I. S. Sokolnikoff and R. M. Redheffer, *Mathematics of Physics and Engineering*, McGraw-Hill, New York, 1958, p. 263.
21. K. Weissenberg as cited by B. Rabinowitsch, *Z. Physi-Chem.*, **A145**, 1 (1929).
22. J. F. Hutton, "Fracture of Liquids in Shear," *Nature*, **200**, 646–648 (1963).
23. A. S. Lodge, *Elastic Fluids*, Academic Press, London, 1964.
24. S. I. Abdel-Khalik, O. Hassager, and R. B. Bird, "Prediction of Melt Elasticity From Viscosity Data," *Polym. Eng. Sci.*, **14**, 859 (1974).
25. J. D. Goddard and C. Miller, "An Inverse for the Jaumann Derivative and Some Applications to the Rheology of Viscoelastic Fluids," *Rheol. Acta*, **5**, 177–184 (1966).
26. W. Noll, *Arch. Rat. Mech. Anal.*, **2**, 197 (1958).
27. J. D. Goddard, "A Modified Functional Expansion for Viscoelastic Fluids," *Trans. Soc. Rheol.*, **11**, 380–399 (1967).
28. A. E. Green and R. S. Rivlin, *Arch. Rat. Mech. Anal.*, **1**, 1 (1957).
29. B. D. Coleman and W. Noll, "Foundations of Linear Viscoelasticity," *Rev. Mod. Phys.*, **33**, 239 (1961).
30. W. O. Criminale, Jr., J. L. Ericksen, and G. L. Filbey, Jr., *Arch. Rat. Mech. Anal.*, **1**, 410 (1958).
31. H. Jeffreys, *The Earth*, First Edition, Cambridge University Press, 1924.
32. J. G. Oldroyd, *Proc. R. Soc., London*, **A200**, 45 (1950).
33. K. Walters, *Q. J. Mech. Appl. Math.*, **13**, 444 (1960).
34. A. G. Fredrickson, "On Stress-relaxing Solids – I Flow and Normal Stress Effects," *Chem. Eng. Sci.*, **17**, 155 (1963).
35. J. D. Ferry, M. L. Williams, and D. M. Stern, *J. Chem. Phys.*, **22**, 987 (1954).
36. B. Bernstein, E. A. Kearsley, and L. J. Zappas, "A Study of Stress Relaxation with Finite Strain," *Trans. Soc. Rheol.*, **7**, 391 (1963).
37. D. C. Bogue, "An Explicit Constitutive Equation Based on an Integrated Strain History," *Ind. Eng. Chem. Fundam.*, **5**, 253–259 (1966); also I. Chen and D. C. Bogue, "Time-Dependent Stress in Polymer Melts and Review of Viscoelastic Theory," *Trans. Soc. Rheol.*, **16**, 59–78 (1972).
38. R. B. Bird and P. J. Carreau, "A Nonlinear Viscoelastic Model for Polymer Solutions and Melts–I," *Chem. Eng. Sci.*, **23**, 427 (1968).
39. W. Ostwald, *Kolloid-Z*, **36**, 99 (1925); also A. de Waele, *Oil and Color Chem. Assoc.*, **6**, 23 (1923).
40. Z. Tadmor, "Non-Newtonian Tangential Flow in Cylindrical Annuli," *Polym. Eng. Sci.*, **6**, 203–212 (1966).

41. S. B. Ellis, Thesis, Lafayette College, PA., 1927; cited in R. W. Whorlow *Rheological Techniques*, Halsted Press, New York, 1980.
42. M. M. Cross, "Rheology of Non-Newtonian Fluids: a New Flow Equation for Pseudoplastic Systems," *J. Colloids Sci.*, **20**, 417–437 (1965); also M. M. Cross, "Relation Between Viscoelasticity and Shear-thinning Behaviour in Liquids," *Rheological Acta*, **18**, 609–614 (1979).
43. P. J. Carreau, Ph.D Thesis, Department. of Chemical.Engineering, University of Wisconsin, Madison (1968).
44. M. Hirshberger, "Flow of Non-Newtonian Fluids in Rectangular Channels," M. S. Thesis, Department of Chemical Engineering, Technion, Israel Institute of Technology, Haifa, 1970.
45. P. E. Rouse, Jr., "A Theory of the Linear viscoelastic Properties of Dilute Solution of Coiling Polymers," *J. Chem. Phys.*, **21**, 1272–1280 (1953).
46. R. B. Bird, W. E. Stewart, and E. N. Lightfoot, *Transport Phenomena*, Second Edition, Wiley, New York, (2002).
47. P. G. deGennes, "Reptation of a Polymer Chain in the Presence of Fixed Obstacles," *J. Chem. Phys.*, **55**, 572–579 (1971).
48. M. S. Green and A. V. Tobolsky, "A New Approach to the Theory of Relaxing Polymeric Media," *J. Chem. Phys.*, **14**, 80–92 (1946).
49. F. T. Wall, "Statistical Thermodynamics of Rubber. II," *J. Chem. Phys.*, **10**, 485–488 (1942).
50. P. J. Flory and J. Rehner, "Statistical Mechanics of Cross-Linked Polymer Networks I. Rubberlike Elasticity," *J. Chem. Phys.*, **11**, 512–520 (1943).
51. H. M. James and E. Guth, "Theory of the Elastic Properties of Rubber," *J. Chem. Phys.*, **11**, 455–481 (1943).
52. L. R. G. Treloar, "The Elasticity of a Network of Long-Chain Molecules–II," *Trans. Faraday Soc.*, **39**, 241–246 (1943).
53. R. G. Larson, *Structure and Rheology of Complex Fluids*, Section 3.4.3, Oxford University Press, New York 1999.
54. S. F. Edwards, "The Statistical Mechanics of Polymerized Material," *Proc. Phys. Soc.*, **92**, 9–16 (1967).
55. W. W. Graessley, *Adv. Polym. Sci.*, **47**, 48 (1982).
56. T. T. Perkins, D. E. Smith, and S. Chu, "Direct Observation of Tube-Like Motion of a Single Polymer Chain," *Science*, **264**, 819–822 (1994).
57. K. Kremer and G. S. Grest, "Dynamics of Entangled Linear Polymer Melts: A Molecular-dynamics Simulation", *J. Chem. Phys.*, **92**, 5057–5086 (1990).
58. M. Doi and S. F. Edwards, *J. Chem. Soc. Faraday Trans. II*, **74**, 1818 (1978).
59. P. G. deGennes, *Scaling Concepts in Polymer Physics*, Cornell University Press, Ithaca, NY, 1979.
60. T. C. B. McLeish and R. G. Larson, "Molecular Constitutive Equations for a Class of Branched Polymers: The Pom-pom Polymer," *J. Rheol.*, **42**, 81 (1998).
61. N. J. Inkson, T. C. B. McLeish, O. G. Harlen, and D. J. Groves, "Predicting Low Density Polyethylene Melt Rheology in Elongational and Shear Flows with 'Pom-pom' Constitutive Equations", *J. Rheol.*, **43**, 873–896 (1999).
62. T. C. B. McLeish, "The Theory of Entangled Polymer Dynamics," *Advances in Physics*, **51**, 1379–1527 (2002).
63. M. H. Wagner and J. Schaeffer, "Constitutive Equations from Gaussian Slip-link Network Theories in Polymer Melt Rheology," *Rheol. Acta*, **31**, 22–31 (1992).
64. M. H. Wagner, H. Bastian, P. Hachmann, J. Meissner, S. Kurtzbeck, H. Münstedt and F. Langouche, "The Strain-hardening Behaviour of Linear and Long-chain-branched Polyolefin Melts in Extensional Flows," *Rheol. Acta*, **39**, 97–109 (2000).

65. M. H. Wagner, P. Ehrecke, P. Hachmann, and J. Meissner, "A Constitutive Analysis of Uniaxial, Equibiaxial and Planar Extension of a Commercial Linear High-density Polyethylene Melt," *J. Rheol.*, **42**, 621–638 (1998).

66. M. H. Wagner, P. Rubio, and H. Bastian, "The Molecular Stress Function Model for Polydisperse Polymer Melts with Dissipative Convective Constraint Release," *J. Rheol.*, **45**, 1387–1412 (2001).

67. J. F. Agassant, F. Baaijens, H. Bastian, A. Bernnat, A. C. B. Bogaerds, T. Coupez, B. Debbaut, A. L. Gavrus, A. Goublomme, M. van Gurp, R. J. Koopmans, H. M. Laun, K. Lee, O. H. Nouatin, M. R. Mackley, G.W. M. Peters, G. Rekers, W. M. H. Verbeeten, B. Vergnes, M. H. Wagner, E. Wassner, and W. F. Zoetelief, "The Matching of Experimental Polymer Processing Flows to Viscoelastic Numerical Simulation," *Int. Polym. Proc.*, **17**, 3–10 (2002).

68. H. Janeschitz-Kriegl, *Polymer Melt Rheology and Flow Birefringence*, Springer-Verlag, Berlin 1983.

69. O. H. Nouatin, Ph.D Thesis, Ecole des Mines de Paris, Sophia Antipolis, France (2000).

70. J. A. Nedler and R. Read, "A Simplex Method for Function Minimization," *Comput J.*, **7**, 308–313 (1965).

71. F. P. T. Baaijens, S. H. A. Selen, H. P. W. Baaijens, G. W. M. Peters, and H. E. H Meijer, "Viscoelastic Flow Past a Confined Cylinder of a Low Density Polyethylene Melt," *J. Non-Newt. Fluid Mech.*, **68**, 173–203 (1997).

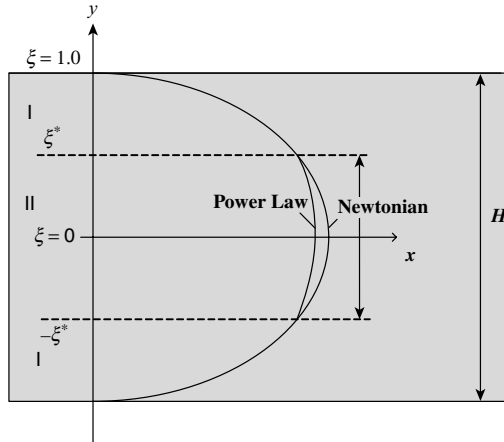
72. C. Braudo, A. Fortin, T. Coupez, Y. Demay, B. Vergnes, and J. F. Agassant, "A Finite Element Method for Computing the Flow of Multi-mode Viscoelastic Fluids: Comparison with Experiments," *J. Non-Newt. Fluid Mech.*, **75**, 1 (1998)

PROBLEMS

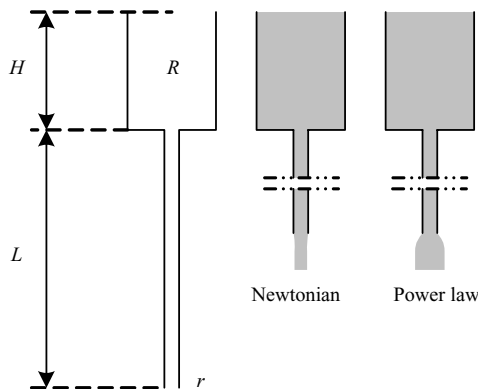
- 3.1 Pressure Flow between Parallel Plates with Various GNF Fluids** Derive expressions for the pressure flow rate of a fully developed, isothermal, steady flow between parallel plates for the following constitutive equations: (a) Power Law model: $\eta = m\dot{\gamma}^{n-1}$, (b) Ellis model: $\eta_0/\eta = 1 + (\tau/\tau_{1/2})^{\alpha-1}$, (c) Bingham Plastic: $\eta = \infty, \tau \leq \tau_0; \eta = \mu_0 + \tau_0/\dot{\gamma}, \tau \geq \tau_0$. (d) Calculate the flow rate per unit width for 2 MI LDPE at 170°C when the pressure gradient is 1.5 MPa/cm and the plate separation is 0.25 cm, using the Power Law model and the Ellis model.
- 3.2 Evaluating the Melt Index (MI) from the Flow Curve** Develop a methodology and computer program logic to evaluate the Melt Index (ASTM Standard D) of a material from its flow curve (non-Newtonian viscosity as a function of shear rate).
- 3.3 Evaluating the Flow Curve from Experimental Data** The flow rate of 3% CMC solution in water was measured in a long capillary as a function of pressure drop. Based on the results given in the following table, compute the non-Newtonian viscosity versus the shear-rate curve.

$4Q/\pi R^3(\text{s}^{-1})$	$\tau_w(\text{N/m}^2)$	$4Q/\pi R^3(\text{s}^{-1})$	$\tau_w(\text{N/m}^2)$
250	220	3500	670
350	255	5000	751
500	298	7000	825
700	341	9000	887
900	382	12500	1000
1250	441	17500	1070
1750	509	25000	1200
2500	584		

3.4 Inherent Errors in Using the Power Law Model in Pressure Flows The shear rate during pressure flow between parallel plates varies from zero at the center to maximum shear rate at the wall, $\dot{\gamma}_w$. Most polymer melts show Newtonian behavior at low shear rates, hence using the Power Law model for calculating flow rate introduces a certain error. How would you estimate the error introduced as a function of ξ^* , where ξ^* is the position below which the fluid is Newtonian? [See Z. Tadmor, *Polym. Eng. Sci.*, **6**, 202 (1966).]



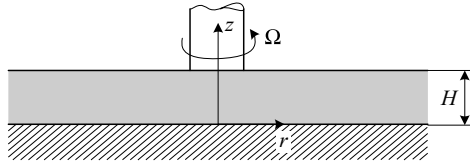
3.5 A Race Between Newtonian and Non-Newtonian Fluids Consider two vertical tubes, side by side, of diameter R and length L , as shown in the following figure, one filled with a Newtonian fluid and the other with a Power Law model fluid. The fluids emerge through a capillary of length l and radius r such that $r \ll R$. As the fluids began to emerge, an interesting phenomenon was observed: first, the level of the non-Newtonian fluids dropped faster than the Newtonian fluid, but then the Newtonian fluid overcame the former. (a) Derive a mathematical model that can explain the observed phenomenon. (b) If, after 10s, the height of both fluids is at $H/2$, what heights will they reach after 20s if the Power Law exponent is 0.5?



3.6 Stresses Generated by CEF Fluids in Various Viscometric Flows What stresses are necessary to maintain a CEF fluid flowing in the following flows: (a) parallel-plate drag flow; (b) Couette flow with the inner cylinder rotating; and (c) parallel-plate pressure flow. Assume the same type of velocity fields that would be expected

from a GNF or a Newtonian fluid. The three just-named flows are all viscometric. You should obtain the results in Eqs. E3.5-12 to E3.5-14.

- 3.7 Torsional Flow of a CEF Fluid** Two parallel disks rotate relative to each other, as shown in the following figure. (a) Show that the only nonvanishing velocity component is $v_\theta = \Omega r(z/H)$, where Ω is the angular velocity. (b) Derive the stress and rate of deformation tensor components and the primary and secondary normal difference functions. (c) Write the full CEF equation and the primary normal stress difference functions.

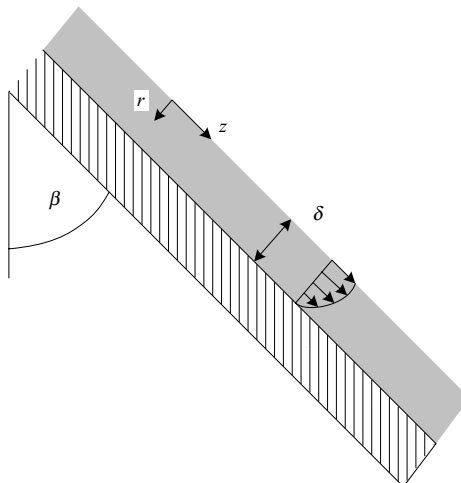


- 3.8 Special Form of the Rabinowitsch Equation** Show that the expression $Q = [\pi R^3/(s + 3)](-R\Delta P/2mL)^s$ is a special form of the Rabinowitsch equation (Eq. E3.1-9) for a Power Law fluid.

- 3.9 The Rabinowitsch Equation for Fluids Exhibiting Slip at the Wall** Derive the Rabinowitsch equation for the case where the fluid has a slip velocity at the wall V_w . [See L. L. Blyler, Jr., and A. C. Hart, *Polym. Eng. Sci.*, **10**, 183 (1970).]

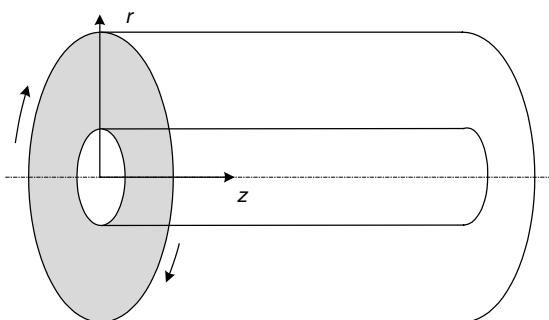
- 3.10 The Flow of Non-Newtonian Fluids in Flows between Almost Parallel Plates** The lubrication approximation was discussed in terms of Newtonian fluids. Considering a nearly parallel plate pressure flow ($H = H_0 - Az$), where A is the “taper,” what additional considerations would have to be made to consider using the lubrication approximation for (a) a shear-thinning fluid flow, and (b) a CEF fluid?

- 3.11 The Flow of a Shear-Thinning Fluid on an Inclined Plate** A shear-thinning viscous liquid defined by $\eta_0/\eta = 1 + (\tau/\tau_{1/2})^{\alpha-1}$ flows at steady state gravitationally on a surface inclined by angle β , as shown in the following figure. (a) Derive an expression for the film thickness δ in terms of the volumetric flow rate. (b) Find its value for $\alpha = 1$.



3.12 Evaluation of GNF Fluid Constants from Viscometric Data Using the flow curve of Chevron/Philips 1409 MI = 50 LDPE in Appendix A, calculate the parameters of the Power Law, Cross and Carreau models.

3.13 Helical Annular Flow Consider the helical annular flow between concentric cylinders with an axial pressure gradient and rotating outer cylinder as shown in the accompanying figure. Specify the equations of continuity and motion (z and θ components) and show that, if a Newtonian fluid is used, the equations can be solved independently, whereas if $\eta = \eta(\dot{\gamma})$, where $\dot{\gamma}$ is the magnitude of $\dot{\gamma}$, the equations are coupled.



3.14 Dimensional Changes in Planar and Biaxial Extensional Flows Determine the rate of dimensional changes that have to be applied on a flat film in order to generate (a) planar extension, and (b) biaxial extension flows.

3.15 Pressure Flow Calculations Using the Equivalent Newtonian Viscosity⁶ Consider fully developed isothermal laminar pressure flow between parallel plates of a shear-thinning liquid with a flow curve fitted to the following polynomial relationship above the shear rate $\dot{\gamma}_0$:

$$\ln \eta = a_0 + a_1 \ln \dot{\gamma} + a_{11} (\ln \dot{\gamma})^2 + a_2 T + a_{22} T^2 + a_{12} T \ln \dot{\gamma} \quad \dot{\gamma} \geq \dot{\gamma}_0,$$

and Newtonian behavior below $\dot{\gamma}_0$:

$$\eta = \eta_0(T), \quad \dot{\gamma} \leq \dot{\gamma}_0$$

The coefficients a_{ij} can be accurately determined from experimental data by standard linear multiple regression methods.

(a) Show that the flow rate per unit width is given by

$$q = -\frac{2h^2}{\tau_w^2} \int_0^{\tau_w} \tau \dot{\gamma} dz$$

where h is half the thickness and τ_w is the shear stress at the wall.

6. E. Broyer, C. Gutfinger, and Z. Tadmor, "Evaluating Flows of Non-Newtonian Fluids," *AIChE J.*, **21**, 198 (1975).

(b) Show that, for a Newtonian fluid, the flow rate can be written as

$$q = \frac{2}{3} \frac{h^2 \tau_w}{\mu}$$

(c) Show that, by defining an equivalent Newtonian viscosity,

$$\bar{\mu} = - \frac{\tau_w^3}{3 \int_0^{\tau_w} \tau \dot{\gamma} d\tau}$$

the flow rate of a non-Newtonian fluid can be calculated with the Newtonian equation in (b) with μ replaced by $\bar{\mu}$.

(d) Show that $\bar{\mu}$ can be expressed uniquely in terms of τ_w and T , for example, by an equation such as

$$\ln \bar{\mu} = b_0 + b_1 \ln \tau_w + b_{11} (\ln \tau_w)^2 + b_2 T + b_{22} T^2 + b_{12} T \ln \tau_w$$

and indicate a procedure for evaluating the coefficients of b_{ij} from a_{ij} .

(e) Using the expression in (d), explain how to calculate the flow rate for a given pressure drop, and the pressure drop for a given flow rate.

3.16 The Secondary Normal Stress Difference as a Stabilizing Force in Wire Coating Dies

Using a CEF equation, it can be shown,⁷ that, if the wire in a wire coating die is off center, a lateral stabilizing force arises proportional to the secondary normal stress-difference function Ψ_2 . Use a bipolar coordinate system ξ, θ, ζ (Fig. P3.16), the components of the equation of continuity, and motion in Table P3.16. Assume that there is no axial pressure gradient and the only nonvanishing velocity component is $v_\zeta(\xi)$, with boundary conditions $v_\zeta(\xi_1, \theta) = V_0$ and $v_\zeta(\xi_2, \theta) = 0$. Further assume the fluid to be incompressible and the flow isothermal.

(a) Show that the velocity profile is given by

$$v_\zeta/V_0 = \frac{\xi - \xi_2}{\xi_1 - \xi_2}$$

(b) Show that the equation of motion reduces to

$$\begin{aligned} \frac{\partial P}{\partial \xi} + X \frac{\partial}{\partial \xi} \left(\frac{1}{X} \tau_{\xi\xi} \right) &= 0 \\ \frac{\partial P}{\partial \theta} - \frac{1}{X} \tau_{\xi\xi} \sin \theta &= 0 \end{aligned}$$

7. Z. Tadmor and R. B. Bird, "Rheological Analysis of Stabilizing Forces in Wire-Coating Dies," *Polym. Eng. Sci.*, **14**, 124 (1974).

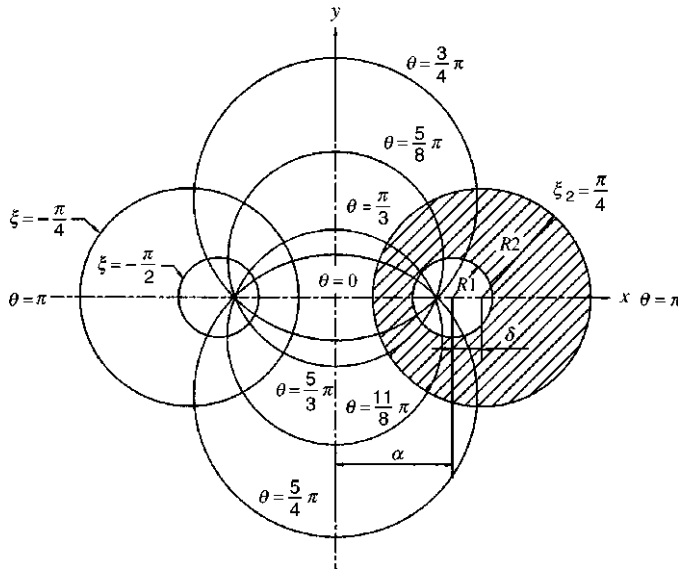


Fig. P3.16 Bipolar coordinate system. The shaded area denotes the cross section of the fluid, and the constant a , the distance of the pole from the origin. [Reprinted by permission from R. Bird, R. Armstrong, and O. Hassager, *Dynamics of Polymeric Liquids, Volume 1, Fluid Mechanics*, Second edition, Wiley, New York, 1987.]

where

$$X = \cosh \xi + \cos \theta$$

(c) Show that the lateral force in the wire per unit length f_x is

$$f_x = -\frac{\Psi_2 \pi V_0^2}{a(\xi_1 - \xi_2)^2}$$

where a is the distance of the poles of the bipolar coordinate system from the origin, which is related to the separation of centers of wire and die δ , via

$$\frac{\delta}{R_2} = \sqrt{1 + \left(\frac{a}{R_2}\right)^2} - \sqrt{\left(\frac{R_1}{R_2}\right)^2 + \left(\frac{a}{R_2}\right)^2}$$

Note that

$$\xi_1 = \sinh^{-1}\left(\frac{a}{R_1}\right) \quad \text{and} \quad \xi_2 = \sinh^{-1}\left(\frac{a}{R_2}\right)$$

3.17 The Single Maxwell Element LVE Constitutive Equation Consider the single Maxwell mechanical element shown in the following figure. The element was at rest for $t < 0$. A shear strain $\gamma_{12}(t)$ is applied at $t = 0$. By stating that the stress is the same in the dashpot and spring, while the total strain is the sum of those

TABLE P3.16 The Equations of Continuity and Motion in Bipolar Coordinates (ξ, θ, ζ)

Continuity

$$\frac{\partial}{\partial t} \rho + \left(\frac{X}{a} \frac{\partial}{\partial \xi} \rho v_\xi + \frac{X}{a} \frac{\partial}{\partial \theta} \rho v_\theta + \frac{\partial}{\partial \zeta} \rho v_\zeta - \frac{1}{a} \sinh \xi \cdot \rho v_\xi + \frac{1}{a} \sin \theta \cdot \rho v_\theta \right) = 0$$

Motion

$$\begin{aligned} & \rho \left[\frac{\partial v_\xi}{\partial t} + v_\xi \left(\frac{X}{a} \frac{\partial}{\partial \xi} v_\xi + \frac{1}{a} v_\theta \sin \theta \right) + v_\theta \left(\frac{X}{a} \frac{\partial}{\partial \theta} v_\xi + \frac{1}{a} v_\theta \sinh \xi \right) + v_\zeta \left(\frac{\partial}{\partial \zeta} v_\xi \right) \right] \\ &= -\frac{X \partial P}{a \partial \xi} - \left[\frac{X}{a} \frac{\partial}{\partial \xi} \tau_{\xi\xi} + \frac{X}{a} \frac{\partial}{\partial \theta} \tau_{\theta\xi} + \frac{\partial}{\partial \zeta} \tau_{\zeta\xi} + \frac{1}{a} (\tau_{\theta\theta} - \tau_{\xi\xi}) \sinh \xi + \frac{1}{a} (\tau_{\theta\xi} + \tau_{\xi\theta}) \sin \theta \right] + \rho g_\xi \end{aligned}$$

$$\begin{aligned} & \rho \left[\frac{\partial v_\theta}{\partial t} + v_\xi \left(\frac{X}{a} \frac{\partial}{\partial \xi} v_\theta - \frac{1}{a} v_\xi \sin \theta \right) + v_\theta \left(\frac{X}{a} \frac{\partial}{\partial \theta} v_\theta - \frac{1}{a} v_\xi \sinh \xi \right) + v_\zeta \left(\frac{\partial}{\partial \zeta} v_\theta \right) \right] \\ &= -\frac{X \partial P}{a \partial \theta} - \left[\frac{X}{a} \frac{\partial}{\partial \xi} \tau_{\xi\theta} + \frac{X}{a} \frac{\partial}{\partial \theta} \tau_{\theta\theta} + \frac{\partial}{\partial \zeta} \tau_{\zeta\theta} + \frac{1}{a} (\tau_{\theta\theta} - \tau_{\xi\xi}) \sin \theta - \frac{1}{a} (\tau_{\theta\xi} + \tau_{\xi\theta}) \sinh \xi \right] + \rho g_\theta \end{aligned}$$

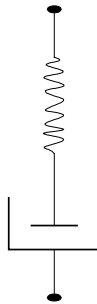
$$\begin{aligned} & \rho \left[\frac{\partial v_\zeta}{\partial t} + v_\xi \left(\frac{X}{a} \frac{\partial}{\partial \xi} v_\zeta \right) + v_\theta \left(\frac{X}{a} \frac{\partial}{\partial \theta} v_\zeta \right) + v_\zeta \left(\frac{\partial}{\partial \zeta} v_\zeta \right) \right] \\ &= -\frac{\partial P}{\partial \zeta} - \left[\frac{X}{a} \frac{\partial}{\partial \xi} \tau_{\xi\zeta} + \frac{X}{a} \frac{\partial}{\partial \theta} \tau_{\theta\zeta} + \frac{\partial}{\partial \zeta} \tau_{\zeta\zeta} - \frac{1}{a} \tau_{\xi\xi} \sinh \xi + \frac{1}{a} \tau_{\theta\theta} \sin \theta \right] + \rho g_\zeta \end{aligned}$$

in which, for Newtonian fluids, $\tau_{ij} = -\mu \{ (\nabla \mathbf{v}) + (\nabla \mathbf{v})^\dagger \}_{ij}$.

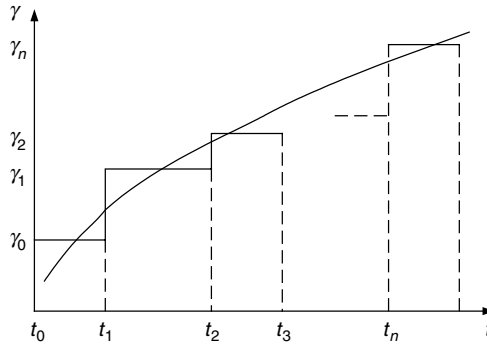
Source: Z. Tadmor and R. B. Bird, "Rheological Analysis of Stabilizing Forces in Wire-Coating Dies," *Polym. Eng. Sci.* **14**, 124 (1974).

Note: For the definition of X and a , see Problem 3.16.

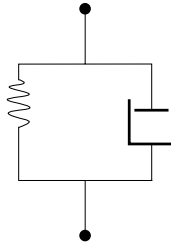
of the spring and the dashpot, obtain Eq. 3.3-9 in shear. Solve the differential equation to obtain $\tau/\gamma_0 = Ge^{-t/\lambda}$ for a stress relaxation experiment, that is, $\dot{\gamma}_{12} = \gamma_0$.



3.18 The Boltzmann Superposition Principle Apply the Boltzmann superposition principle to obtain the LVE (Eq. 3.3-8) using $\tau(t) = \gamma_0 Ge^{-t/\lambda}$. Consider the applied strain $\gamma(t)$ as being applied discretely in a series of small steps $\Delta\gamma$, as shown in the following figure:

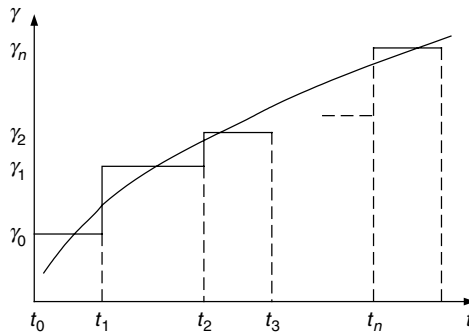


3.19 The Single Voigt Element LVE Constitutive Equation In the Voigt mechanical element shown in the following figure, the total stress is the sum of the stresses on the dashpot and spring. On the other hand, the strain in each component is equal to the total strain. (a) Use these facts to develop the constitutive equation for a single Voigt element. (b) Solve the differential equation for a creep experiment ($\tau = 0, t < 0; \tau = \tau_0, t \geq 0$).



3.20 The Boltzmann Superposition Principle: Alternate form of the LVE Equation

Apply the Boltzmann superposition principle for the case of a continuous stress application on a linear viscoelastic material to obtain the resulting strain $\gamma(t)$ in terms of $J(t - t')$ and $d\tau/dt'$, the stress history. Consider the applied stress in terms of small applied $\Delta\tau_i$, as shown on the accompanying figure.



- 3.21 Creep in Structural Design** A pendulum clock manufacturer wants to replace the metal pendulum arm of the clocks with a polymer rod. Is his idea a good one? Use the answer to Problem 3.20.
- 3.22 Prediction of $\bar{\eta}^+(t)$ by the Rubberlike Liquid Constitutive Equation** Calculate the extensional viscosity as a function of time after the start-up of a steady uniaxial extension of a Lodge rubberlike liquid, Eq. 3.4-3, having a single relaxation time λ_0 and modulus G_0 , Eq. 3.4-4. Before the initiation of the steady extensional flow the sample is and had been at rest, thus the stretch ratio history is: $\lambda(t', t) = \exp[\dot{\epsilon}(t' - t)]$ for $t' > 0$ and $\lambda(t', t) = \exp(\dot{\epsilon}t')$ for $t' \leq 0$ (independent of t')
- 3.23 Prediction of the Steady-State Viscosity in a Simple Shearing Flow by the K-BKZ Constitutive Equation** The K-BKZ (Kaye-Bernstein, Kearsley, and Zappas) constitutive equation [A. Kaye, Note No. 134, College of Aeronautics, Cranford University, U.K. (1962)] has the same integral form as the Green and Tobolsky Lodge rubberlike liquid, but utilizes a strain-dependent modulus $G[(t - t'), \gamma] = m(t - t')h(\gamma) = h(\gamma) \sum_i \frac{G_i}{\tau_i} \exp[(t - t')/\lambda_i]$. Thus, it has the general form $\tau = \int_{-\infty}^t m(t - t')\gamma_{[1]}(t', t) dt'$. Consider a fluid with a single relaxation time, λ_0 , and modulus, G_0 , and with $h(\gamma) = e^{-\gamma}$. Calculate the steady-state shear viscosity function $\eta(\dot{\gamma})$.